ANALYSIS AND DESIGN OF WIDEBAND ANTENNA ARRAYS

A THESIS SUBMITTED TO
THE GRADUATE SCHOOL OF NATURAL AND APPLIED SCIENCES
OF
MIDDLE EAST TECHNICAL UNIVERSITY

BY

KENAN ÇAPRAZ

IN PARTIAL FULFILLMENT OF THE REQUIREMENTS
FOR
THE DEGREE OF MASTER OF SCIENCE
IN
ELECTRICAL AND ELECTRONICS ENGINEERING

JANUARY 2014

Approval of the Thesis:

ANALYSIS AND DESIGN OF WIDEBAND ANTENNA ARRAYS

submitted by **KENAN ÇAPRAZ** in partial fulfillment of the requirements for the degree of **Master of Science in Electrical and Electronics Engineering Department, Middle East Technical University** by,

Prof. Dr. Canan Özgen _____
Dean, Graduate School of **Natural and Applied Sciences**

Prof. Dr. Gönül Turhan Sayan _____
Head of Department, **Electrical and Electronics Engineering**

Assoc. Prof. Dr. Lale Alatan _____
Supervisor, **Electrical and Electronics Engineering Dept., METU**

Examining Committee Members:

Prof. Dr. Sencer Koç _____
Electrical and Electronics Engineering Dept., METU

Assoc. Prof. Lale Alatan _____
Electrical and Electronics Engineering Dept., METU

Prof. Dr. Gülbin Dural _____
Electrical and Electronics Engineering Dept., METU

Prof. Dr. Özlem Aydın Çivi _____
Electrical and Electronics Engineering Dept., METU

Mehmet Erim İnal (M.Sc.E.E) _____
ASELSAN Inc.

Date: **31.01.2014**

I hereby declare that all information in this document has been obtained and presented in accordance with academic rules and ethical conduct. I also declare that, as required by these rules and conduct, I have fully cited and referenced all material and results that are not original to this work.

Name, Last name : Kenan ÇAPRAZ

Signature :

ABSTRACT

ANALYSIS AND DESIGN OF WIDEBAND ANTENNA ARRAYS

ÇAPRAZ, Kenan

M. Sc. Department of Electrical and Electronics Engineering

Supervisor: Assoc. Prof. Dr. Lale Alatan

January 2014, 112 pages

Two methods of wideband array design are studied. The aim of this study is to investigate arrays with aperiodic spacings which are designed with these methods in order to obtain wideband behavior. These methods are genetic algorithm and wavelength scaled arrays that have active regions with variable interelement spacings. Genetic algorithm is utilized for array antennas with aperiodic spacing to optimize sidelobe levels of the antenna array in wide frequency band. Wavelength scaled spacing concept in designing arrays is benefited to design array with frequency independent radiation characteristics such as constant gain and beamwidth in the operational bandwidth. MATLAB® codes are developed in order to examine array factor of designed arrays with these methods. A feed network in order to implement active region concept is designed and realized. A fabricated linear Vivaldi antenna array with designed feed network is measured and its performance is compared with simulation results.

KEYWORDS: Wideband Array Design, Genetic Algorithm, Wavelength Scaled Array, Aperiodic Spacing, Sidelobe, Frequency Independence Radiation

ÖZ

GENİŞ BANTLI ANTEN DİZİLERİNİN ANALİZİ VE TASARIMI

ÇAPRAZ, Kenan
Yüksek Lisans, Elektrik ve Elektronik Mühendisliği Bölümü
Tez Yöneticisi: Doç. Dr. Lale ALATAN

Ocak 2014, 112 sayfa

Geniş bantlı dizi tasarımı konusunda iki yöntem incelenmiştir. Bu çalışmanın amacı, bu yöntemlerle tasarlanmış değişken aralıklı dizi antenlerini geniş bantlılık elde etme konusunda incelemektir. Bu metotlar, genetik algoritma ve elemanlar arası uzaklıkların değişken olduğu aktif bölgelere sahip dalga boyu ile orantılanmış dizilerdir. Genetik algoritma aperiyodik dizilimli dizi antenlerinde, dizi antenin yan huzme seviyesini geniş bantta optimize etmek için kullanılmaktadır. Dalga boyu ile orantılanan uzaklık konseptinden dizi tasarımlarında, çalışılan frekans bandında, sabit kazanç ve huzme genişliği gibi frekanstan bağımsız yayın karakteristiklerini elde etmek için faydalanılmaktadır. Bu metotları sınamak için MATLAB® programında kodlar tasarlanılmıştır. Dizi antenine aktif bölge konseptini uygulamak için bir besleme devresi tasarlanmıştır ve üretilmiştir. Üretilmiş tek boyutlu Vivaldi anten dizisi bu besleme devresi ile ölçülmüş ve performansı benzetim sonuçlarıyla karşılaştırılmıştır.

ANAHTAR KELİMELER: Geniş Bantlı Dizi Tasarımı, Genetik Algoritma, Dalga Boyu ile Orantılanmış Dizi, Aperiyodik Dizilim, Yan Huzme, Frekanstan Bağımsız Yayın

To my Family …

ACKNOWLEDGMENTS

The author would like to express his sincere appreciation to his supervisor, Assoc. Prof. Dr. Lale ALATAN for her valuable guidance and supervision. Without her support this work would not be possible.

The author would like to acknowledge his gratitude to his friends and colleagues in ASELSAN Inc. Special thanks goes to Mehmet Erim İnal, Erhan Halavut, Mert Kalfa and Hakan Paruldar who supported the author with their experience about the topic and motivation.

I would like to thank TÜBİTAK for providing financial support during the study.

Last but not the least; the author would like to express his deepest gratitude to his family, without whom he would have never been able to reach where he is.

TABLE OF CONTENTS

LIST OF TABLES

TABLES

LIST OF FIGURES

FIGURES

LIST OF SYMBOLS

ϵ_r	relative permittivity
λ	wavelength
λ_0	free space wavelength at frequency f0
λ_i	wavelength of an element of a layer inside array antenna
d_i	distance of an element of a layer inside array antenna
HPBW	Half Power Beamwidth
f_0	design frequency
N	number of elements in a part of array or in entire array
$AF(\theta, \phi)$	array factor in terms of θ and ϕ
a_n	excitation coefficient of nth array element
d_{nx}	positions of nth array element in x direction
d_{ny}	positions of nth array element in y direction
f_{min}	minimum operating frequency of an array antenna
f_{max}	maximum operating frequency of an array antenna
f_n	any operating frequency of an array antenna
S_m	active S parameter of mth array element
S_{mn}	coupling between mth and nth array element
ϕ_n	phase coefficient of nth array element
k	free space wave number
v_{ph}	phase velocity
c	speed of light in vacuum
p	opening rate of exponential Vivaldi taper
w_1	minimum width of Vivaldi taper
w_2	maximum width of Vivaldi taper
AUT	Antenna Under Test

CHAPTER 1

INTRODUCTION

Array antenna systems are one of the inevitable parts of today's radar and electronic warfare (EW) systems. They can produce beams with high scanning rates to operate simultaneously against multiple targets. For such systems, survivability, low observability, cost and weight issues can be challenging technical obstacles [1]. Apertures and T/R modules in those systems have to be not only wideband but also modular and reconfigurable in order to meet the design specifications in some parameters such as antenna gain and beam shape.

For a usual design of phased arrays, antenna element sizes and the distance between elements are chosen as fixed distances. This fixed distance between the elements is often nearly $\lambda/2$ at the highest operational frequency of the array in order not to observe the grating lobe at high frequencies. As a result, the elements can be electrically small at the low end of the frequency band for wideband applications.

In conventional array design, the length of elements is determined according to the specified beamwidth at the lowest frequency whereas the element spacing is determined according to the wavelength at the highest frequency. This results in unnecessarily large number of elements at the lowest frequency for very wideband arrays. Moreover, the beamwidth at the highest frequency will be narrower than the specified value. If the phased array's feed is frequency independent, the beamwidth of the array will decrease, and the gain will increase with increasing frequency. Thus, with conventional approach, wideband phased arrays are subject to disadvantages of frequency dependent radiation and high cost because of the large number of T/R modules required to feed the array. As a

result, there is a need for a proper design of the array and the antenna feed so that the phased array can perform less frequency dependent radiation compared to a conventional phased array.

The studies conducted in this thesis are mainly focused on investigation of the array design concepts that allows design of arrays with aperiodic lattice and wideband characteristics.

Firstly, the methods and results found in literature for the design of wideband arrays will be presented to understand the key issues in the design of such arrays.

Rumsey et al. [2] studied a dipole array indicated with crosses as shown in Figure 1.1. All elements are fed in phase, so the array has a broadside radiation. This array is designed to have active regions. The frequency band is divided into subbands and an active region is assigned for each subband. Element spacing in each active region is determined by the center frequency of the corresponding subband, so frequency independent radiation is achieved.

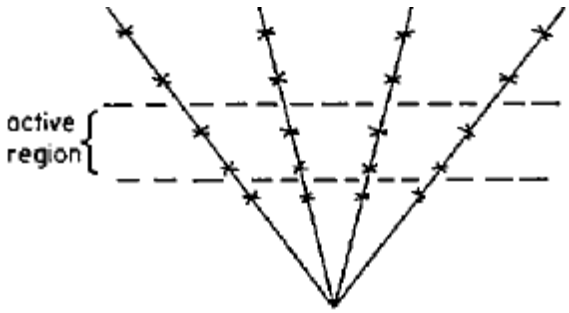

Figure 1.1 Arrangement of dipole array (From [2])

A similar study about dipole arrays is conducted by James K. Breakall [3]. He extended the concept presented in [2] for 3D arrays. He designed a 3 dimensional frequency independent phased array with dipole elements as shown in Figure 1.2 (plus sign represents dipole elements). This array is an application of log-periodic principle. With this principle, the element spacings are determined in a similar manner like the design of log-periodic antennas. Advantages of this antenna over the conventional approach are

constant gain and beamwidth within the whole frequency band, less number of radiating elements, less physical volume and area.

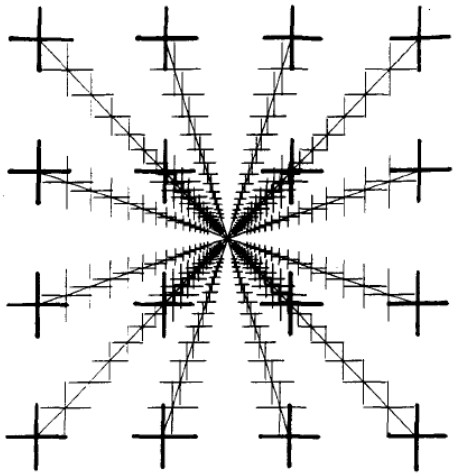

Figure 1.2 Three dimensional frequency independent phased array + : dipole elements (From [3])

Another study was conducted by Gunnarsson et al. [1] where three phased array concepts were compared in terms of reducing the frequency dependence of the radiation for very wideband phased arrays. Conventional array, frequency tapered array and array with varying elements size and spacings were those mentioned concepts. Schematic of conventional array can be seen in Figure 1.3 with active region illustration.

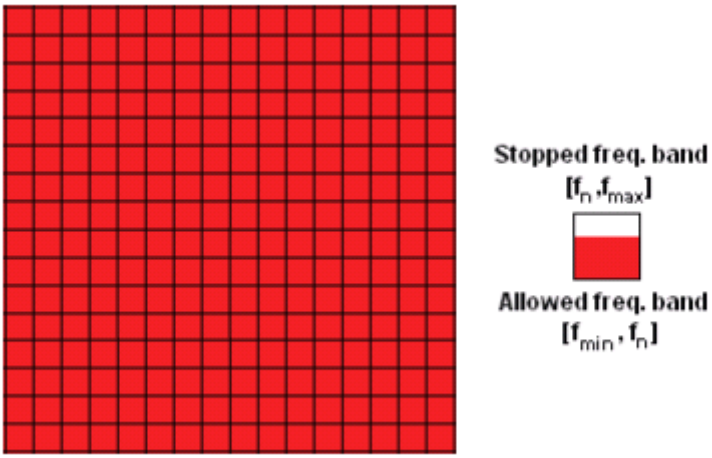

Figure 1.3 Schematic illustration of frequency operation of conventional array

Active region illustration in Figure 1.3 shows that all of the elements in the aperture have the same size so that spacing between adjacent elements are the same in all possible directions. Spacing between elements is nearly λ/2 at the maximum frequency within the band, f_{max}, so that no grating lobe exists in visible space for any scan of the array. Frequency band meter at the right of the figure indicates the frequency of operation for any element in the array. The red color denotes the operational bandwidth of the corresponding element. As can be seen, all elements of conventional array operate for all the frequencies in the bandwidth. Frequency tapered array and conventional array differs from each other with changing active region with respect to frequency in the bandwidth. Such an example of frequency tapered array with 6 subbands can be seen in Figure 1.4.

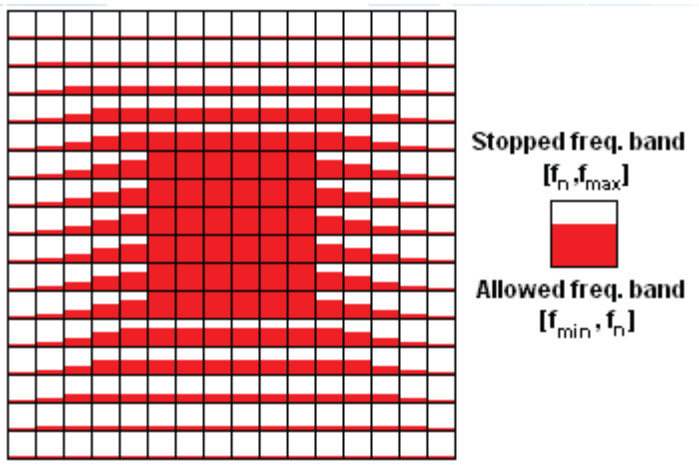

Figure 1.4 Schematic illustration of a frequency tapered phased array (From [1])

As can be seen in the figure, for frequencies at the highest subband, only the elements in the core region are active. As frequency of operation in the bandwidth decreases, more elements adjacent to core region are active. Furthermore, all of the elements are active for frequencies at the lowest subband. Such an operation of elements is a frequency taper that results in frequency independent radiation of the array. In Figure 1.3 and Figure 1.4, it is observed that size of elements, spacing between elements and number of elements can be same for conventional array and frequency tapered array for the same requirements such as HPBW. However, it is also possible to have frequency independent radiation with less number of elements and varying element sizes and spacings with variable element size

array concept. Figure 1.5 shows an example of an array with varying element size having 4 subbands in its operational band.

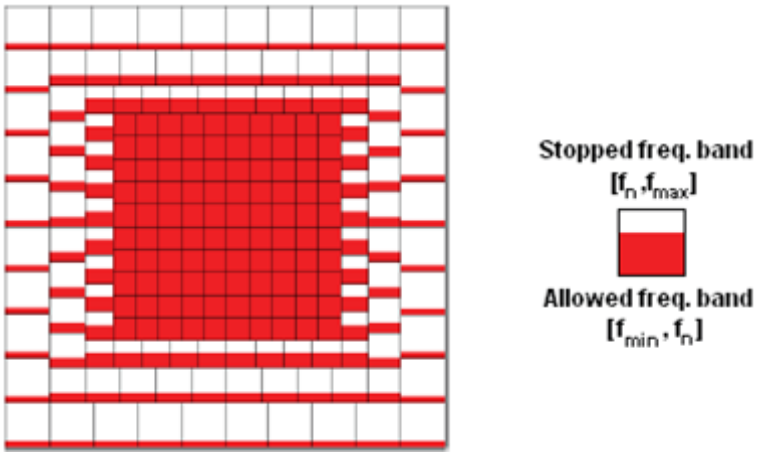

Figure 1.5 Schematic illustration of the antenna concept proposed by Cantrell et al. [4] (From [1])

For the third alternative method to reduce frequency dependence, i.e. the variable element size array, the concept is to obtain approximately frequency independent and beamwidth for very wide frequency range which was proposed by Cantrell et al. [4]. Basic idea is to design a wideband phased array with antenna elements with varying element sizes and element distances. First step in the design is to build a core region with the same and very wideband elements with $\lambda/2$ apart at the maximum frequency. Then, layers are added to the border of the core region such that element sizes and distances are increasing in proportion with the increase in the wavelength as in Figure 1.5. In some references, this type of array configuration is called as variable element size array and in some others it is referred as wavelength scaled array. Since the wavelength scaled spacing concept can be used even with elements of same size, wavelength scaled array terminology is preferred and adopted in this thesis. The core region consists of $N*N$ elements. The number of elements in the next layer is also N. However, for adjacent layers, N identical inner elements will have the same length as the N-2 identical outer elements. This relation is valid for the all adjacent layers as in Figure 1.5. The element distance in each layer, d_i, is equal to $\lambda_i/2$. The relation between adjacent layers as seen in Figure 1.6 can be shown as in (1.1).

$$\lambda_{i+1} = \frac{N}{N-2} * \lambda_i,\ d_{i+1} = \frac{N}{N-2} * d_i \qquad (1.1)$$

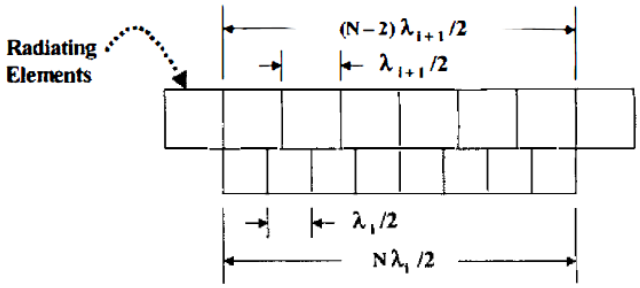

Figure 1.6 Illustration of the relationship between element size and inter-element spacing in adjacent layers (From [4])

As can be seen in frequency illustration of Figure 1.5, elements in core region are active at the highest frequency of operation. For the lower frequencies the core region plus one or more layers are active. The frequency of the operation determines the number of layers of the phased array. For the lowest frequency, all elements are active. The power density has to be kept constant over the aperture so that gain and beamwidth of the array can be frequency independent for this phased array. This requires that input power to each element must vary linearly with the element area of each element.

Some comparison is performed by designing array with the same specifications but with different concepts [1]. Results of such a comparison are given in Table 1.1. Number of elements, and variation in HPBW in 5:1 bandwidth, can be seen for a HPBW requirement of 10º at low frequency in the band.

Table 1.1 Number of elements required and change in HPBW in 5:1 bandwidth for the investigated array concepts (From [1])

Array Concept	Number of elements	$HPBW_{f_{min}} - HPBW_{f_{max}}$
Conventional Array	2500	10.2º-2.0º
Frequency Tapered Array	2500	10.2º-9.3º
Wavelength Scaled Array	441	10.2º-9.3º

For conventional and frequency tapered array, number of elements required to give 10º HBPW is nearly 5.7 times that of wavelength scaled array. The change in HPBW in bandwidth is the same for frequency tapered and wavelength scaled arrays; however, the change in the same parameter is greater for conventional array than that for those concepts. As a result, for the applications requiring frequency independence, conventional arrays are not suitable due to change in HPBW in bandwidth. Moreover, if such applications also require less number of elements or modules, wavelength scaled array is better than frequency tapered array.

Realization of wavelength scaled phased arrays has also been found in some studies. Kindt designed ultrawideband wavelength scaled antenna which can be seen as a progress of wavelength scaled phased array as seen in Figure 1.7 [5]. This architecture is seen to be a version of that in Figure 1.5 with N=4. Design of Vivaldi elements with different size is performed in this study.

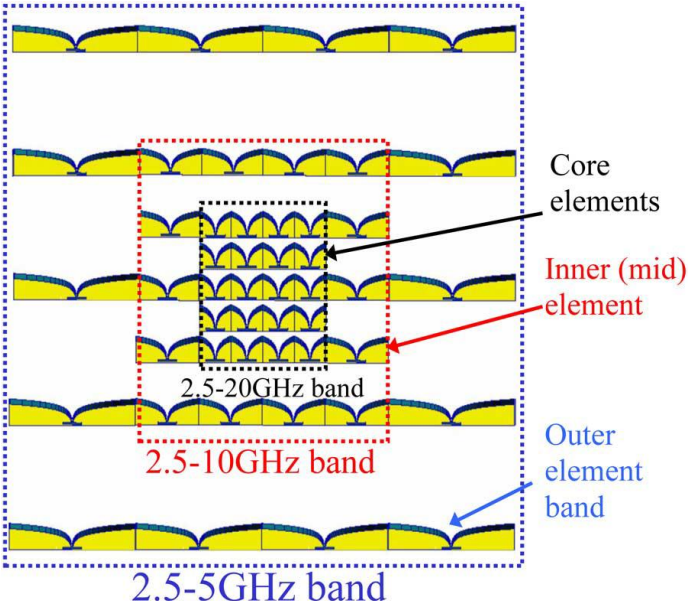

Figure 1.7 Variable size Vivaldi array operating in 2.5-20 GHz (From [5])

In addition to the previous study, wavelength scaled array with 1:8 bandwidth is also designed by Kindt, giving a constant beamwidth of 12 degrees [6]. The array has dual polarized flared notched elements with variable size. The array architecture is such that core region is in the corner rather than in the center as can be seen in Figure 1.8. Moreover this array's adjacent layer does not satisfy (1.1). As a result, it can be possible to design wavelength scaled arrays with arbitrary adjacent layers.

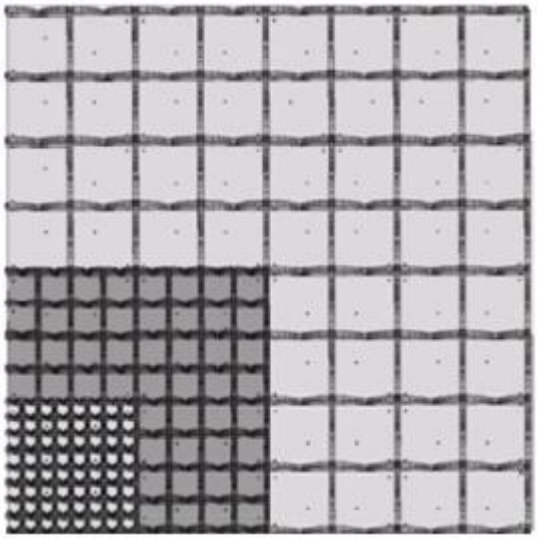

Figure 1.8 Architecture of wavelength scaled array (From [6])

In order to get frequency independent radiation from an array antenna, Hohlfeld and Cohen [7] also utilized the idea of changing active region with changing frequency as in the previous studies. According to their study, the concept of frequency independent phased arrays is very similar to the concept of frequency independent antennas.

They benefited from the studies of frequency-independent antennas carried out by Rumsey [7]. Sufficient conditions for frequency independence of antennas are showed in his study with definition of antenna geometry in terms of angles. The extension of this work was performed by Hohlfeld and Cohen. Properties of a frequency independent antenna are developed from symmetry properties of Maxwell's equations. As a result of the latter study the set of frequency independent antennas is extended. Moreover, Rumsey's Principle is demonstrated to be a subset of the overall properties which are required for frequency independence.

Hohlfeld and Cohen showed that radiating structure being both self-similar and origin symmetric, about a point is necessary and sufficient for frequency independence in their previous studies [8]. This symmetry point can be a feed point for the radiator because symmetry of the current distribution is mentioned.

Hohlfeld and Cohen use this principle (the HCR Principle) in the design of a planar array [7]. Antenna elements in array were placed in origin-symmetric pairs so that the conditions of the HCR Principle were satisfied at each stage of the construction. Some design objectives such as minimization of grating sidelobes in a sparse array was also aimed with the introduction of origin-symmetric antenna pairs. Arrays, designed with the HCR principle, consist of subarrays which are designed for a set of design frequencies. As a result, the same spatial frequency spectrum for all design frequencies could be maintained in this way.

Positions of each antenna element are optimized by using genetic algorithm [7]. Positions of half of the antenna elements were determined by the positions on the other half due to the symmetry principles existing in the HCR Principle. As a result, there were fewer bits in the genome encoding element positions in the phased array synthesized with HCR Principle. A planar array is synthesized for 2.5:1 band. Array consists of three regions

which are active at different frequency bands. Element locations in each region are optimized to give low sidelobes and independently from each other. The element positions were given on Figure 1.9.

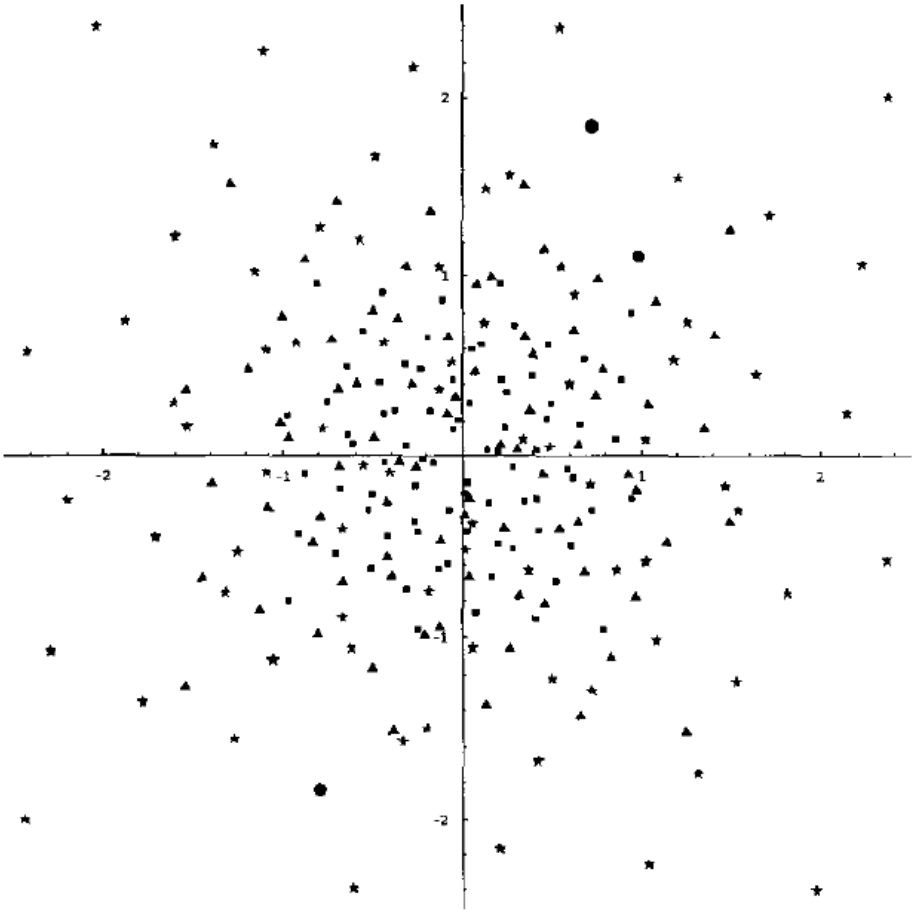

Figure 1.9 Frequency independent phased array constructed using the HCR Principle and using a genetic algorithm. Filled boxes represent high-frequency subarray, filled triangles represent middle-frequency subarray, and stars represent low-frequency subarray. Border frequencies are $2.5f_o$, $\sqrt{2.5}\,f_o$ and f_o (design frequency) (From [7]).

In the literature, other studies performed using genetic algorithm mainly focuses on optimization of side lobe levels of array with aperiodic spacing between elements for wideband operation. Micah D. Gregory and Douglas H. Werner studied the optimization of position of array elements to minimize sidelobe levels and have no grating lobes [9].

They can maintain low sidelobes for a linear array in 1:20 frequency band. Designed array is seen in Figure 1.10.

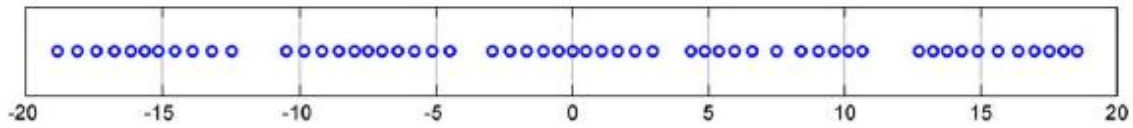

Figure 1.10 Locations in wavelengths (λ_0) (From [9])

Array in Figure 1.10 involves elements with spacing $0.5\lambda_0$ at minimum and $0.69\lambda_0$ at average. Array factor of this array at $20f_0$ has no grating lobes and sidelobe level nearly -15dB which is equal to sidelobe level at f_0. Array factor of linear array at f_0 and $20f_0$ can be seen in Figure 1.11 and Figure 1.12, respectively.

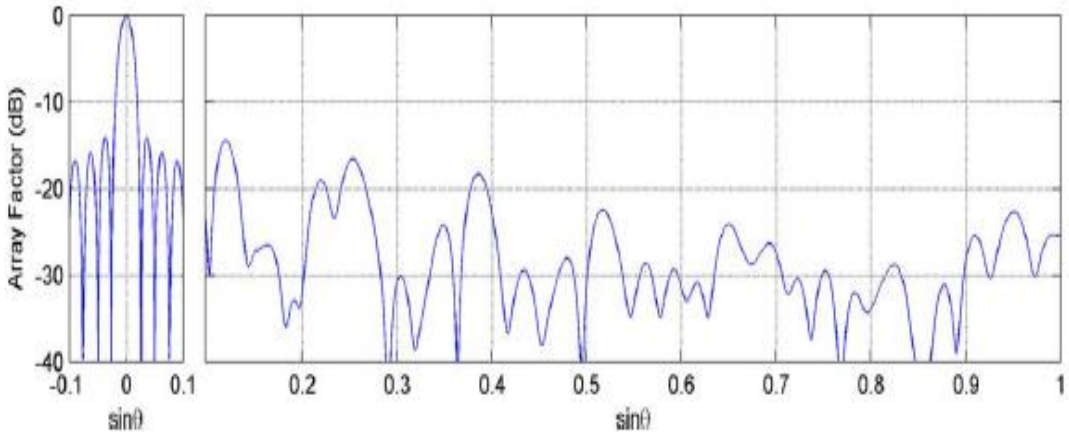

Figure 1.11 Array factor at f_0 (From [9])

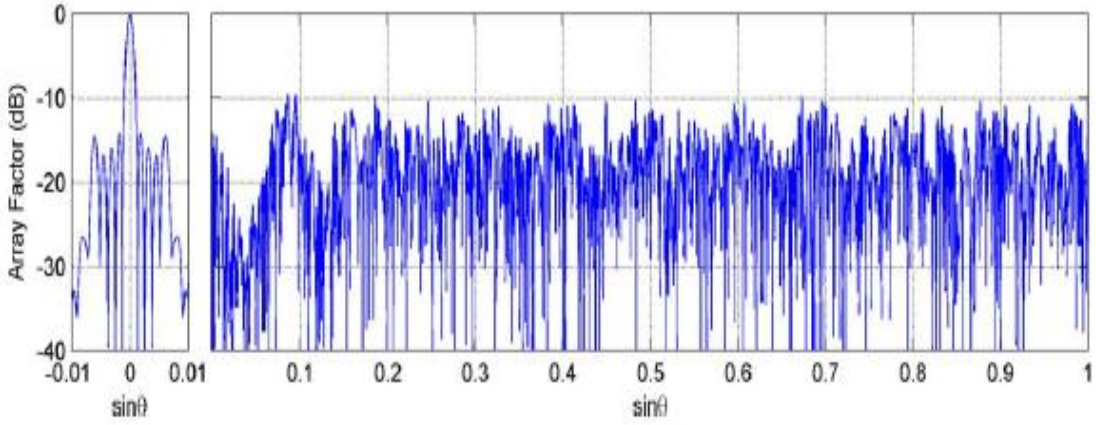

Figure 1.12 Array factor at $20f_0$ (From [9])

Ren et al. [10] performed sidelobe optimization with aperiodic spacing with a different approach, using Fourier Transform. By using Fourier transform and aperiodic lattice of elements with equal amplitude patterns like Chevbyshev are synthesized in this study. Such an example of a linear array with 23 elements is given in Figure 1.13.

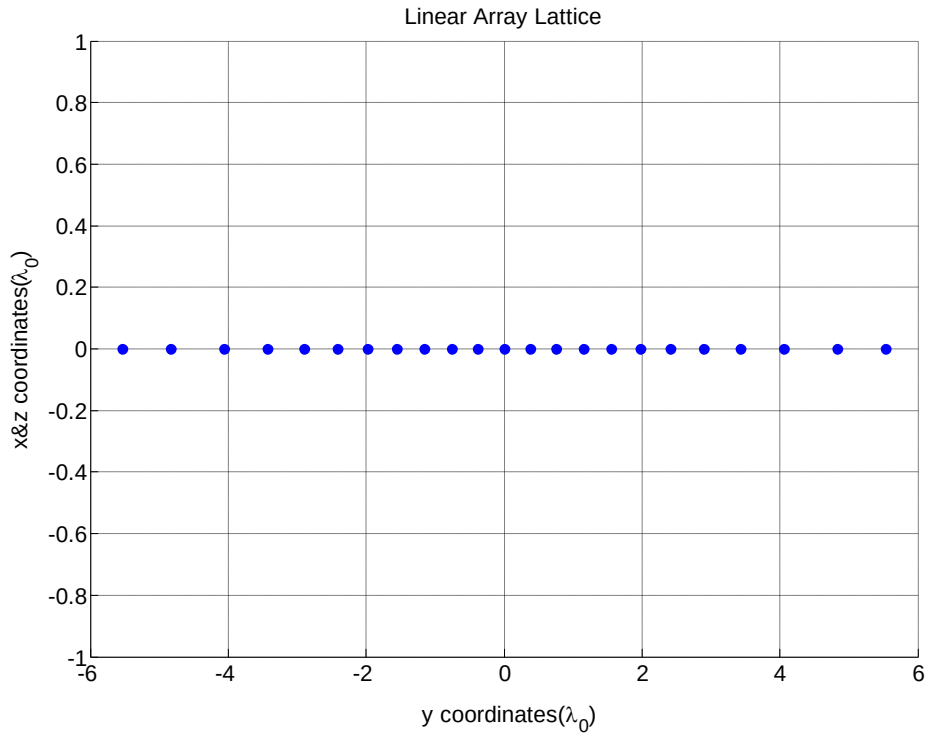

Figure 1.13 Linear array lattice (From [10])

All of elements seen in Figure 1.13 are with equal amplitude. The tapering along the array aperture is achieved by increasing the interelement spacing towards the edges of the array. As the interelement distance increases the amount of radiated power from a unit length decreases. This type of tapering is called spatial tapering. This array is designed to perform Chevbyshev pattern with equal sidelobe levels of -23 dB. Array factor of this array can be seen in Figure 1.14 at f_0 frequency.

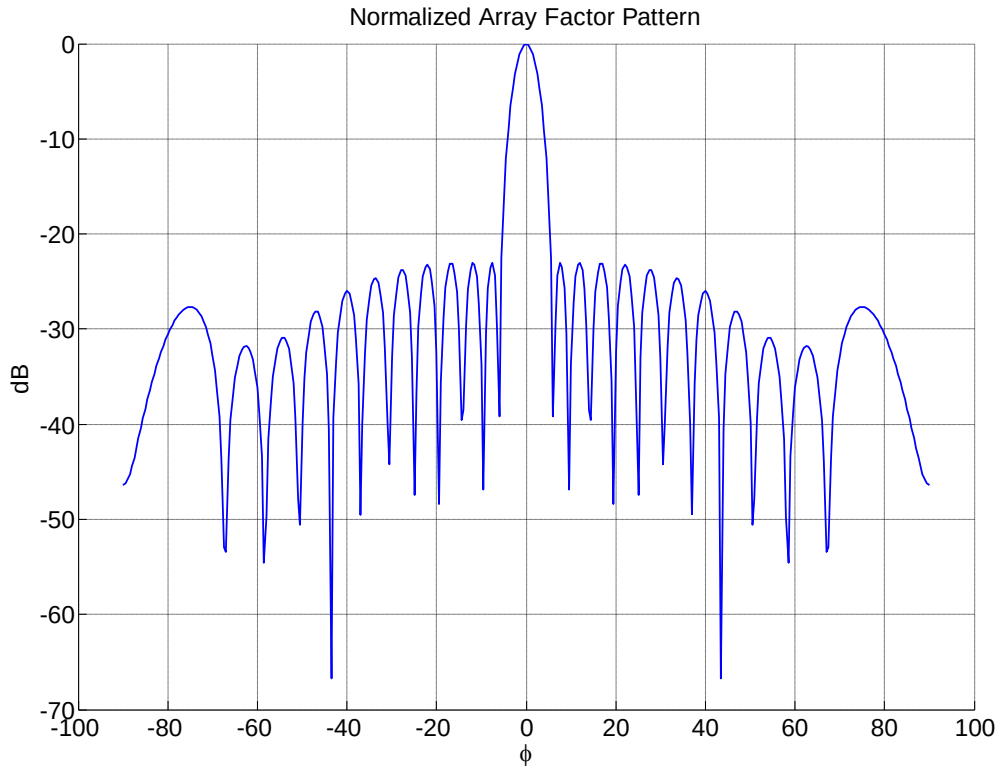

Figure 1.14 Array factor of the linear array seen in Figure 1.13 at f_0 frequency

Pattern seen in Figure 1.14, have low sidelobes under -23 dB. A number of lobes near mainlobe are nearly with equal amplitude as expected because of Chevbyshev pattern which is aimed to be synthesized. It is possible to have low sidelobes with aperiodic spacing, in other words, using space tapering.

A similar study is conducted by Milligan [11] for circular arrays. Array patterns with Taylor distributions are achieved in this study with uniform amplitude array elements. A planar array is formed by using a number of concentric circular arrays. The radius of each

circular array is determined from circular Taylor distribution in this study. The lattice of an array designed to give -30 dB Taylor distribution and consisting of 10 concentric rings can be seen in Figure 1.15.

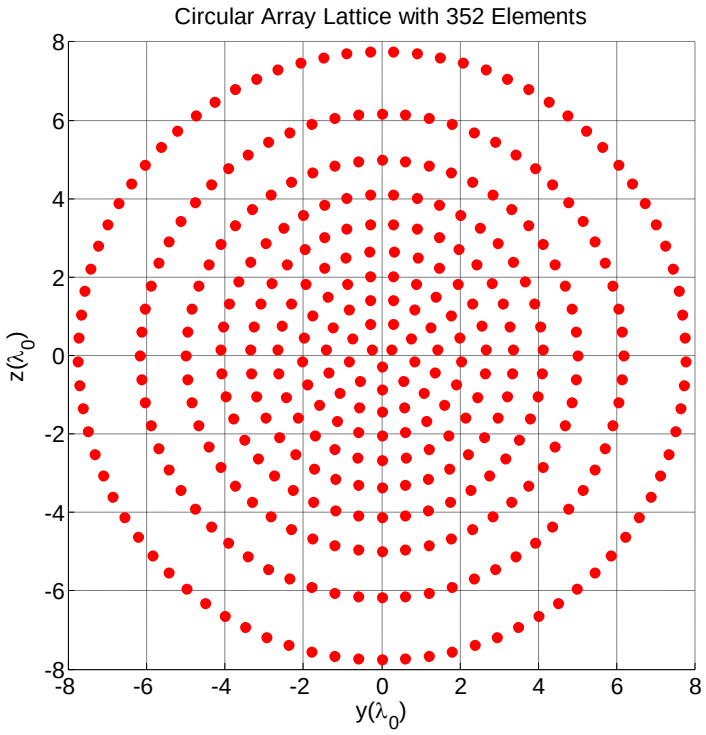

Figure 1.15 Circular array lattice designed to give -30 dB Taylor distribution (From [11])

The distance between adjacent radii of array increases as seen in Figure 1.15. Array lattice occupies an aperture of ±8λ at design frequency. Array factor of this array is given in Figure 1.16 for one of the major axis at f_0 design frequency.

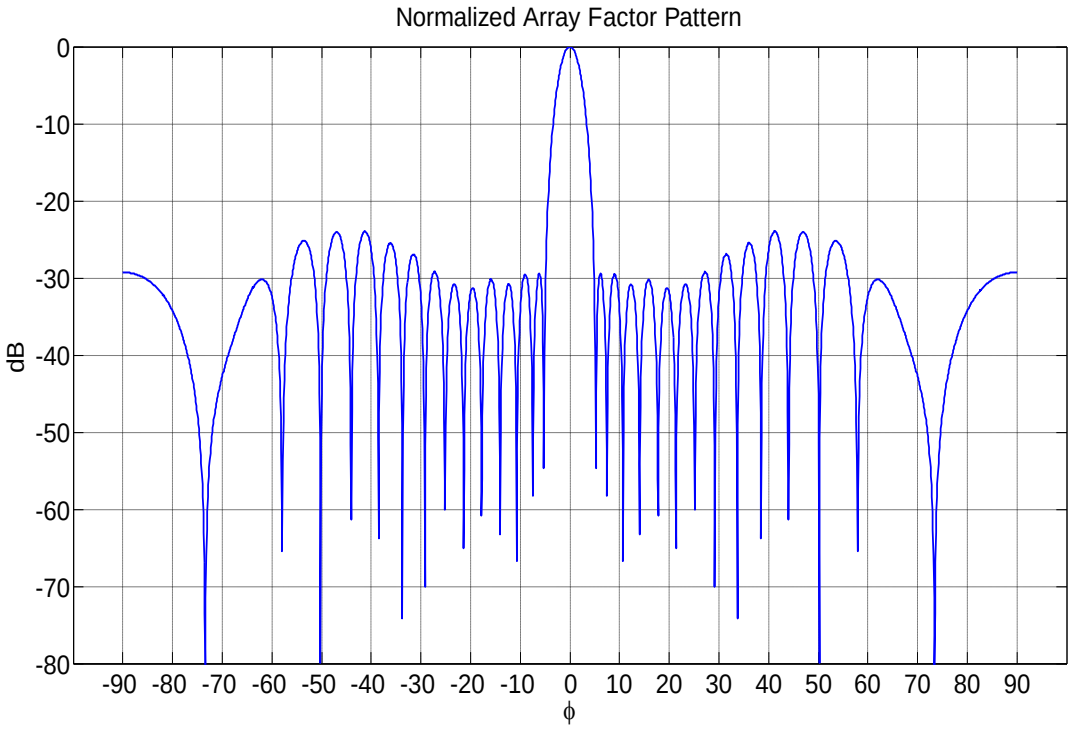

Figure 1.16 Array factor of the circular array designed to give -30 dB Taylor distribution

The pattern seen in Figure 1.16 satisfies -30 dB for a number of lobes near to mainlobe; however it can be higher for the angles over ±30º on that plane.

1.1 Objective of the Thesis

Up to now, some approaches for the design of wideband arrays are discussed. For the genetic optimization approach, array elements must be origin symmetric according to HCR principle. As a benefit of this principle, half of the array element positions can be optimized rather than all the element positions. For the wavelength scaled array approach, a lattice of elements as in Figure 1.5 can be utilized. Frequency independent radiation characteristic can be observed with this approach. Moreover, a drastic reduction in the number of elements in the array compared to conventional phased arrays can be attained. As a result, this research is devoted to design of wideband arrays with genetic optimization and wavelength scaled array concept.

In the second and third chapter of the thesis, the required numerical studies for the evaluation of the two mentioned frequency wideband array design techniques, i.e. genetic optimization and wavelength scaled array concept, are introduced. Moreover, arrays are designed for each approach with the help of numerical studies. The success of each technique is evaluated. In the fourth chapter, realization of a linear array with changing active region is discussed. A linear array with Vivaldi elements is designed and manufactured. Array performance is investigated with changing active region of the array with frequency. Performance of this array in simulation and measurements are also compared.

1.2 Thesis Outline

This thesis includes 5 chapters as the following:

Chapter 2 provides an introduction to the design of arrays using genetic algorithm. Steps in the algorithm are explained. Studies include the optimization of sidelobe levels and beamwidth for aperiodic arrays with linear and circular lattice. Results for the linear and circular arrays designed using genetic algorithm are presented and compared with the results found in literature. Evaluation of this technique has been made in this chapter.

In Chapter 3, the introduction of the GUI (Graphical User Interface) [12] that was utilized for the examination of properties of the arrays designed with wavelength scaled array concept is provided. Wavelength scaled array concept is investigated in details for some crucial parameters of array antennas, such as, bandwidth of the array, number of elements and beamwidth. Comparison of the designed wavelength scaled arrays with conventional arrays is the main concern in this chapter.

Chapter 4 covers the realization of a linear array with changing active region. Characterization of the designed feed network for such a realization is performed. The effects of switching on the performance of a manufactured linear array with Vivaldi elements are investigated. Comparison of the measured and simulated results of the array is included in Chapter 4. The evaluation of this array in terms of the desired frequency independent radiation characteristics is the scope of this chapter.

Finally, in Chapter 5, conclusions of this thesis work are provided with the suggested future works.

CHAPTER 2

GENETIC ALGORITHM APPROACH FOR THE DESIGN OF WIDEBAND ARRAYS

In this chapter of the thesis, one of the wideband array design techniques, namely genetic algorithm, is introduced. The technique is explained step by step manner. Element positions are optimized in order to optimize sidelobe level and beamwidth of array factor patterns for linear and circular array whose elements are uniformly excited. The positions of the elements are set to be origin symmetric with the application of the HCR principle [7]. After explanation of this method, results of linear and circular arrays which are designed within this study are given in this chapter. Finally, success of this technique in wideband array design is discussed.

2.1 Array Design Using Genetic Algorithm

The positions of the array elements are determined by genetic algorithm in MATLAB® [13]. Position vector representing one of the linear arrays in the genetic optimization is called an individual. Individuals are represented as binary numbers consisting of '1' and '0'. This binary string can be called a genome. Element positions in an array are set to specific values according to binary numbers in the individual. Therefore, an individual represents one of the linear arrays in the optimization. The optimization includes a set of individuals that can be called population. The success of each individual in terms of its closeness to the desired characteristics in the population is called as the fitness of that individual.

The optimization starts with a specified number of individuals, namely population density. Individuals are randomly organized initially, i.e. positions of '1' and '0's in the

individuals are distributed randomly. The optimization is performed iteratively. The fitness of each individual is calculated at the end of the each iteration. Then, individuals are sorted according to their fitness. This sorting procedure can be regarded as ordering them from healthiest to weakest. New individuals in the population are generated. These new individuals are called children and the individuals contributing some parts of children are called as parents. First and the second parent's genome are separated at the same position and the resultant parts of first genome are combined with the corresponding parts of the second genome. This is called as crossover and demonstrated in Figure 2.1.

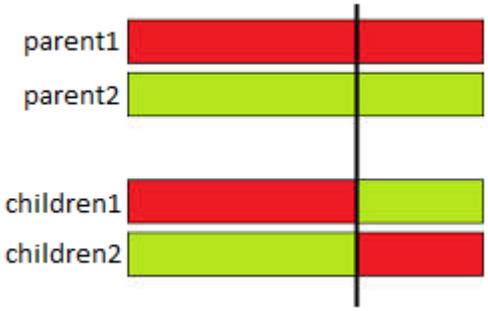

Figure 2.1 Crossover procedure in genetic algorithm

There is also mutation in individuals in order to increase variety in the population before crossover. To realize mutations, there are some parameters such as probability of mutation and randomly selected individuals exist in the optimization. Randomly selected bits of randomly selected individuals are mutated, i.e. some bits of randomly chosen individuals are changed from 0 to 1 or 1 to 0 to maintain mutation in the population. Mutation is a key factor that can protect genetic algorithm against stacking in poor local solutions.

The health of each individual is the factor that increases the probability of selection for the generation of children. Roulette wheel selection strategy is utilized in selection of parents to produce children. The number of individuals in the population throughout the optimization is protected, so weak individuals are replaced by children at each iteration of the optimization. After generation of children, fitness of the new population is evaluated. If the best or the least error in the current generation satisfies the design goal or error

criteria, algorithm stops. Otherwise, iterations continue until desired error level is satisfied or the maximum number of iterations is reached in the algorithm. The flowchart of genetic algorithm can be seen in Figure 2.2.

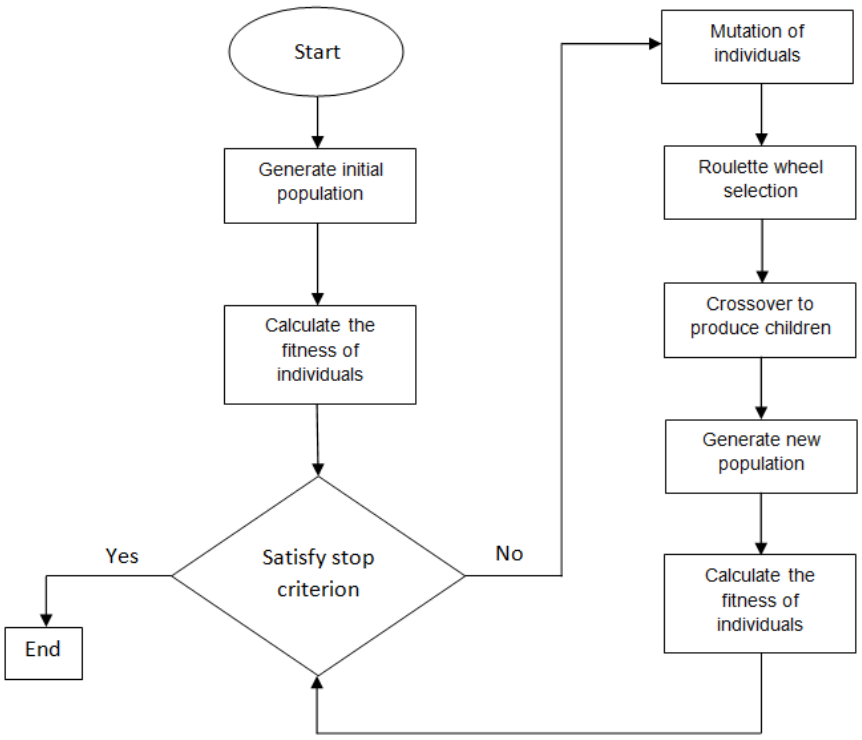

Figure 2.2 Flowchart of genetic algorithm

In the next sections of this chapter, sidelobe level optimization is performed for linear and circular arrays with the algorithm whose flowchart is given in Figure 2.2.

2.2 Sidelobe Level Optimization

In order to optimize sidelobe level of array factor patterns, some genetic algorithms are performed. The first optimization is started to determine the positions of a linear array whose all elements are equally excited. Number of elements is set to 23 in order to design linear arrays as in Figure 1.13. All the elements are located in ±y direction. They are confined within ±8λ aperture at the design frequency. An element can be any position on ±8λ aperture. In the algorithm, minimum difference in spacing between adjacent elements is set to 0.375λ as in Figure 1.13. Individuals not obeying this distance setting give an

error so that they are forced to be unfit in the population. Position of each element is represented by 9 bits. An element of the array is located at origin for the entire array generated in this algorithm. Only positions of 11 elements are optimized so that arrays with 23 elements are designed by symmetry condition with respect to origin. Results of this study are compared with the results of study conducted by Ren et al. [10]. Sidelobe level of each individual is desired to be -23 dB as in mentioned study and that's the second error criterion in this algorithm. Optimization started with 500 individuals and stopped after 1000 iterations. Element positions of the array for the fittest individual in genetic algorithm and the array in Figure 1.13 can be seen in Figure 2.3. Sidelobe of both arrays are compared in terms of their maximum value and wideband behavior.

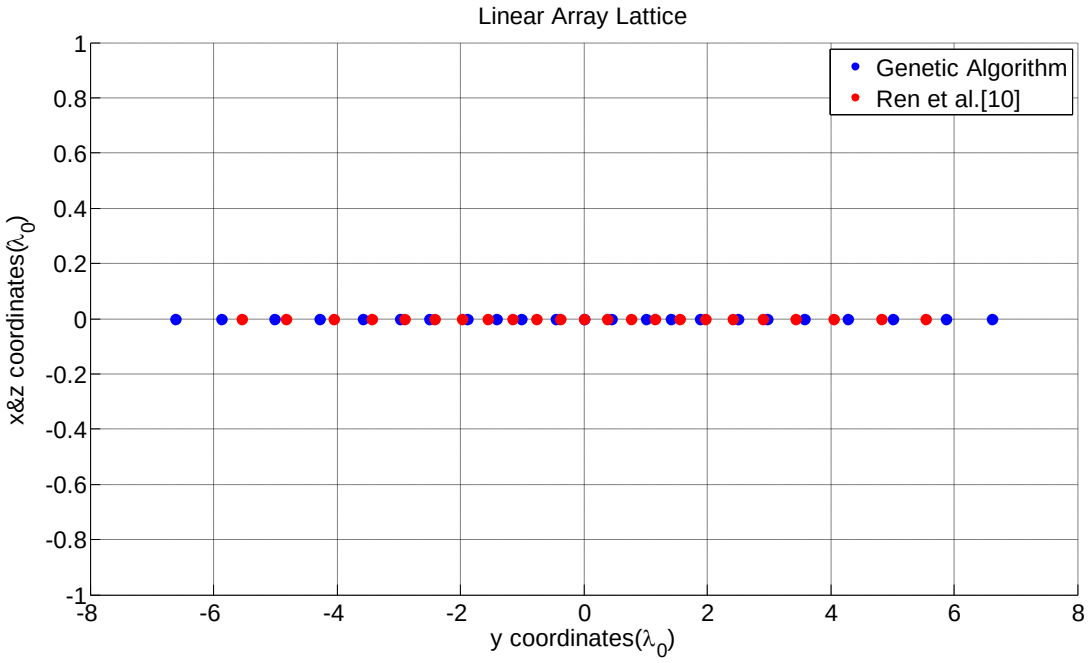

Figure 2.3 Positions of elements designed by genetic algorithm and Ren et al. [10]

Positions found by genetic algorithm occupy wider aperture. Array factor at the frequency of f_0 can be seen in Figure 2.4.

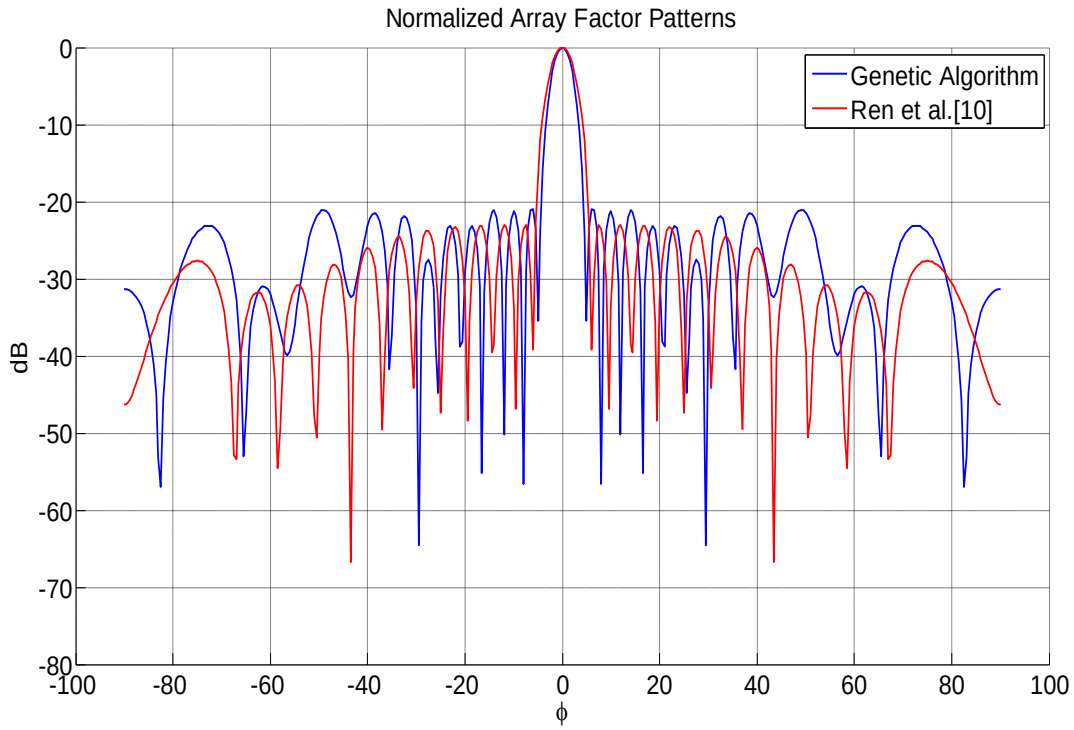

Figure 2.4 Normalized array patterns generated by genetic algorithm and Ren et al. [10]

As can be seen in Figure 2.4, pattern generated by genetic algorithm has higher sidelobes. As a result, sidelobe levels under -23 dB cannot be achieved due to difference in element positions designed by genetic algorithm and the mentioned study. Two element distributions are also investigated in terms of sidelobes in wider frequency bands. For frequencies lower than f_0, sidelobes are not higher than sidelobes at f_0 frequency. However, as the frequency increases sidelobes begin to increase. This behavior can also be seen in Figure 2.5 and Figure 2.6 for the array generated by genetic algorithm.

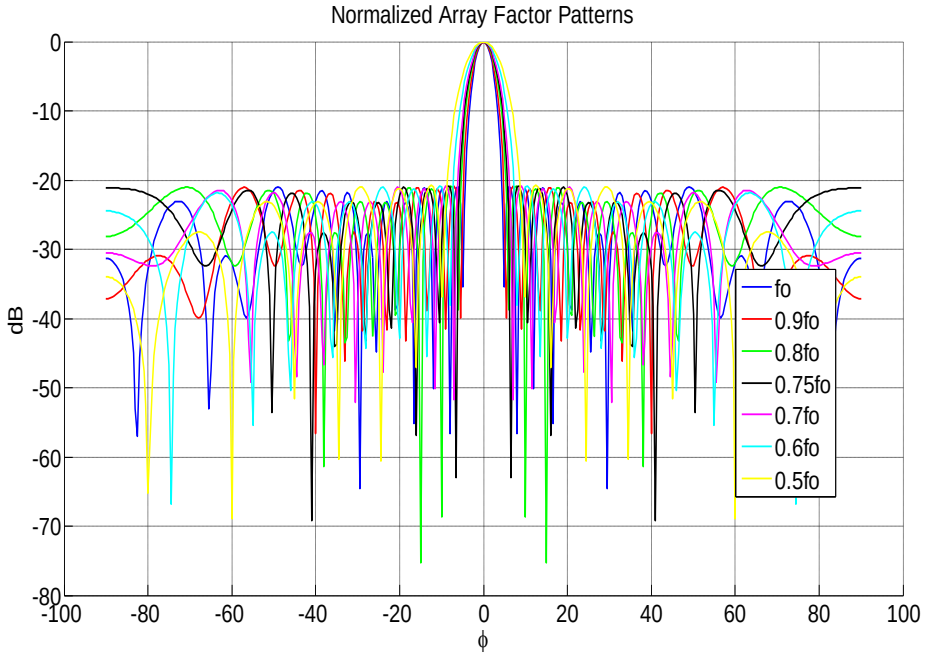

Figure 2.5 Normalized array patterns for the array generated by genetic algorithm for frequencies lower than f_0

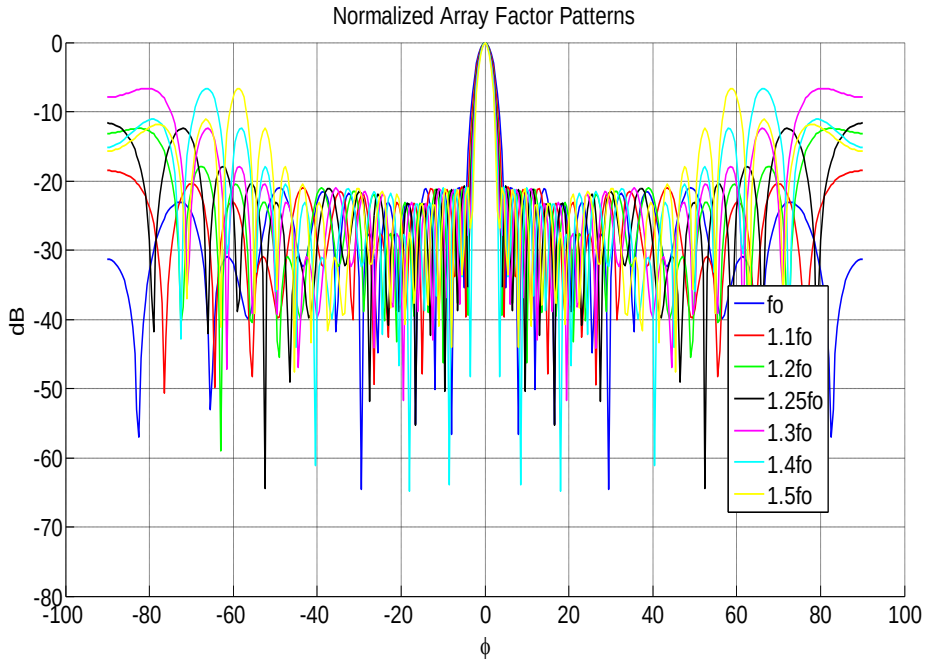

Figure 2.6 Normalized array patterns for the array generated by genetic algorithm for frequencies higher than f_0

Sidelobes in Figure 2.6 are higher than -10 dB for the frequencies higher than $1.25f_0$. However for the array designed by Ren et al. [10], sidelobe for higher frequencies are lower than -10 dB as in Figure 2.8. Similarly, sidelobes are not higher than sidelobes at f_0 frequency for this array, for the frequencies below f_0 as in Figure 2.7.

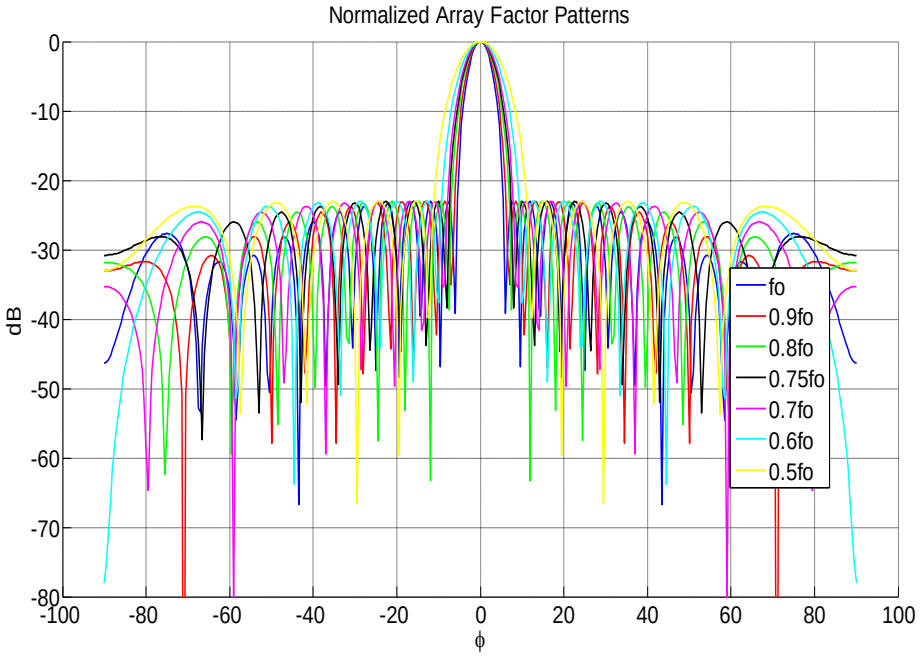

Figure 2.7 Normalized array patterns for the array in the study conducted by Ren et al. [10] for frequencies below f_0

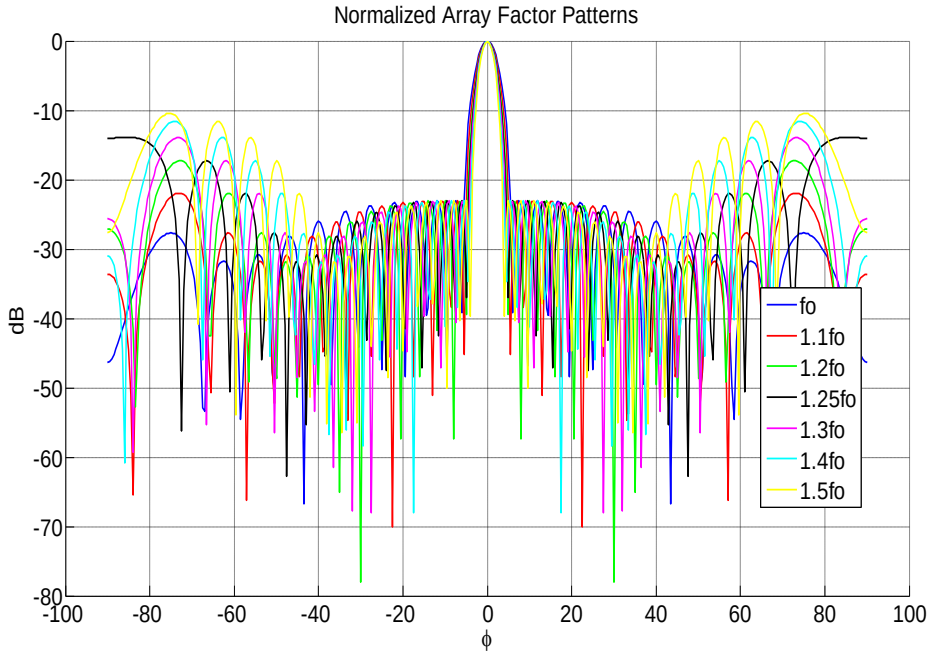

Figure 2.8 Normalized array patterns for the array in the study conducted by Ren et al. [10] for frequencies over f_0

Up to now, it is seen that sidelobes for the array designed by genetic algorithm are higher than that of the mentioned study at f_0 frequency and higher frequencies. This is mainly due to algorithm used in element positioning of the designed arrays by genetic algorithm. For the first optimization, elements can be on anywhere in $\pm 8\lambda$ region at f_0. As a result of this algorithm, difference between adjacent element positions can decrease or increase. However, in the study of Ren et al. [10], distance between adjacent elements mostly increases as the distance increases from the origin as seen in Figure 2.3. From this observation, algorithm used in element positioning in genetic algorithm is changed to give increasing distance between adjacent elements in the array. This is beneficial in terms of narrowing the search space of the algorithm, in other words, finding better solutions with genetic algorithm. After this change in the algorithm, second optimization is started for the problem with same settings such as minimum 0.375λ spacing requirement between adjacent elements, existence of 23 elements in array design, and -23 dB sidelobe level requirement (only error criterion in genetic algorithm). However, designed arrays are not confined in $\pm 8\lambda$ region as in the previous algorithm. This

optimization is also started with 500 individuals and stopped after 1000 iterations. Positions of the fittest individual in genetic algorithm and the array designed by Ren et al. [10] can be seen in Figure 2.9.

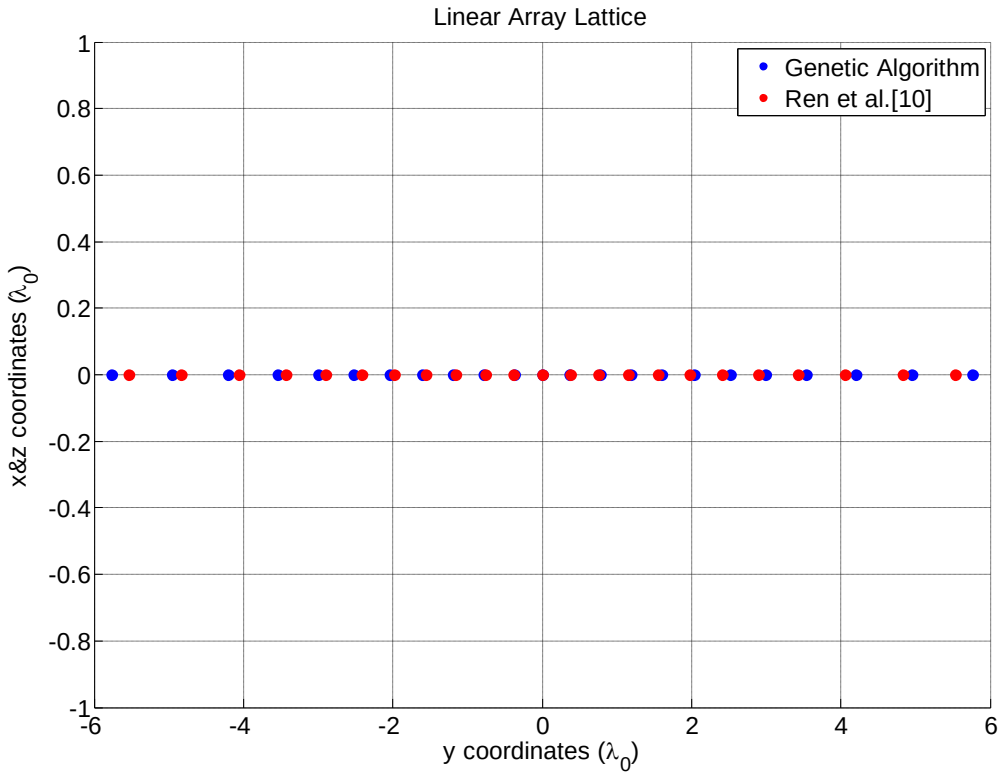

Figure 2.9 Positions of elements designed by second optimization and Ren et al. [10]

The positions of elements for both designed array are very close as in Figure 2.9. Array factor of these arrays can be seen in Figure 2.10.

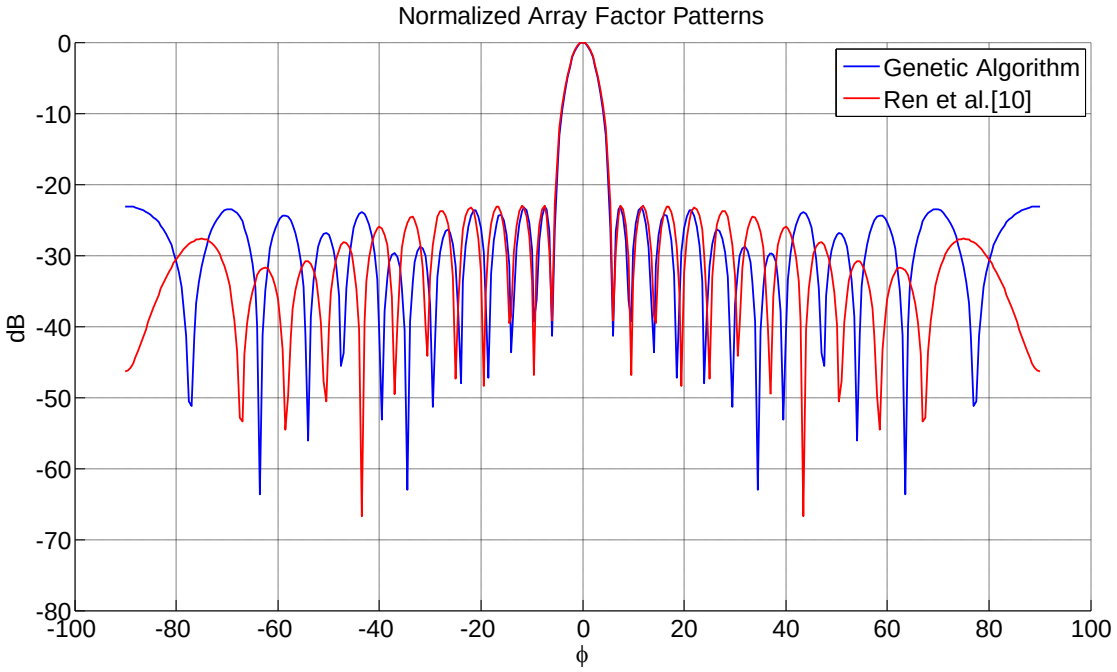

Figure 2.10 Normalized array patterns generated by second algorithm and Ren et al. [10]

Both arrays have nearly the same sidelobe levels at f_0 frequency. Then it is necessary to investigate sidelobe levels of the array designed by second algorithm in wideband to make a better comparison with the study of Ren et al. [10]. Array factors of designed array in low and high band can be seen in Figure 2.11 and Figure 2.12 respectively.

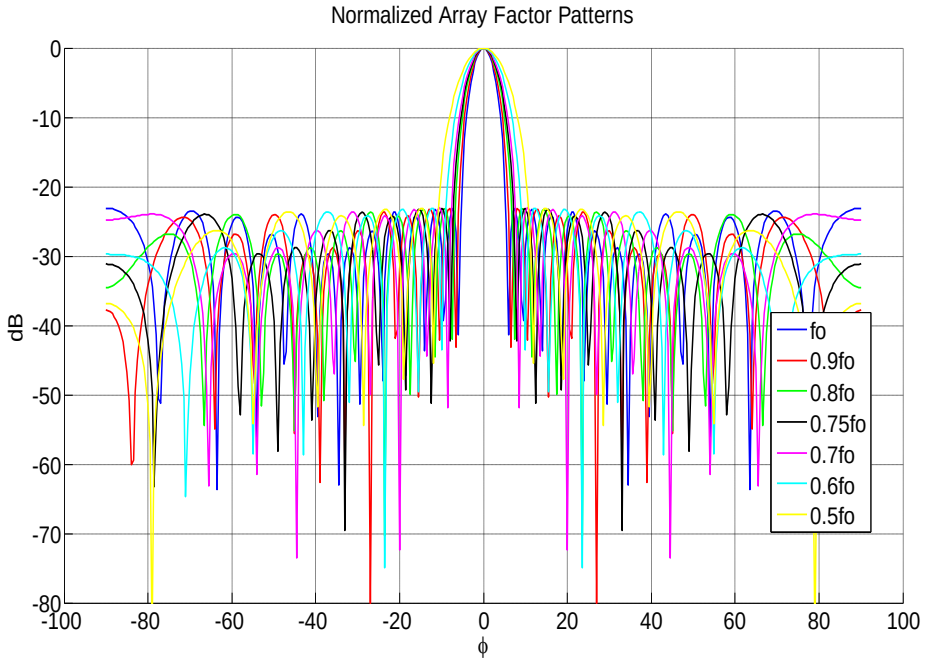

Figure 2.11 Normalized array patterns for the array generated by second algorithm in low band

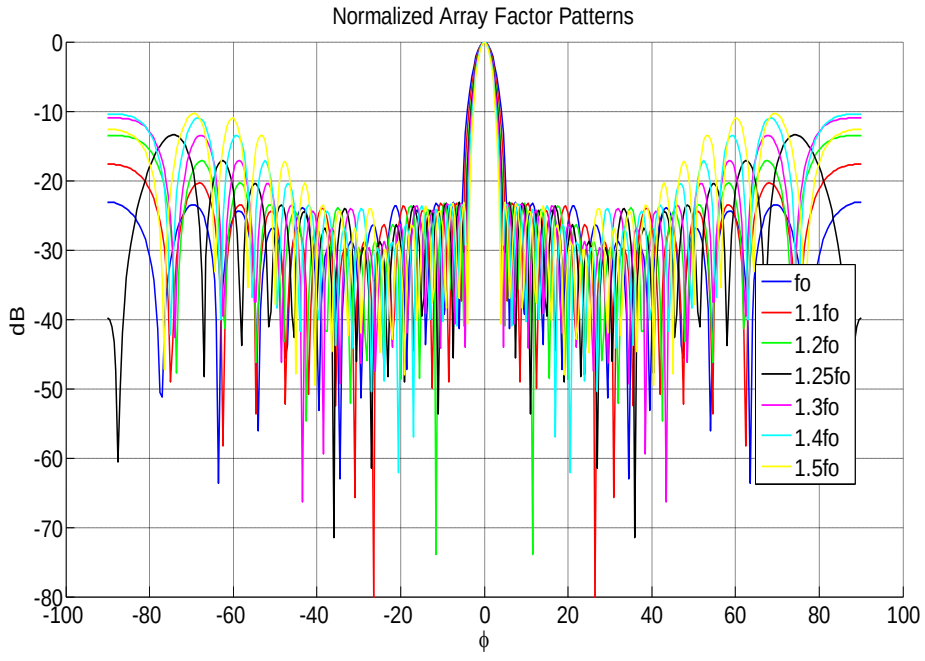

Figure 2.12 Normalized array patterns for the array generated by second algorithm in high band

As can be seen in Figure 2.8 and Figure 2.12 both arrays have nearly the same performance in $0.5f_0$-$1.5f_0$ band. It is seen that second algorithm in which adjacent element spacing is increasing with increasing distance with respect to origin is more suitable than the first one for sidelobe optimization of arrays both for the design frequency and wideband operation.

After the algorithm for element positioning is determined, same genetic algorithm is used for different minimum element spacing between adjacent elements. For this case, the mentioned setting is 0.5λ. The positions of elements of the fittest individual after 1000 iterations of this algorithm can be seen in Figure 2.13.

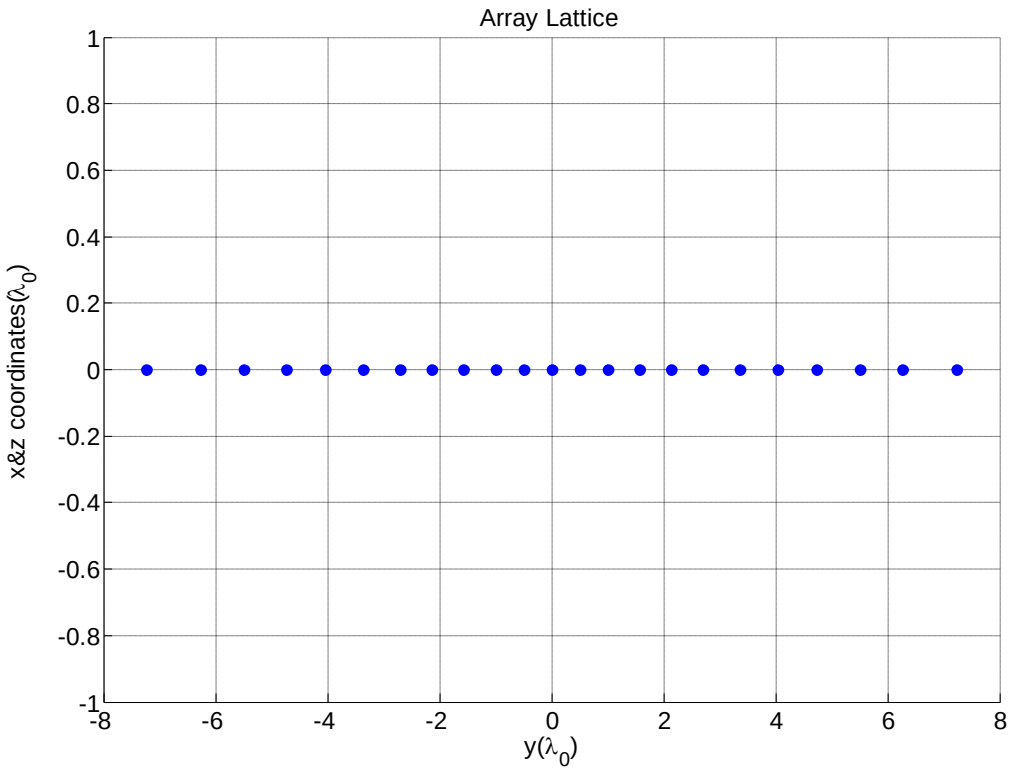

Figure 2.13 Positions of elements designed by second optimization with minimum adjacent element spacing of 0.5λ

Elements of the array exceeds ±6λ region at the design frequency of f_0 with the mentioned setting as can seen in Figure 2.13. Array factor of designed array in low and high band can be seen in Figure 2.14 and Figure 2.15 respectively.

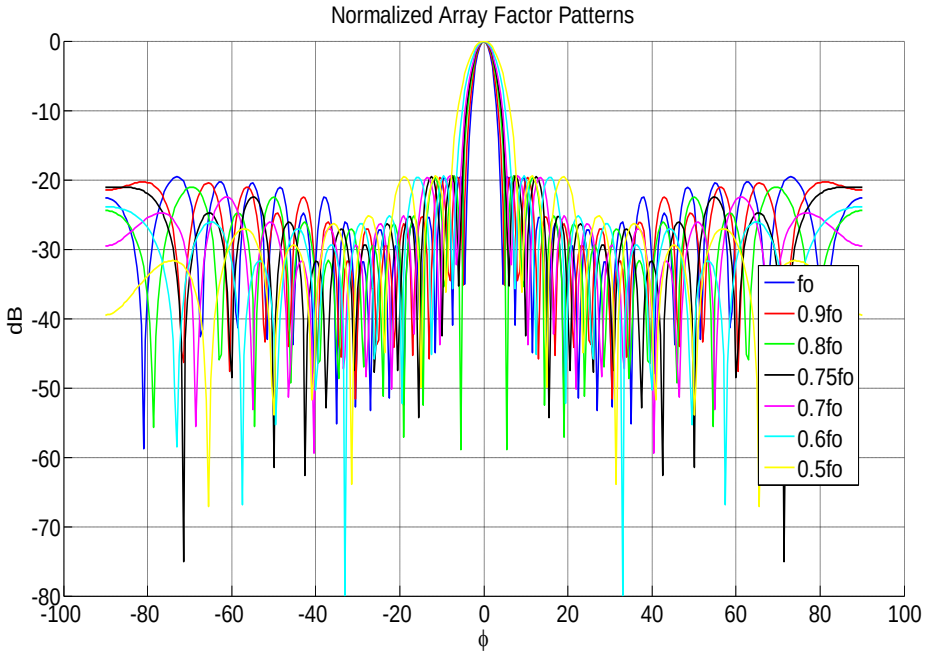

Figure 2.14 Normalized array patterns for the array generated by second algorithm with minimum adjacent element spacing of 0.5λ for low band

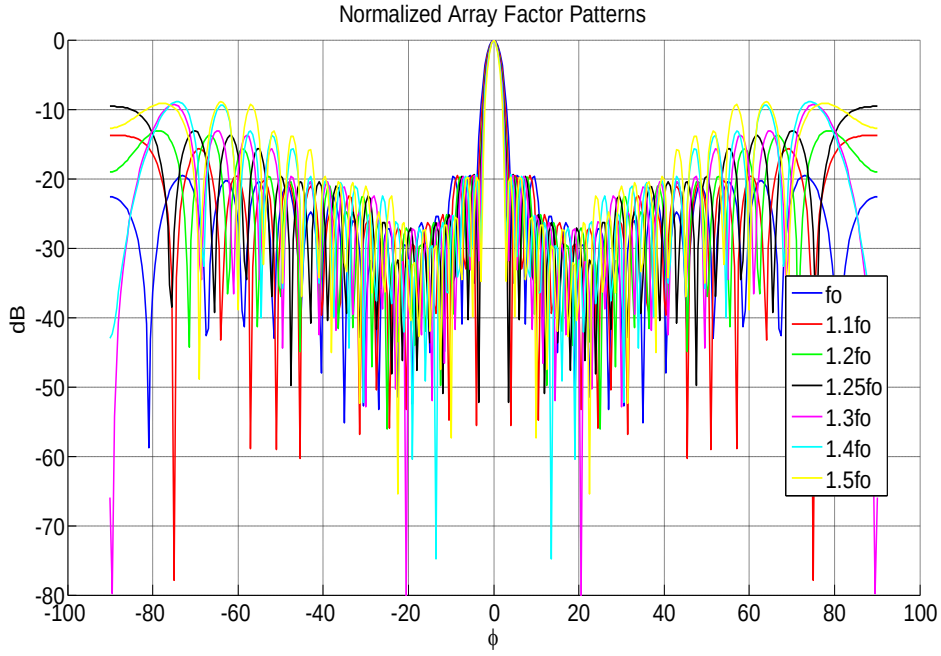

Figure 2.15 Normalized array patterns for the array generated by second algorithm with minimum adjacent element spacing of 0.5λ for high band

Sidelobe of array patterns for the low band are higher than that of second algorithm with minimum adjacent element spacing of 0.375λ. Sidelobe level for this array at high band is also higher. As a result, changing minimum adjacent element spacing to 0.5λ lowers the sidelobe performance of the array.

For the high band, whatever minimum adjacent element spacing setting is, sidelobe level increases with increasing frequency as seen in Figure 2.8, Figure 2.12 and Figure 2.15. In order to increase this sidelobe performance at high frequencies, error criterion in second algorithm is changed. Sidelobe level difference from the desired value at frequencies f_0 and $1.5f_0$ are included in error criterion with the mentioned change. Error weights of sidelobe level error for both frequencies are defined as the same. Minimum adjacent element spacing for this algorithm is set as 0.375λ. Array lattices of elements of the fittest individual of this algorithm with modified error criterion and with previous error criterion are given in Figure 2.16.

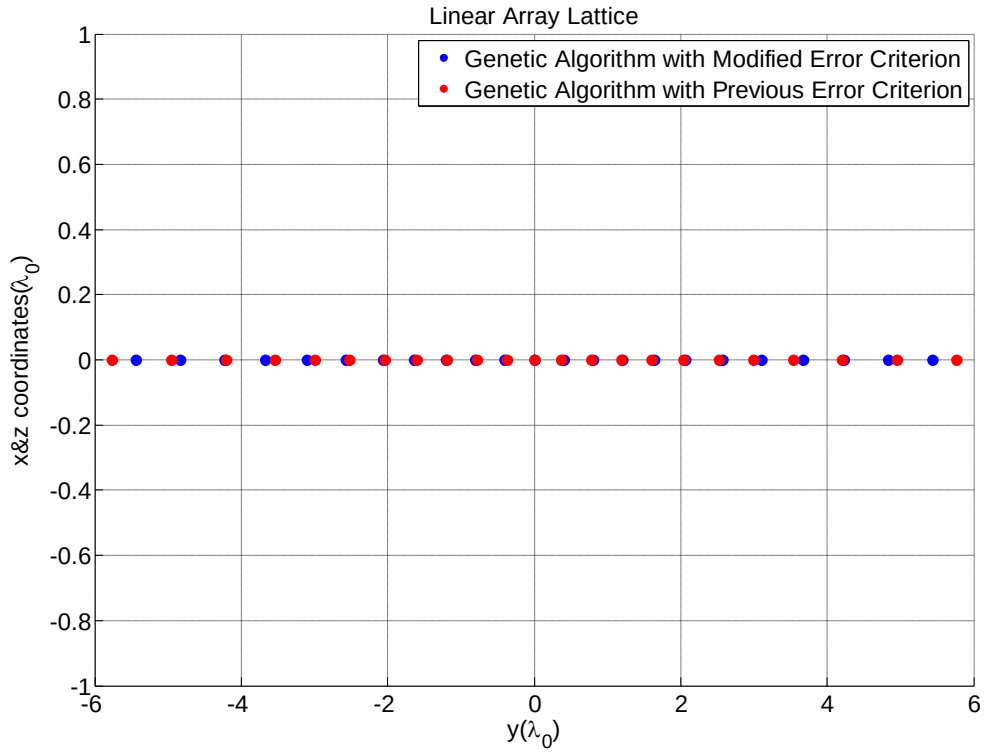

Figure 2.16 Positions of elements designed by the algorithm with modified error criterion and previous error criterion

With modified error criterion, length of the array becomes shorter with respect to array designed by algorithm with previous error criterion as in Figure 2.16. Array patterns of this array for low and high frequencies can be seen in Figure 2.18 and Figure 2.18. With this modification on error criterion in the algorithm, sidelobe level at f_0 increases from -23 dB to -18.5 dB. However, maximum sidelobe level of array factor for this array remains the same for low and high frequencies. As a result, sidelobe level remains nearly constant for wider frequency operation with such a modification in algorithm.

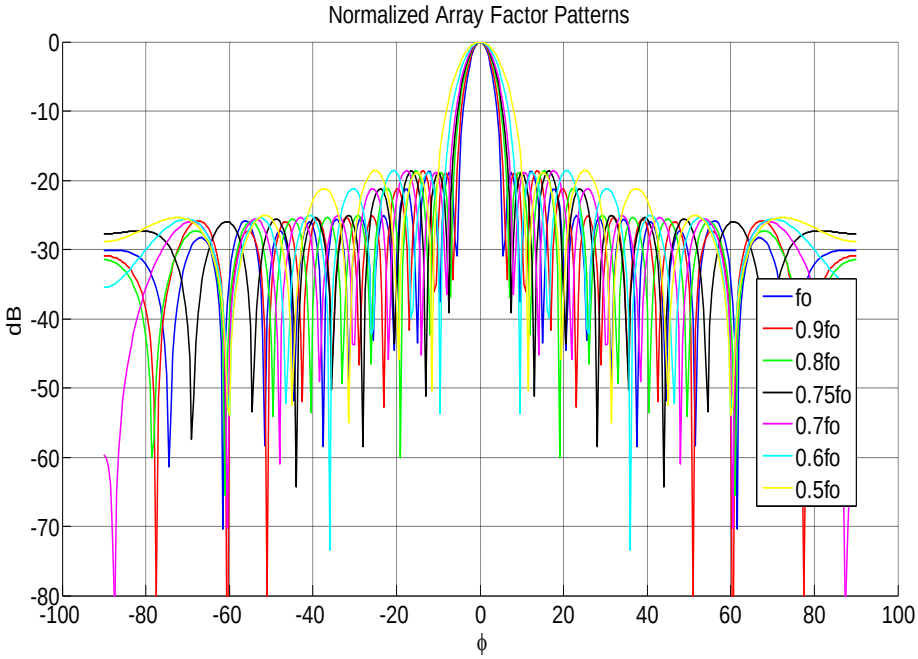

Figure 2.17 Normalized array patterns for the array generated by second algorithm with modified error criterion in low band

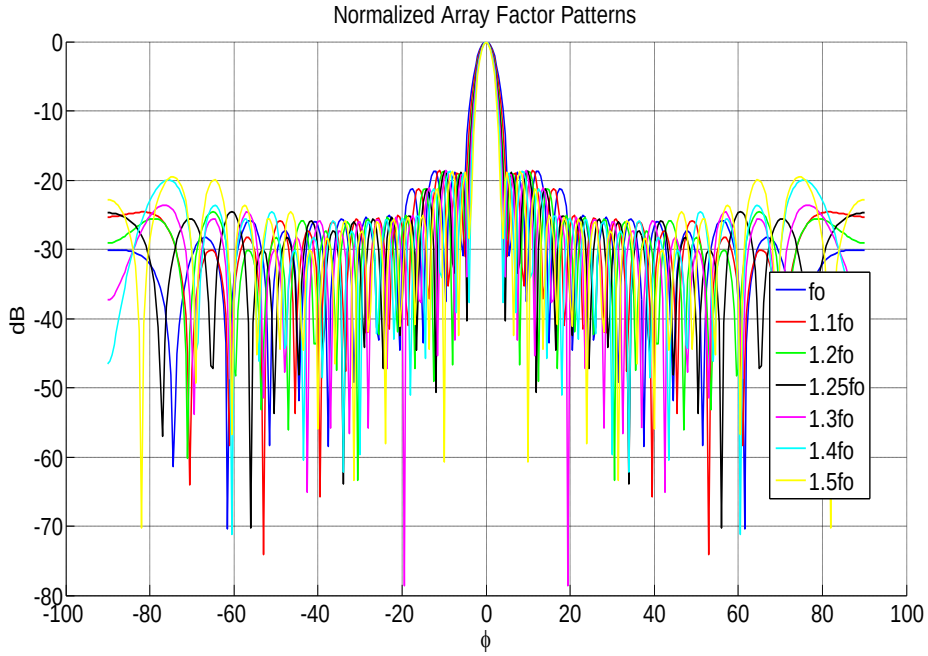

Figure 2.18 Normalized array patterns for the array generated by second algorithm with modified error criterion in high band

Same algorithm is also used with a change in minimum adjacent element spacing. This variable is set as 0.5λ rather than 0.375λ. After this change, an array in Figure 2.19 is generated.

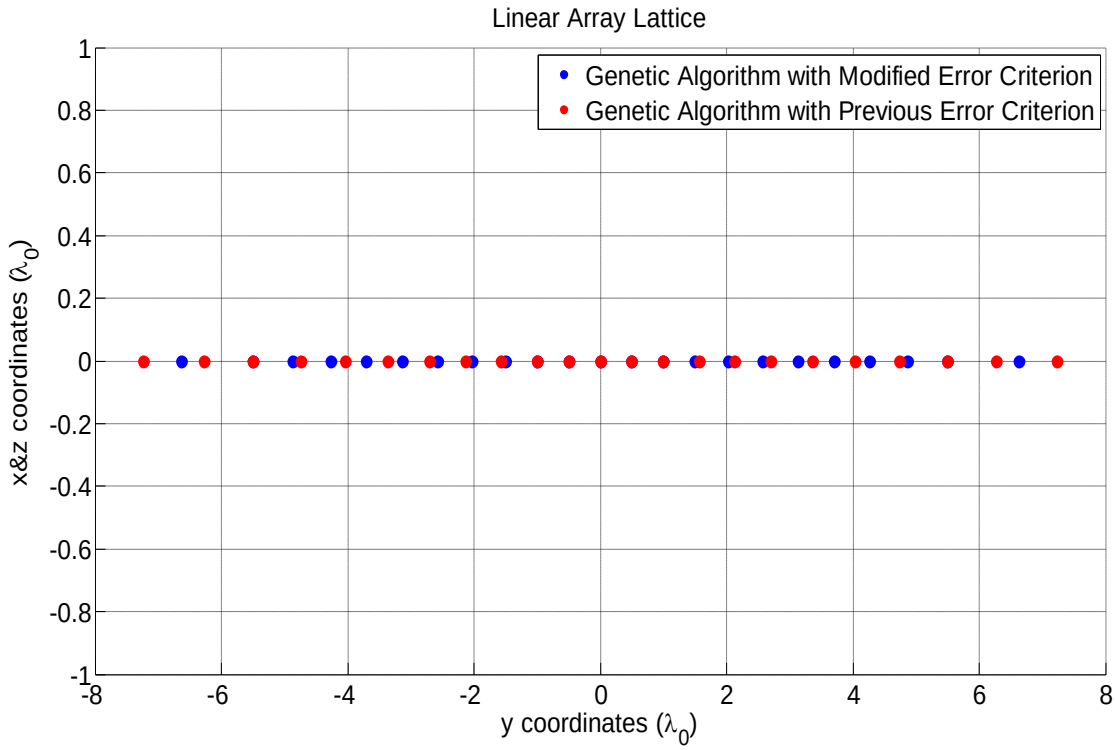

Figure 2.19 Array lattice created by algorithm with modified and previous error criterion for minimum adjacent element spacing of 0.5λ

For minimum adjacent spacing of 0.5λ, length of the array again becomes shorter with modified error algorithm as in Figure 2.19. Array factors of this designed array in low and high band can be seen in Figure 2.20 and Figure 2.21 respectively.

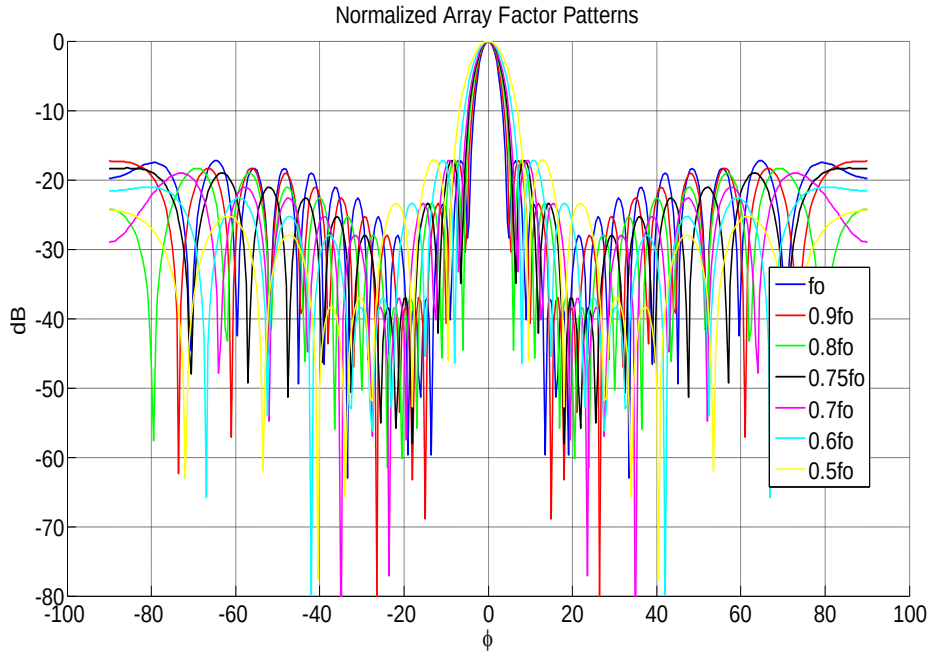

Figure 2.20 Normalized array patterns for the array generated by second algorithm with modified error criterion and minimum adjacent element spacing of 0.5λ in low band

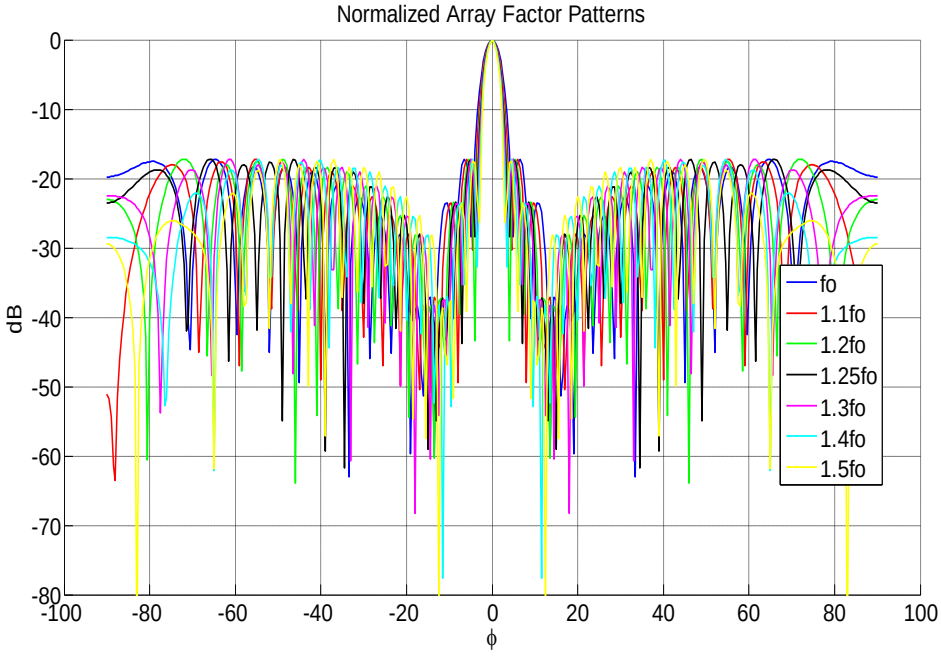

Figure 2.21 Normalized array patterns for the array generated by second algorithm with modified error criterion and minimum adjacent element spacing of 0.5λ in high band

For the mentioned changes in error criterion of the algorithm and minimum adjacent element spacing sidelobe level increases to -17 dB at f_0. However, error criterion change results in an increase of nearly 2 dB for this minimum element spacing setting as can been from Figure 2.14 and Figure 2.20. These levels for sidelobe also remain constant for wide frequencies. In other words, array factors seen in Figure 2.18 and Figure 2.21 have low sidelobe levels for wide frequency bands. Up to now, studies show that linear arrays can be designed using genetic algorithm with low sidelobe levels -23 dB at one frequency and -18 dB for a wideband frequency region.

Planar arrays nearly 400 elements were also studied with genetic algorithm. However, they couldn't give low sidelobe levels such as -18 dB. This was due to the fact that finding the solution space for such a problem becomes harder when the number of variables in the problem increases. Similarly, genome vector representing a planar array with 400 elements become very long and this results in a dramatic increase of varieties that genome can have. Those facts also force the solution for an iteration of the algorithm to take long time. On the other hand, planar arrays can be formed extending the lattices found for linear arrays to the z direction and these arrays can also give low sidelobes in three dimensional space. Such an array is formed from the linear lattice shown in Figure 2.16 which found by genetic algorithm with a modified error criterion to satisfy wideband sidelobe level condition. Planar array that is formed from this linear array can be seen in Figure 2.22.

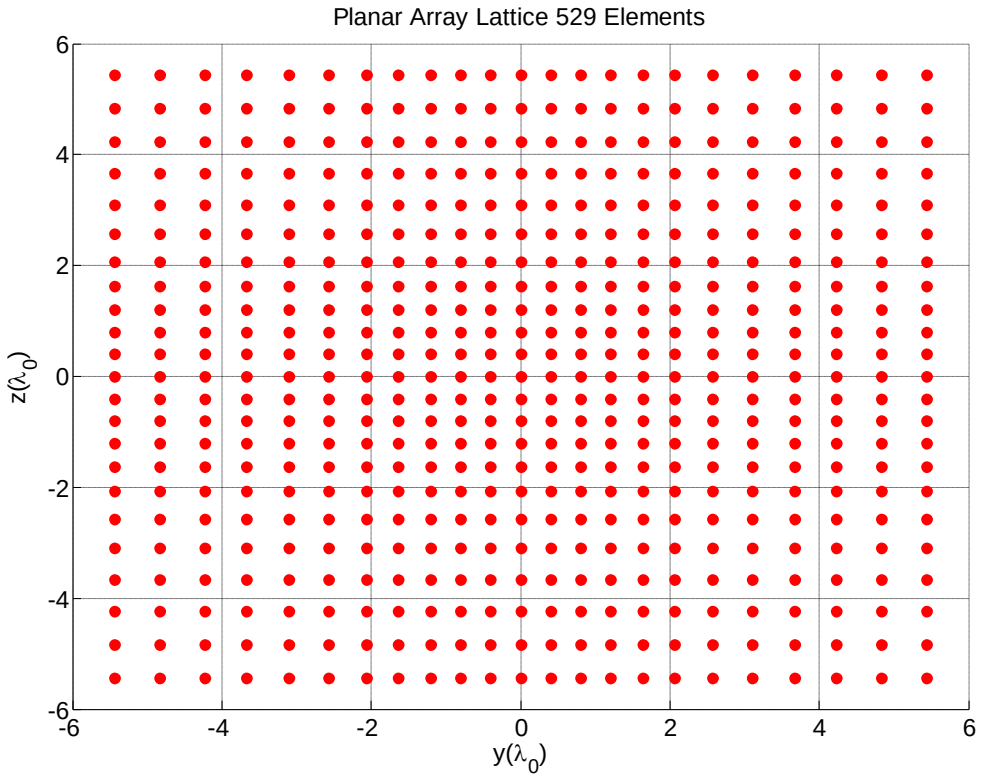

Figure 2.22 Planar array which is formed by extension of linear array to z direction

Planar array seen in Figure 2.22 has a square lattice. Array factor of this array can be seen in Figure 2.23.

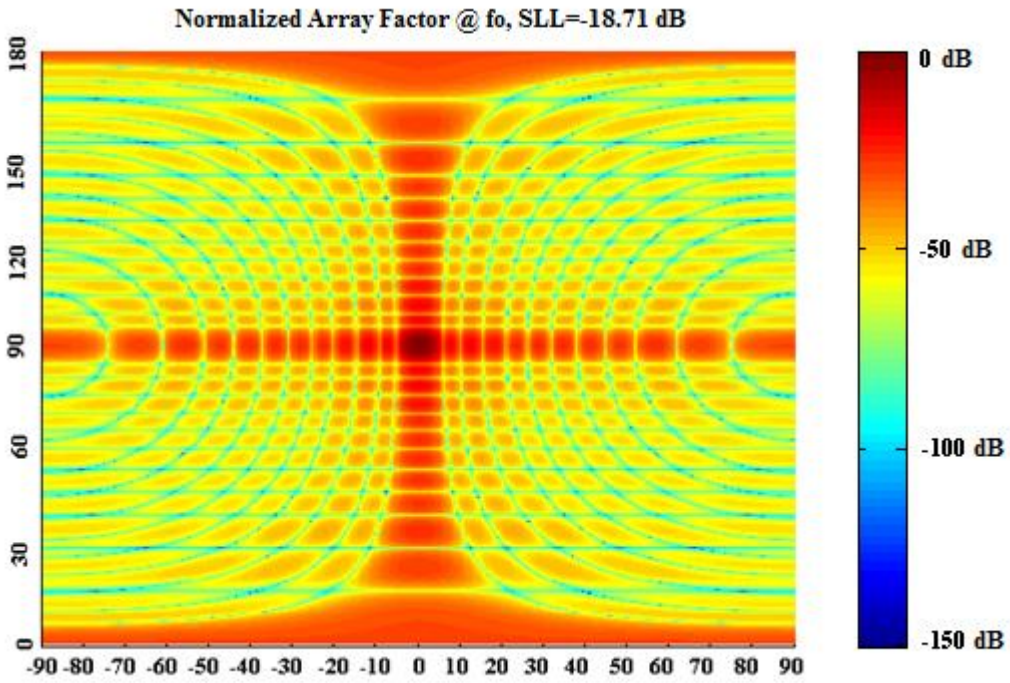

Figure 2.23 Three dimensional array factor of planar array with 529 elements

As can be seen in Figure 2.23, maximum sidelobe levels occur on two scan major axis with equal amplitude. Maximum sidelobe level at f_0 frequency has the same value with that of linear array.

Studies about sidelobe level optimization using genetic algorithm is also performed by designing circular arrays. In order to design circular arrays with genetic algorithm used for designing linear arrays, some modifications have been made. Firstly, individuals in the population represented the radius of the circles inside a circular array rather than elements in linear array. Number of circles was defined in circular array as the definition of number of elements in linear arrays. Moreover, number of elements on the circle with minimum circle was also optimized by some bits inside genome in order to determine the arc length between the elements on any circle of circular arrays to be designed. This parameter is constant between all the elements of the array as in the study of Milligan [11]. Radius of minimum circle is also set to some ratio of λ at the design frequency of f_0 so that distance between elements cannot be very close. Distance between radii of circular arrays are set to be increasing with increasing distance from the origin as

in the algorithm used for designing linear arrays. In this algorithm, number of circles is 10 in any circular array. Radius of minimum circle is defined between 0.2λ and 0.5λ. Moreover, number of elements on the minimum circle can be 3 or 4 depending on the bits of the mentioned section of the genome which are determining this parameter. In order to find the fitness of individuals, sidelobe level of the first sidelobe is aimed to be below -30 dB and other sidelobes levels are aimed to be below -25 dB in order to obtain a design similar to the one presented in [11]. This is the error criteria in the algorithm.

After these settings, algorithm is started. Position of elements in circular array of the fittest individual and that in Figure 1.15 can be seen in Figure 2.24 after 1000 iterations of this algorithm.

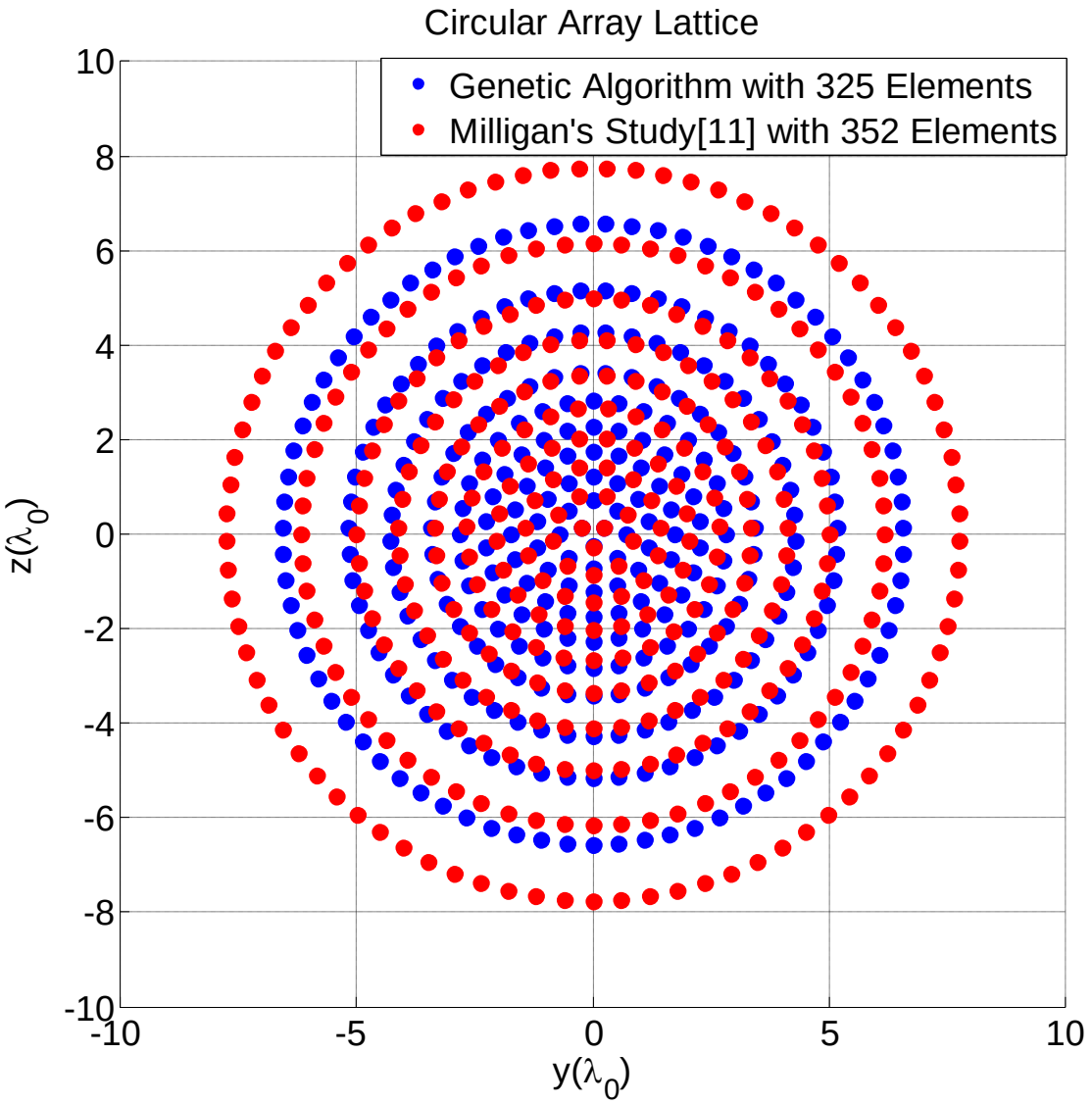

Figure 2.24 Element positions of the circular array generated by genetic algorithm and in Milligan's study [11]

Radii of concentric rings for both studies seem to be very close for the first two rings. Other rings' radii are greater in Milligan's study [11]. Array factor patterns of these arrays in 0º scan plane are given in Figure 2.25.

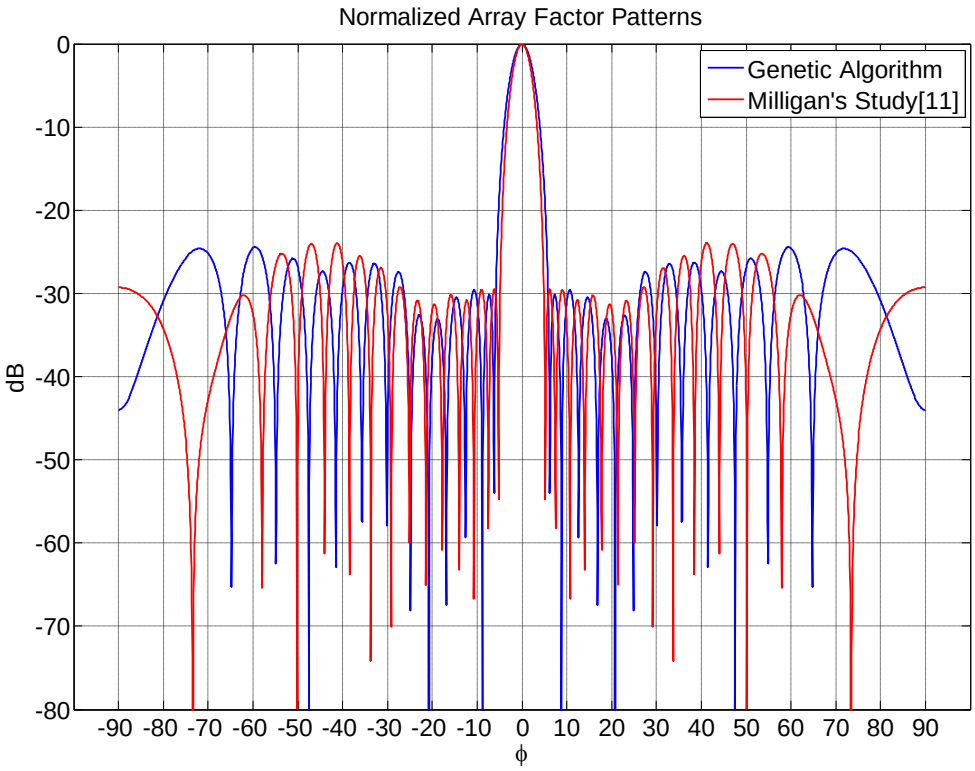

Figure 2.25 Array factor of the circular arrays generated by genetic algorithm and in Milligan's study [11]

The first sidelobe level of the designed circular array is below -30 dB and other sidelobe levels are below nearly -25 dB. Patterns in Figure 2.25 are very similar to each other except the width of the mainlobe which is mainly due to difference between the maximum radii of those arrays. Sidelobe performance of the designed array is also investigated for wideband operation. Figure 2.27 and Figure 2.27 show array factors of the array in low and high frequency bands.

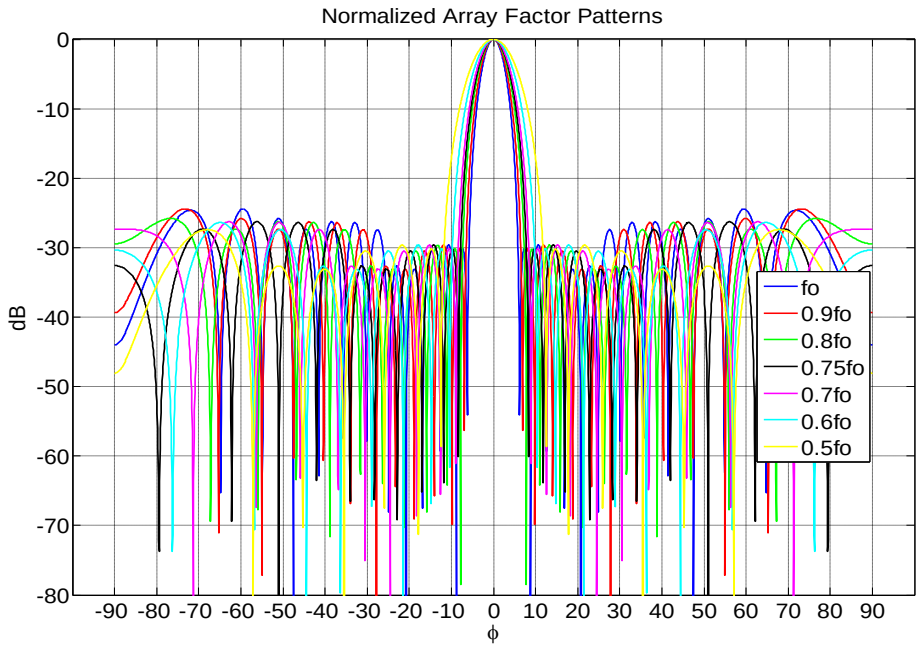

Figure 2.26 Array factor of the designed array with genetic algorithm in low band

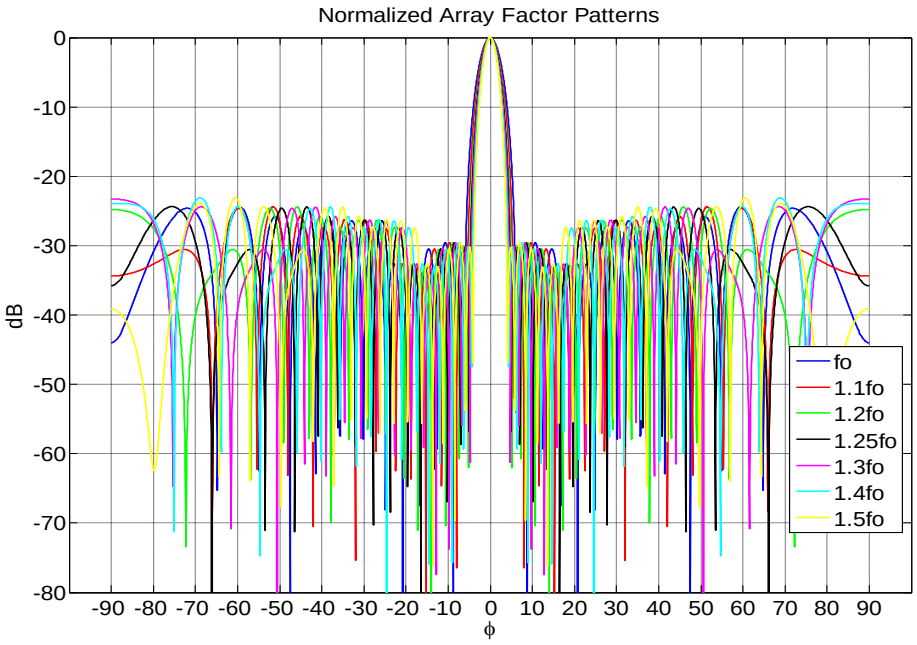

Figure 2.27 Array factor of the designed array with genetic algorithm in high band

Sidelobe performance of the designed circular array is wideband as can be seen in previous figures not only in low band but also in high band. Therefore, circular arrays with low sidelobes for wideband frequencies can also be designed by genetic algorithm.

Some studies to evaluate the performance of genetic algorithm during those iterations are also conducted. They are mainly focused on change of error with respect to iteration and investigation of other possible solutions. Second algorithm used in design of linear array is started again with the same design goals for such purposes. However, sidelobe performance of the designed arrays is investigated not only at the end of 1000 iterations but also at the end of some iterations for this case. Error of the fittest individual at the end of each iteration during 1000 iterations of algorithm is given in Figure 2.28.

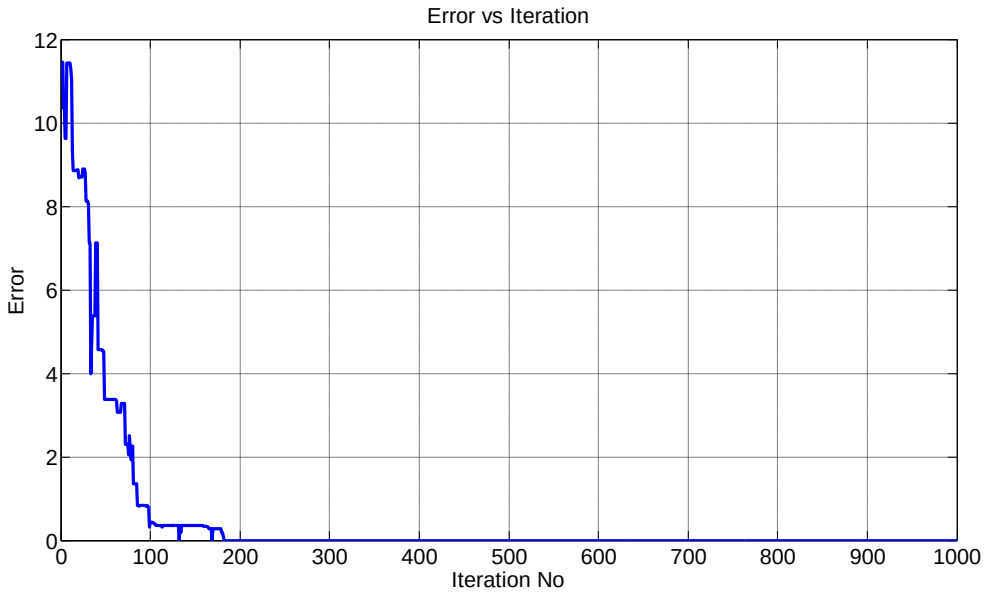

Figure 2.28 Error change with respect to number of iterations

As seen in Figure 2.28, error at the end of each iteration does not always decrease. This is due to mutations that can occur even inside elite selection of population that are not protected against mutation. Moreover, convergence has reached after near 200 iterations. Until then, error remains zero; however, the fittest individuals can give different solutions due to mutations which can occur at any iteration. There is a need to investigate possible solutions in order to understand whether solution space is narrow or broad; therefore,

array lattice and pattern comparison at those iterations are performed and these are given in Figure 2.29 and Figure 2.30.

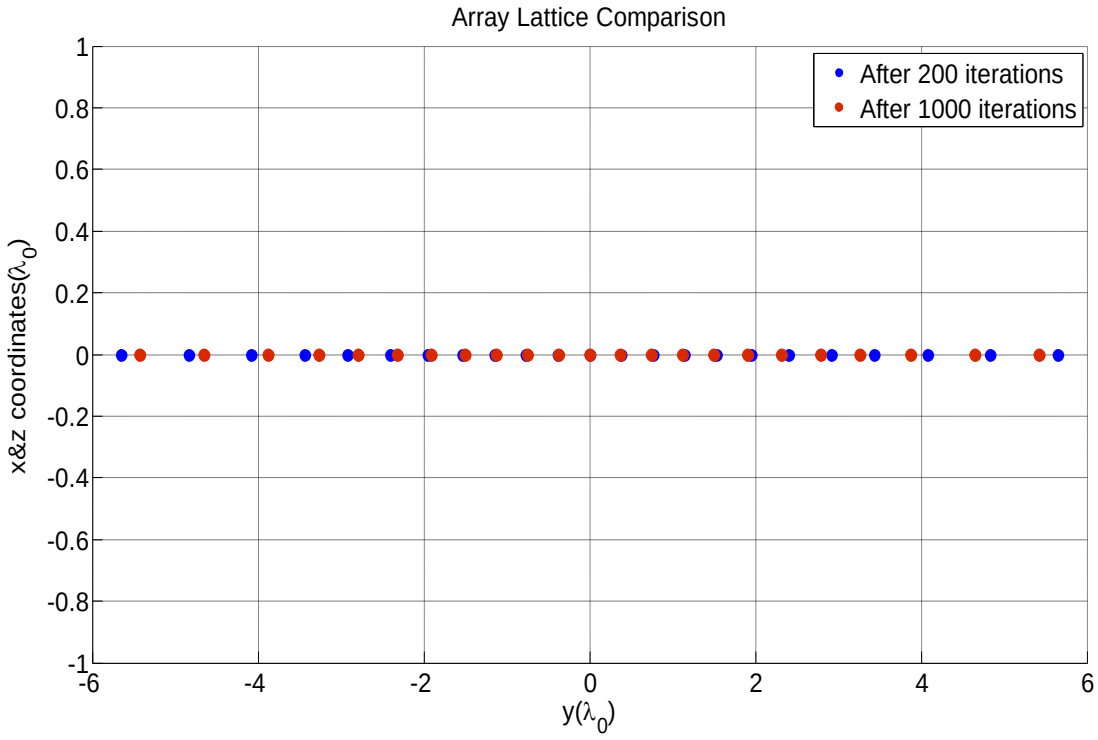

Figure 2.29 Array lattice of the fittest individuals with different number of iterations

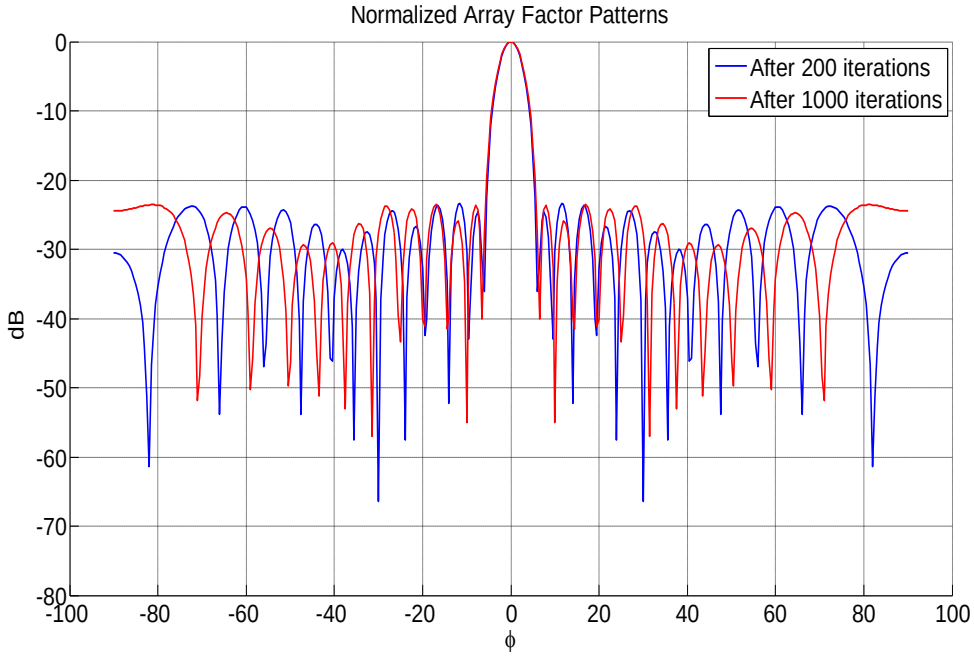

Figure 2.30 Patterns of the fittest individuals at different iterations

Array lattice are very similar as can be seen in Figure 2.29. Maximum difference in element positions is 0.225λ. Both arrays are in ±6λ aperture. Their patterns are similar in terms of mainlobe, first sidelobe and the maximum level of sidelobes; however, null positions of sidelobes can be a little different as seen in Figure 2.30. Therefore, genetic algorithm could generate not only single solution but also a number of possible solutions for this problem. However, solution space can be said to be very narrow for this problem because there is a little difference in element positions of array generated at different iterations of genetic algorithm.

2.3 Beamwidth Optimization

Beamwidth of an array antenna is another parameter for optimization. Normally, beamwidth of an array with uniform spacing and whose aperture is fully illuminated inversely scales with changing frequency in its operational frequency band. For an array with aperiodic spacing and fully illuminated aperture, there is need to investigate beamwidth performance in order to understand whether it can be frequency independent

for some bandwidth. In this section, genetic algorithm is also used to optimize the positions of a linear array to have constant beamwidth in wide frequency band.

In order to design a linear array with constant beamwidth there should be at least two frequencies which are in the band of interest, and they must be taken into account so that beamwidth difference in the band could be minimized. Similarly, array factors are calculated for frequencies f_0 and $1.5f_0$ in the optimization. Moreover, difference in beamwidth of the array factors for these frequencies is represented in error criteria of this algorithm. However, that is not the only criteria to calculate the fitness of individuals in the population of the algorithm. A sidelobe level requirement is also present such that there will be no grating lobes in the patterns of array factor for an array. Similarly, error criterion for sidelobes is adjusted to have maximum -13 dB sidelobe level at f_0 frequency.

Linear arrays designed by the algorithm have a minimum of 0.375λ spacing between adjacent elements. After these settings, algorithm is started. Position of elements of the linear array for the fittest individual can be seen in Figure 2.31, after 1000 iterations of this algorithm.

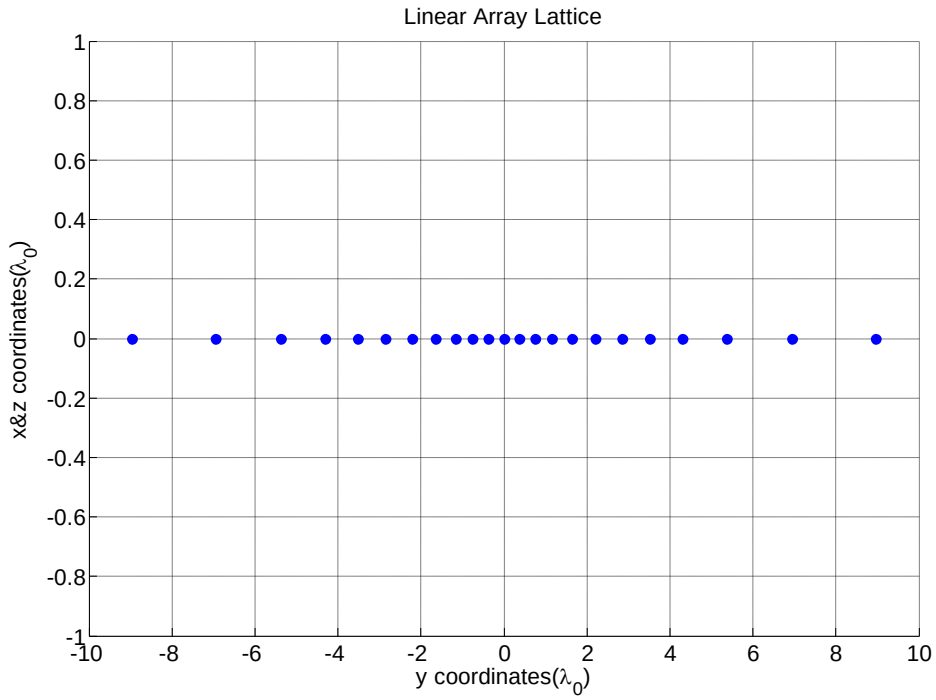

Figure 2.31 Array lattice for the fittest individual in beamwidth optimization

For the array seen in Figure 2.31, spacing between adjacent elements for the elements close to origin is nearly constant, whereas it increases very dramatically for the elements far from origin. Array factor of this array at f_0 frequency can be seen in Figure 2.32.

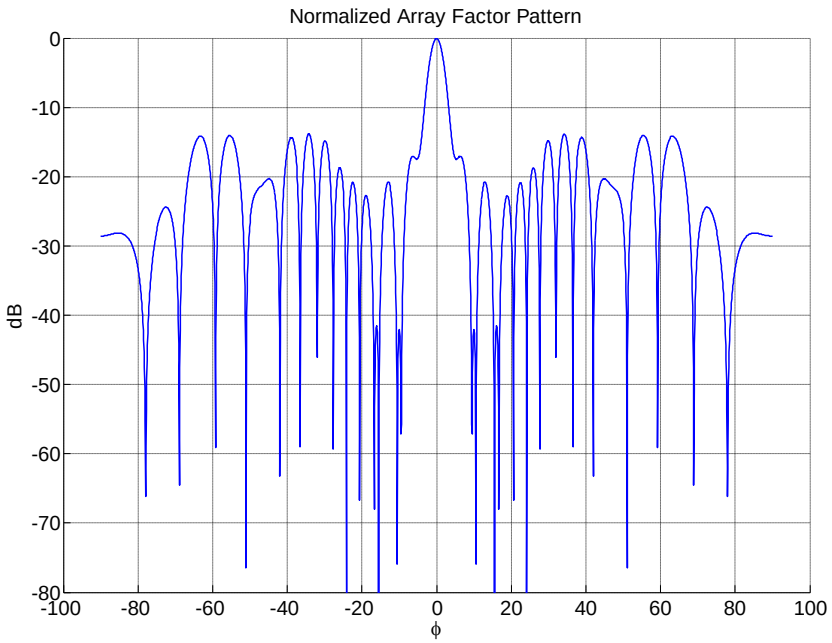

Figure 2.32 Array factor of the array at f_0 frequency

As can be seen in Figure 2.32, sidelobe level of the array pattern is below -13 dB. In other words, sidelobe requirement is satisfied in this algorithm. Array factor of this array is also investigated for different frequencies in the band between f_0 and $1.5f_0$. Array factors patterns are given in Figure 2.33.

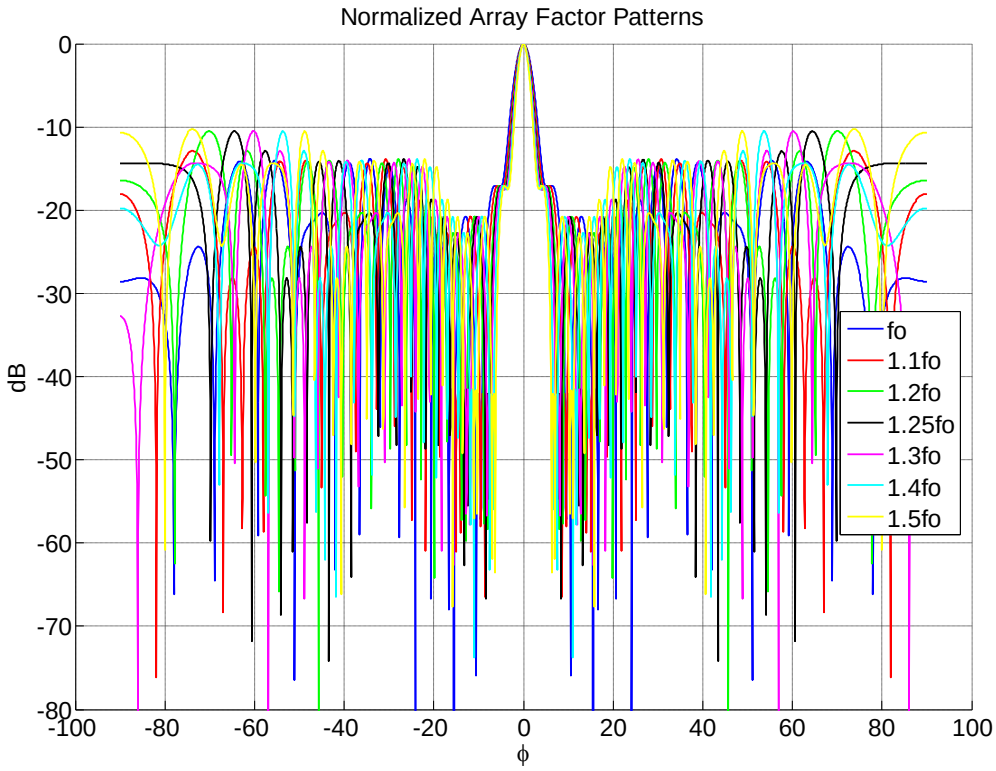

Figure 2.33 Array factor patterns in the band between f_0 and $1.5f_0$

Sidelobe level can increase to -10 dB as can be seen in Figure 2.33 with the increasing frequency. Therefore, no grating lobe can be seen for f_0-$1.5f_0$ band. Beamwidth performance is given in Figure 2.34. Moreover, there is a red line in the same figure showing the values which are found by inverse scaling of the beamwidth at f_0.

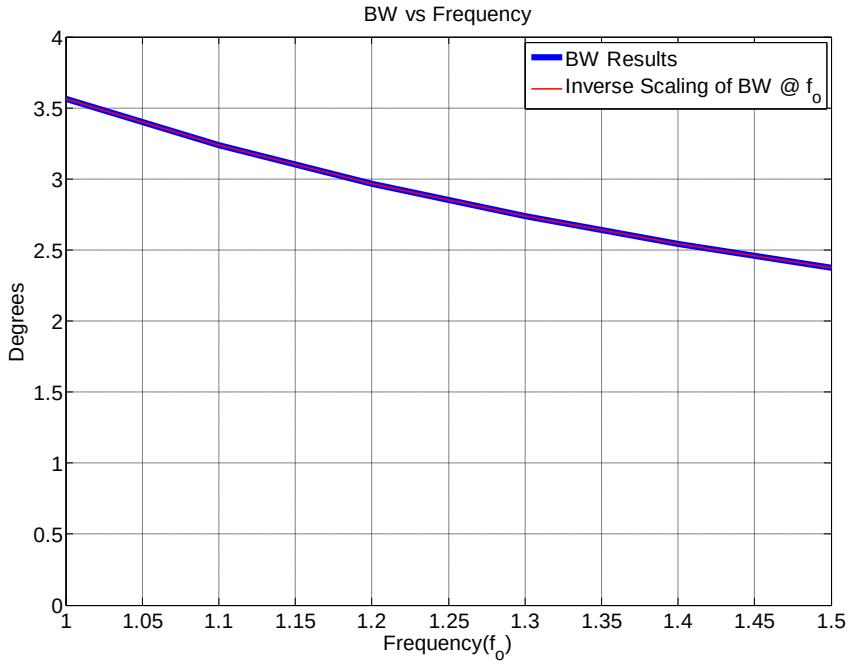

Figure 2.34 Beamwidth performance of the array in f_0-1.5f_0 band

Beamwidth results (blue line) and values found by inverse scaling (red line) are very close to each other as can be seen in Figure 2.34. In other words, beamwidth in the designed aperiodic array also scales inversely with changing frequency. This is due to the fact that active region of the array stay same, in other words, not changing with respect to frequency. Therefore, beamwidth of aperiodic arrays with uniform illumination cannot be optimized since it just scales inversely with changing frequency. In order to have a constant beamwidth, different array structures such as wavelength scaled array concept which is studied in the next chapter must be investigated.

CHAPTER 3

WAVELENGTH SCALED ARRAY CONCEPT

3.1 Introduction to Graphical User Interface

In this chapter, wavelength scaled arrays are studied. In order to examine the characteristics of array as in Figure 1.5, some numerical studies have been studied in MATLAB® environment. Array factors of such arrays are examined by Graphical User Interface (GUI) in this environment. Two interfaces were designed. The first interface, namely "dizi_analizi" was to design the array at the maximum operating frequency. An example of this GUI is given in Figure 3.1.

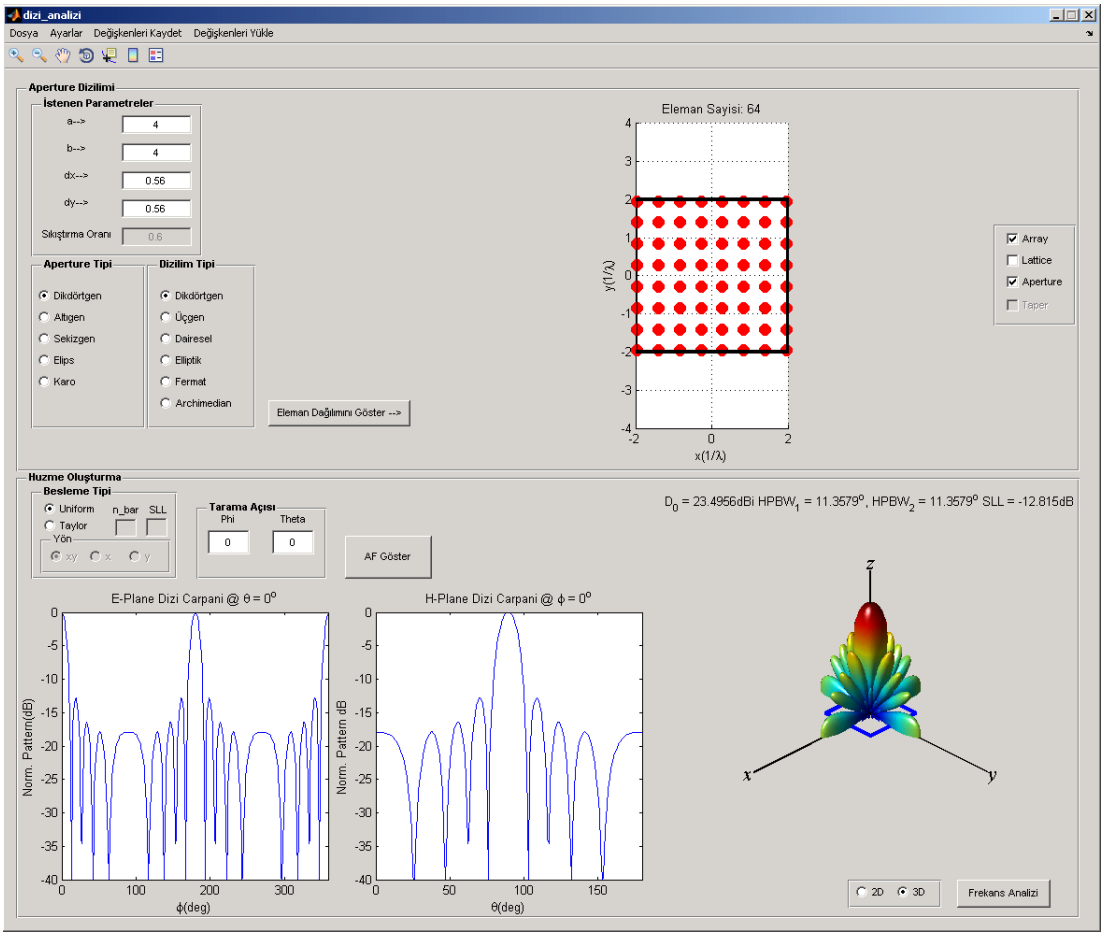

Figure 3.1 Interface utilized to examine array factor at the maximum operating frequency

With the help of this GUI, array antennas with isotropic radiators can be designed the desired aperture type and lattice. After those are specified, the distribution of the elements on xy plane can be given by this GUI. Then, the pattern generated by the element distribution of the array, patterns on the maximum scan angle planes and 3D pattern can be examined in the next section of this GUI. By the button existing on the right bottom side of this GUI, a second GUI will appear. The second GUI, namely "freqGUI", allows user to examine the characteristics of the designed array by the first GUI, which was designed at its maximum operating frequency, with the changing frequency. An example of this second GUI can be seen in Figure 3.2.

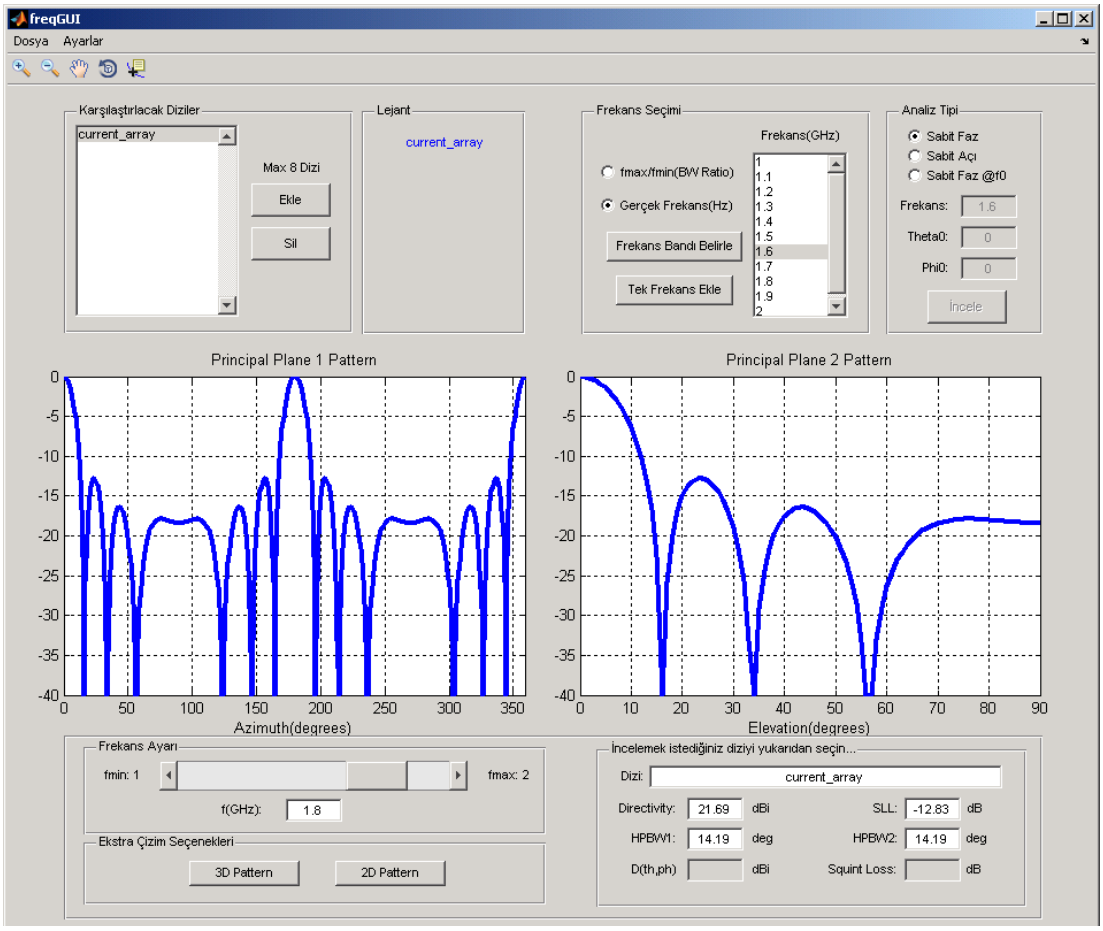

Figure 3.2 Interface utilized to examine array factor with the changing frequency

With the “current array” selection in the right top of this GUI, the designed array in the first GUI can be studied with the change in frequency. Selection of the range of frequency can be made in the right box. Then, the patterns of the designed array can be generated by entering the scan angles in phi and theta coordinates. Directivity, sidelobe level with respect to main beam and half power beamwidths on scan axes can be seen for all the frequencies specified in this GUI.

3.2 Design of Wavelength Scaled Array with GUI

The designed GUIs was firstly utilized to investigate wavelength scaled array by Cantrell et al. [4] shown in Figure 1.5. The array with the same element spacing is formed in GUI which was named as “dizi_analizi” as in Figure 3.3. Points on the figure represent the centers of elements.

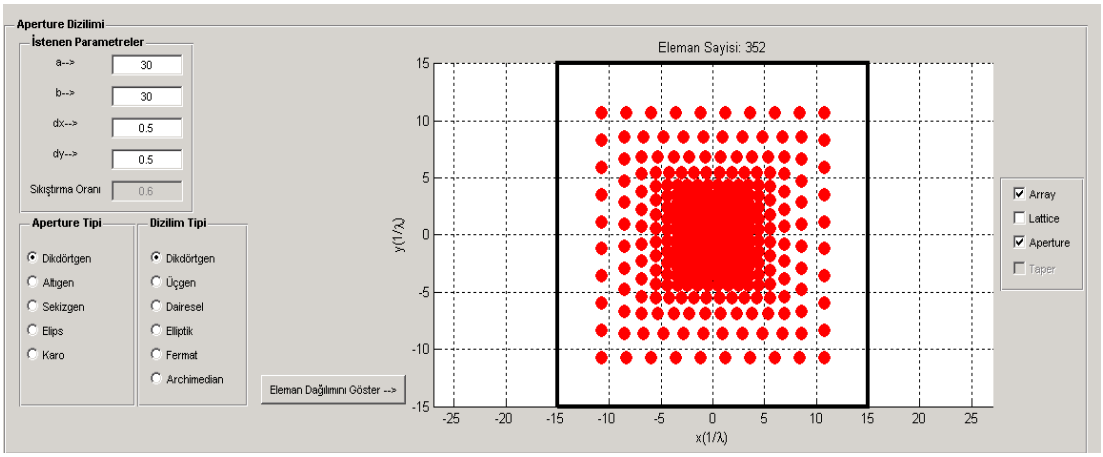

Figure 3.3 Wavelength scaled array by Cantrell et al. [4]

The frequency characteristics of this designed array are investigated in the following GUI, named as "freqGUI". Calculation of the array factor of this phased array can be explained by the following array factor formula:

$$AF(\theta,\phi) = \sum_{n=1}^{N} a_n * e^{kd_{nx}\sin\theta\cos\phi} * e^{kd_{ny}\sin\theta\sin\phi} \tag{3.1}$$

In (3.1), array factor is shown as $AF(\theta,\phi)$ in θ and ϕ coordinates. a_n represents element excitation coefficients, and d_{nx} and d_{ny} are x and y coordinates of the nth element of the array respectively.

This array consists of elements which will be on or off according to operating frequency in the band 4-18 GHz. Active regions of the array for some frequencies can be seen in Figure 3.4. In 16.6-18 GHz band, only 10x10 elements in the core region are active. As the frequency decreases, in order to maintain constant beamwidth and gain, area of active region increases.

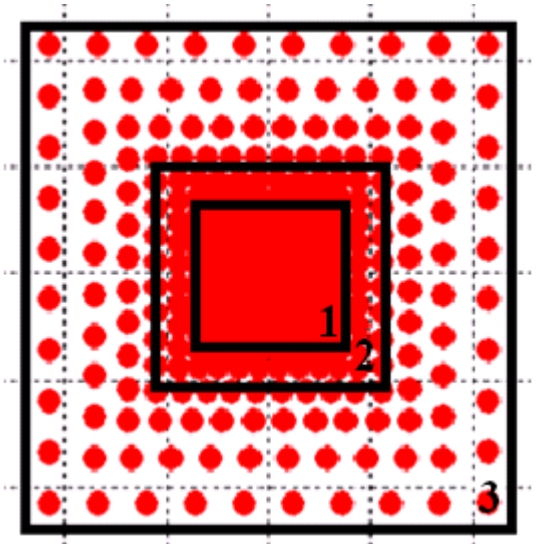

Figure 3.4 Active regions of the wavelength scaled array. (1) Only 10x10 core region is active for 16.6-18 GHz band. (2) Core region plus two adjacent layers are active for 9.3-11.2 GHz band. (3) All elements are active for 4-4.9 GHz band.

For most of the frequencies, active region of the array includes elements with variable size. Those elements will contribute to array factor in proportion with their length in x and y coordinates. In order to see this contribution, a_n of each element is distributed in proportion with length of each element in x and y coordinates. Then, maximum of this coefficient is normalized to 1 before the calculation of the array factor. Array factor for this array is calculated for 0° scan for both scan axes. Some frequency characteristics of this array at 4, 11 and 18 GHz frequencies can be seen in Figure 3.5, Figure 3.6 and Figure 3.7 respectively.

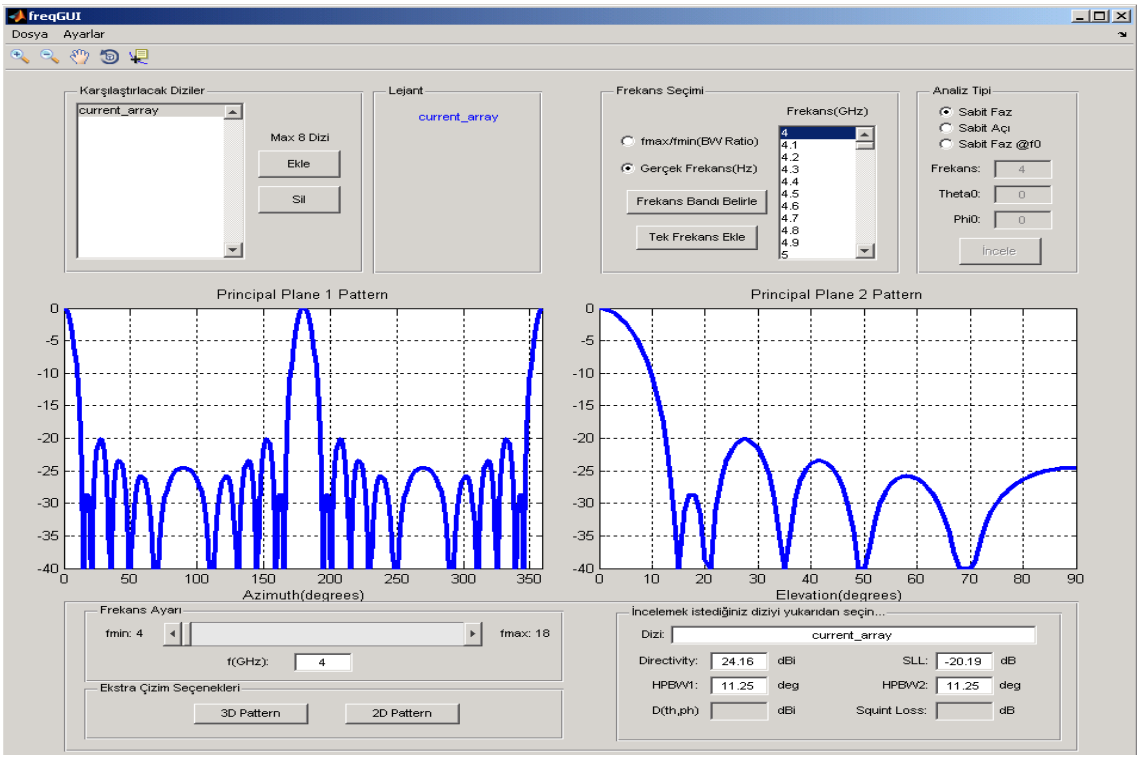

Figure 3.5 Wavelength scaled array performance at 4 GHz

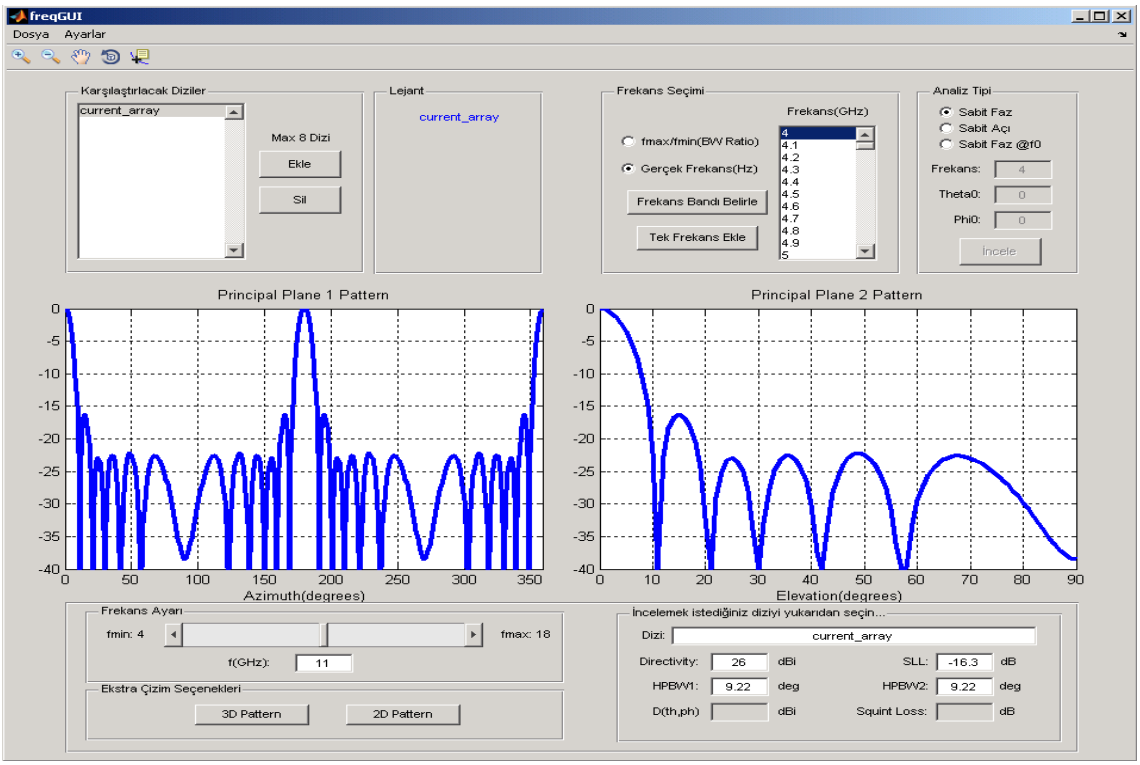

Figure 3.6 Wavelength scaled array performance at 11 GHz

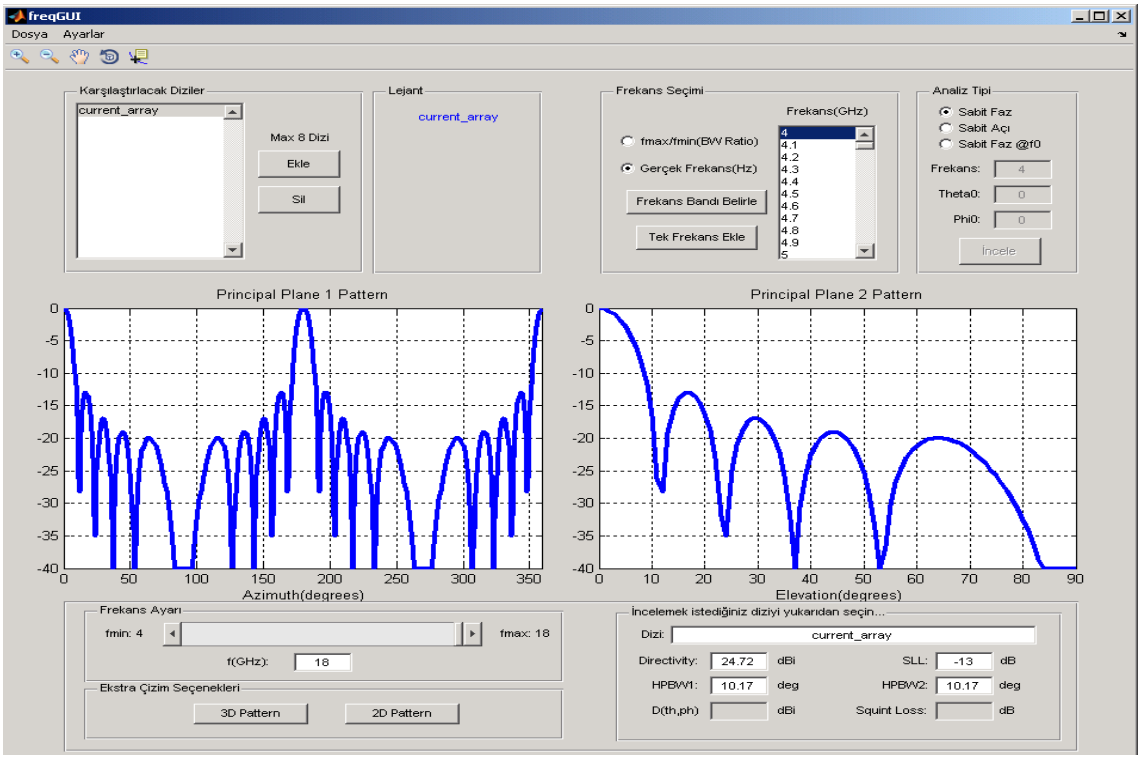

Figure 3.7 Wavelength scaled array performance at 18 GHz

As can be seen in Figure 3.5, Figure 3.6, and Figure 3.7 wavelength scaled arrays are able to show nearly independent frequency characteristics. Note that Plane1 in these figures corresponds to azimuth and Plane2 corresponds to elevation planes. Generally full coverage is required for azimuth plane so the scan angle extends from -180° to 180°. However, in elevation plane scanning only the range from 0° to 90° is found sufficient. The difference in the scan range is the reason why the beamwidths in the two planes seem different eventhough they are the same.

3.3 Comparison Between Wavelength Scaled Array and Conventional Array

In this part of the study, wavelength scaled arrays are examined for linear arrays and for frequency bands with different bandwidth. Their HPBW performances and number of elements in these arrays are compared with uniform phased arrays in the same frequency bands. A wavelength scaled (Figure 3.8) and a conventional (uniform spacing) array (Figure 3.9) are designed to have 10° HPBW at 18 GHz. A number of active regions are defined for each array in order to keep the beamwidth between 9° and 11°.

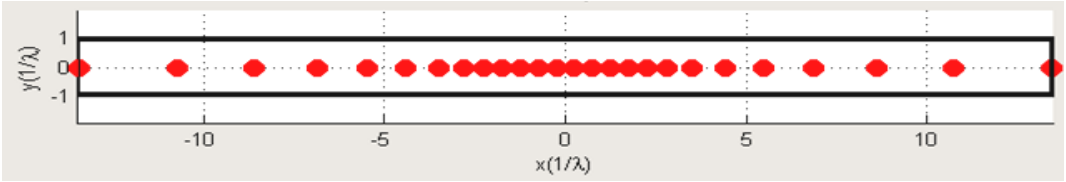

Figure 3.8 4-18 GHz wavelength scaled linear array

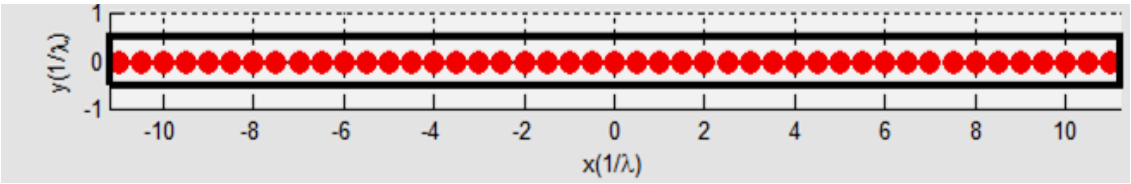

Figure 3.9 4-18 GHz uniform linear phased array

Number of active elements increase as frequency decrease in order to have nearly constant HPBW. HPBW of these arrays in 4-18 GHz band for 141 frequency points can be seen in Figure 3.10. Each jump in this figure represents a transition to a new active region. Therefore, to keep the beamwidth between 9° and 11°, 11 active regions are required for the uniform array whereas 8 active regions are enough for WSA. There is 42.2% reduction in the number of elements with wavelength scaled array.

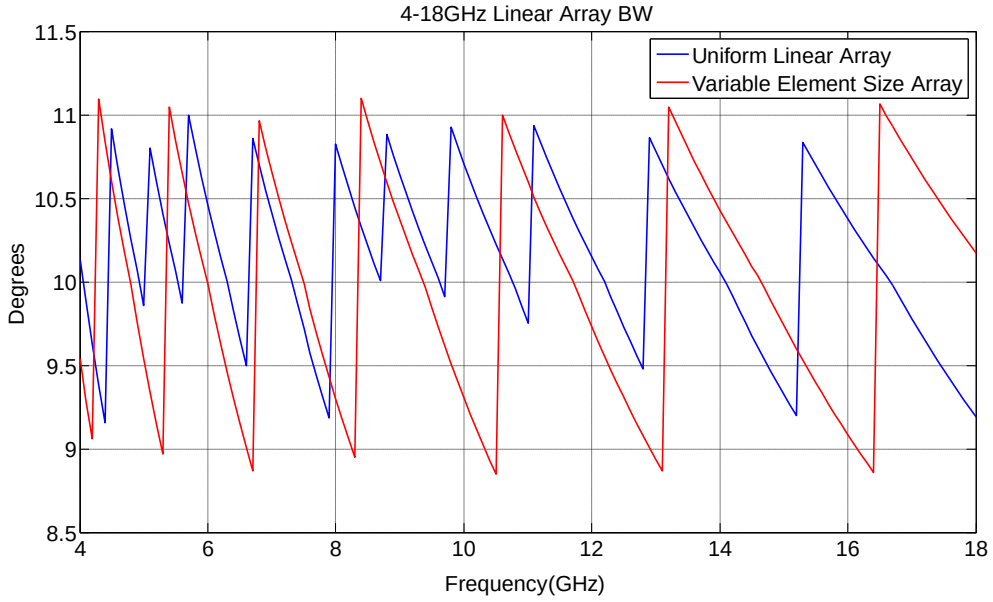

Figure 3.10 HPBW of 4-18 GHz linear arrays

This study is also performed for 4-8 GHz, 4-12 GHz and 8-12 GHz bands. Summary of this study can be seen in Table 3.1. As can be seen, as the bandwidth of the operation increases, reduction in the number of elements increases.

Table 3.1 Difference in the number of elements for wavelength scaled array and uniform linear array for 10° HPBW

Bandwidth	#Elements for Wavelength Scaled Array	#Elements for Uniform Linear Array	Reduction % in #Elements
1:4.5	26	45	42.2
1:3	20	30	33.3
1:2	16	20	25
1:1.5	14	14	0

CHAPTER 4

REALIZATION OF AN ARRAY WITH CHANGING ACTIVE REGIONS

This chapter includes implementation of a linear array with changing active region. A linear array with Vivaldi elements and feeding network are designed because implementation of this concept requires a linear array and a network to feed that array. This chapter consists of three main parts, namely linear array design, feed network design, and the measurement results of the overall designed system.

Feed network design is one of the crucial parts of phased array systems. In order to implement changing active aperture with respect to frequency, feed network plays the most important role. For this concept switching is required in feed network as well as beam steering, and power dividing with amplitude balance. Bandwidth is also determined by feed network. As a result, components used in feed network affect the bandwidth of all system. In this thesis, a feed network is designed between 1.5-4.5 GHz to feed a linear array of 8 elements.

For linear array design, Vivaldi elements are selected because they are one of the best candidates for RF applications requiring wideband operating frequency and wide angle scanning performance. These antennas can be produced easily by printed circuit applications. Their input impedance can be matched to feed lines via microstripline or stripline. In this thesis, a manufactured Vivaldi array with constant size is used.

4.1 Feed Network Design

Feed networks are one the most important parts of phased array systems. Sidelobe level control, beam steering, active aperture control, and impedance matching can be done by feed networks. Operating bandwidth is also determined by feed network as well as array antenna. In this thesis, a feed network with dividers, phase shifting units and also switching abilities is required in order to satisfy required characteristics of changing active region. For the switching abilities, directional coupler of diplexer is required in order to determine the way of input signal, i.e. active region of the array [4]. For the design of feed network in this thesis, a 3 port diplexer operating in 1-12 GHz band as in Figure 4.1 is utilized. Diplexer is a device that is used to split incoming signals from a common port into two paths (channels) dependent on frequency. These devices involve RF filters, usually a low pass on one channel and high pass filter on the other or bandpass filters with different cutoff frequencies for both channels.

Figure 4.1 Diplexer utilized in feed network

Return loss of the input port and insertion loss characteristics of output ports can be seen in Figure 4.2 and Figure 4.3 respectively. Diplexer has bandpass characteristics for both of the output channels. As seen in Figure 4.3, first output, J1, is bandpass in 1.5-2 GHz band, and the second output is bandpass in 2-4.5 GHz.

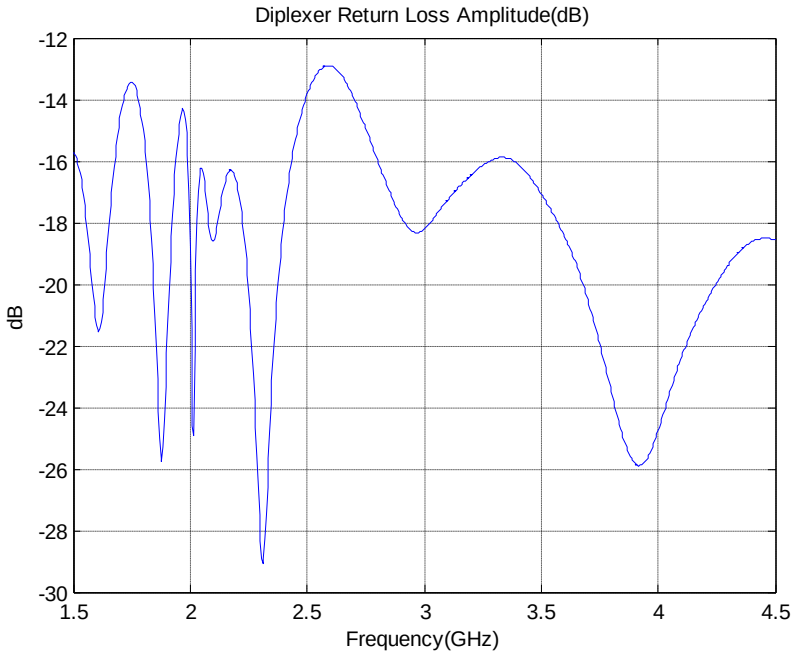

Figure 4.2 Return loss characteristics of diplexer used in feed network

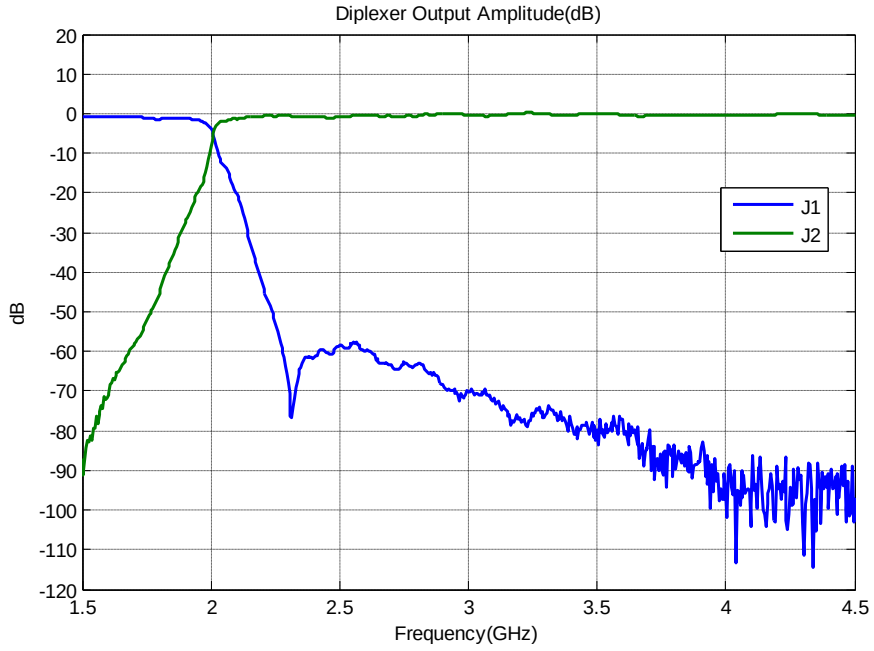

Figure 4.3 Insertion loss characteristics of diplexer used in feed network

Nominal values of these measured parameters are given Table 4.1.

Table 4.1 Nominal values of diplexer (From [14])

Return loss (dB)	**1-4.5 GHz band**	
Input	-12 dB min	
Insertion loss (dB)	**1-1.9 GHz band**	**2.1-4.5 GHz band**
Input-J1	-1 dB max	-30 dB min
Input-J2	-30 dB min	-1.5 dB max

In addition to diplexer, phase shifting units and power dividers are also required to feed the designed linear array. In this feeding network 2 way and 4 way divider are designed. Power divider chips are used in order to split or combine power [16]. Delay lines are used for phase shifting units. These delay lines set to give same phase shift, so array will be steered to 0° (boresight). Parallel feed structure is used in these dividers as shown in Figure 4.4 and Figure 4.5. Substrate material for these circuits is RO4003® [15]. Port numbering can also be seen in these figures.

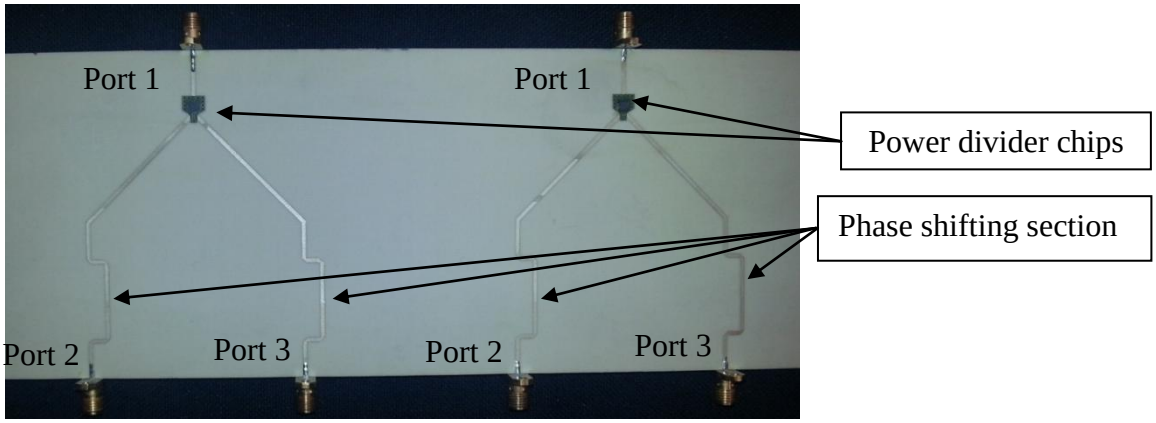

Figure 4.4 2 way dividing and phase shifting unit

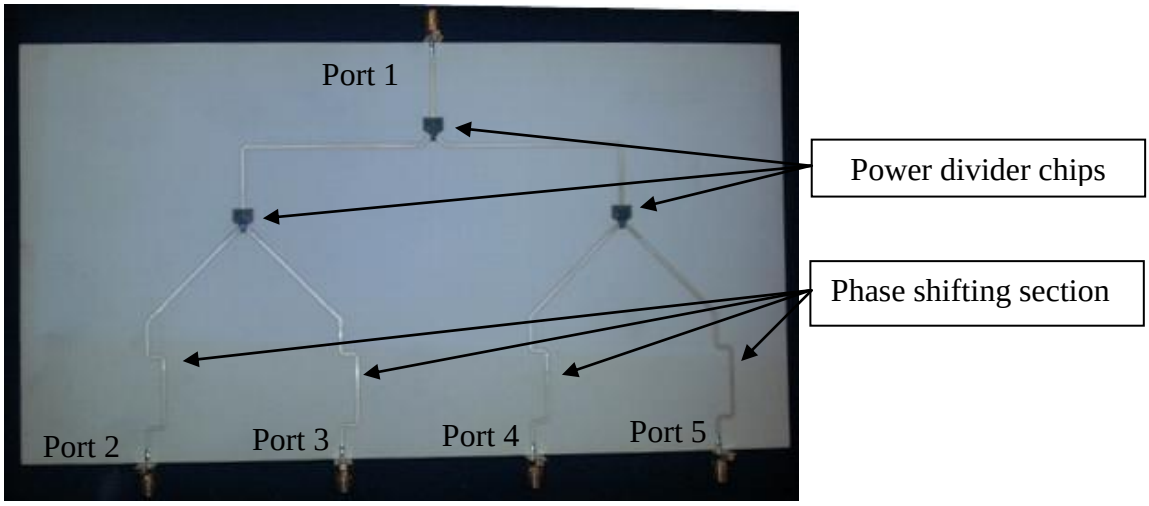

Figure 4.5 4 way dividing and phase shifting unit

Output phase characteristics and insertion loss of 2 way divider are in Figure 4.6 and Figure 4.7, respectively. Phase differences between output ports are below 2° in 1.5-4.5 GHz band. Moreover, insertion loss of output ports are close to each other, maximum difference between ports is 0.3 dB. Expected insertion loss for an ideal 2 way divider is 3 dB. At this point of view, this divider could be inappropriate to utilize due its high insertion loss especially at high frequencies. On the other hand, it is used in the feed network due to its availability and very similar characteristics between output ports.

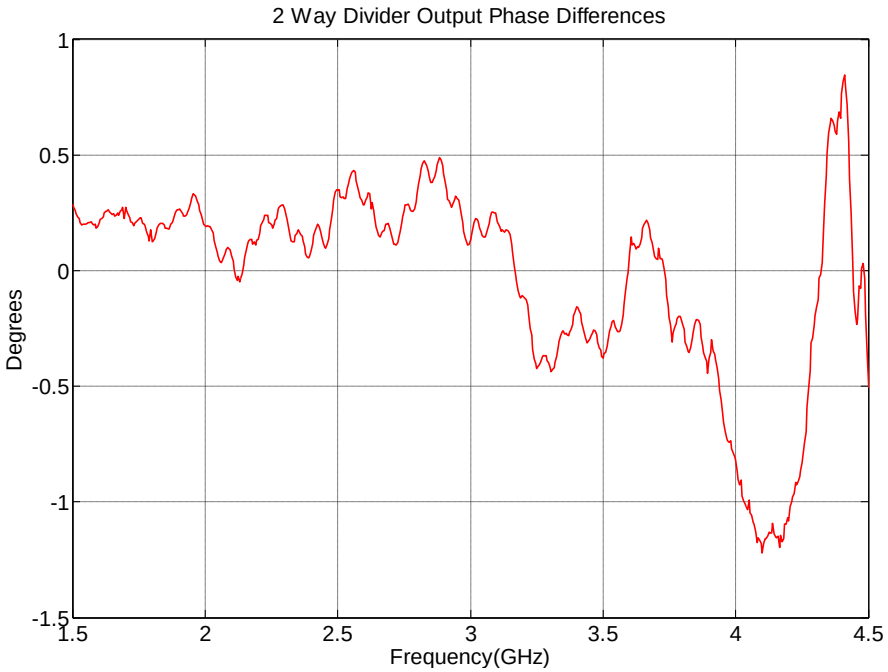

Figure 4.6 Output phase differences of 2 way divider

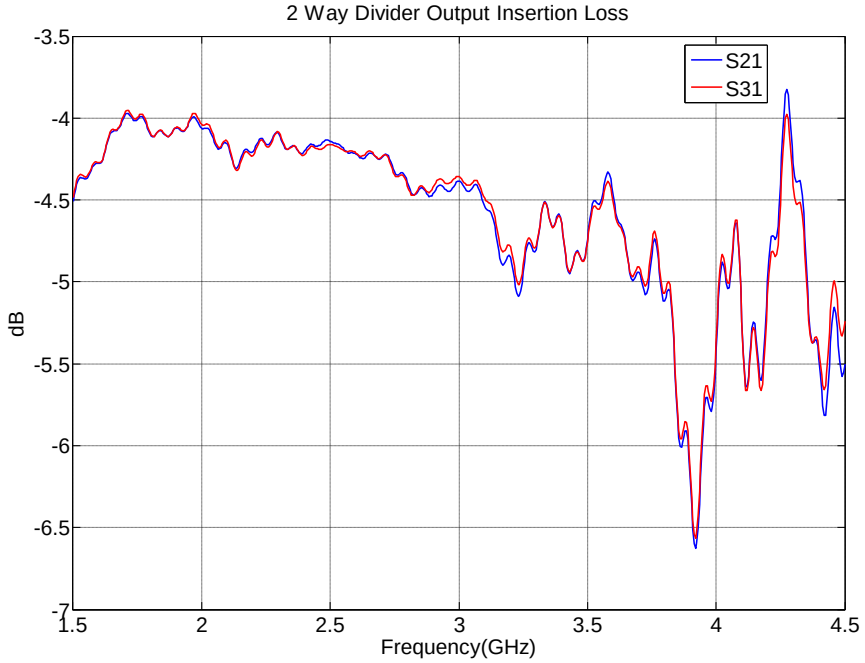

Figure 4.7 Insertion loss characteristics of 2 way divider

Electrical specifications reported in the datasheet of the chip used in the 2 way divider circuit are given in Table 4.2.

Table 4.2 Electrical specifications of the chip used in divider and combiners (From [16])

Frequency (GHz)	**Isolation (dB)**		**Insertion Loss (dB)**		**Phase Unbalance (Degrees)**	**Amplitude Unbalance (dB)**	**VSWR(:1)**	
f_{min}- f_{max}	**Typ.**	**Min.**	**Typ.**	**Max.**	**Max.**	**Max.**	**Input Port**	**Output Ports**
1.55-4.4	20	12	4	4.9	6.0	0.3	1.4	1.4

As can be seen from Table 4.2, characteristics of 2 way divider satisfies typical insertion loss, phase unbalance and amplitude unbalance values. However, it fails for the maximum insertion loss criteria, and this can be due to inappropriate copper lines causing impedance mismatch for some frequencies in the band.

Output phase characteristics and insertion loss of 4 way divider are in Figure 4.8 and Figure 4.9 respectively. Phase differences between output ports are below 15° in 1.5-4.5 GHz band. Moreover, insertion loss of output ports are close to each other, maximum difference between ports is 0.6 dB. Phase unbalance between output ports are normalized with respect to phase of insertion loss of Port 2. Maximum phase unbalance is 14° which is not far from the specifications. High insertion loss could be also observed for high frequencies.

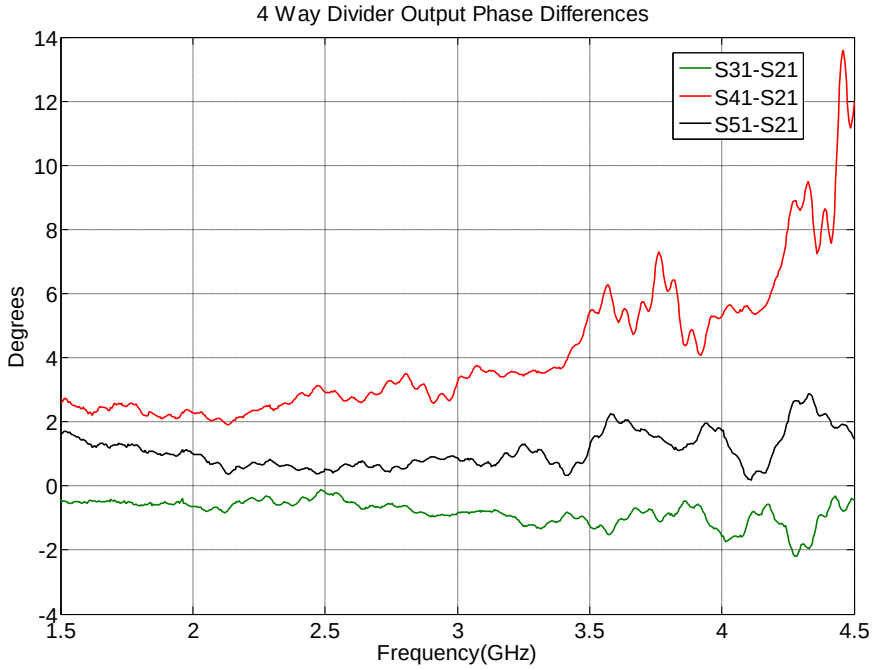

Figure 4.8 Output phase differences of 4 way divider

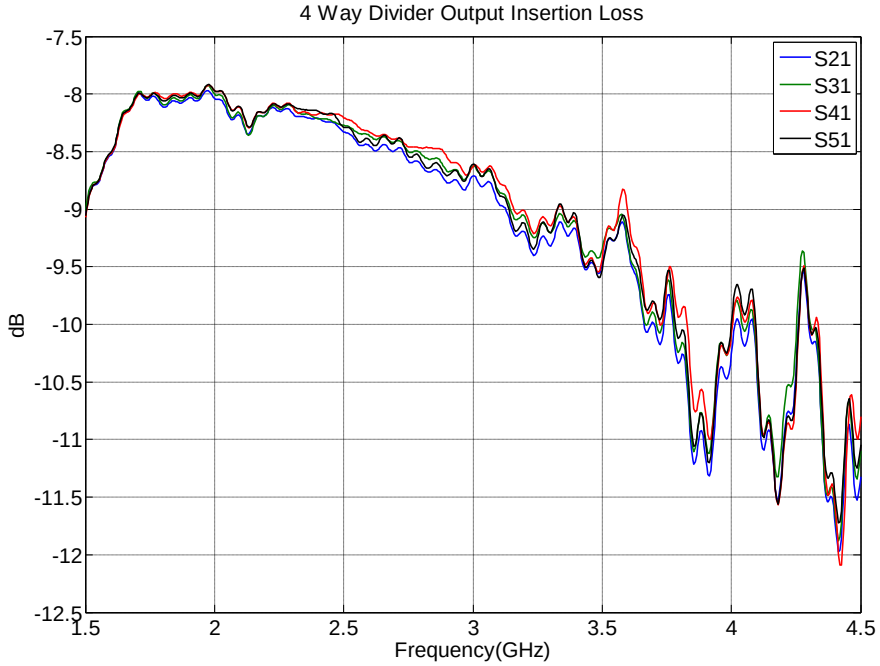

Figure 4.9 Insertion loss of 4 way divider

In addition to dividers/combiners mentioned above, another 2 way divider is utilized in 1.5-2 GHz band channel, in order to design an 8 way divider in this channel with two

4 way dividers. Output phase and insertion loss characteristics of this 2 way divider are given in Figure 4.10 and Figure 4.11, respectively. Eventhough the insertion loss performance of this 2 way divider is much better than the previous one; it couldn't be utilized to replace the previous dividers since only a single one is available.

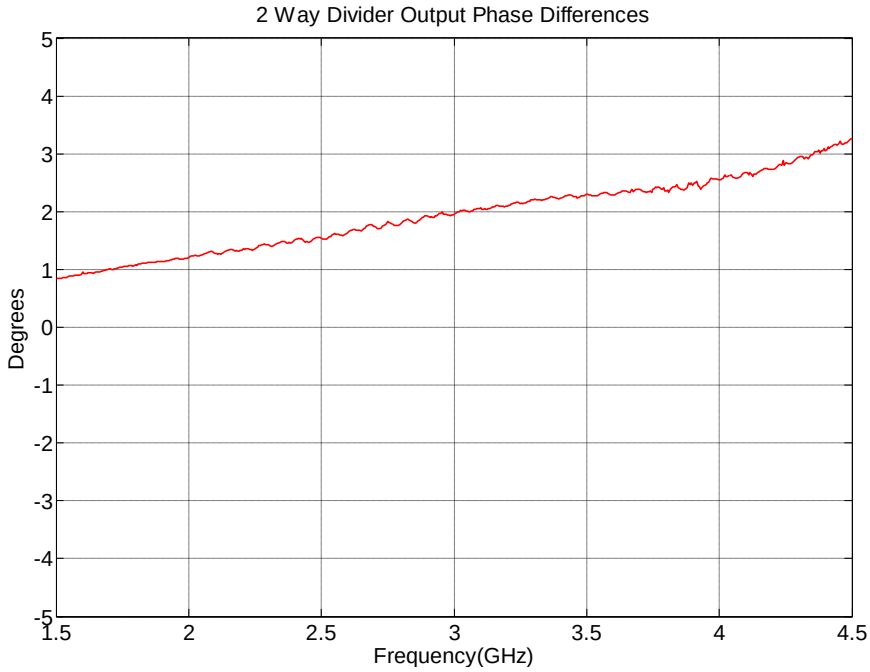

Figure 4.10 Output phase differences of 2 way divider utilized in 1.5-2 GHz channel

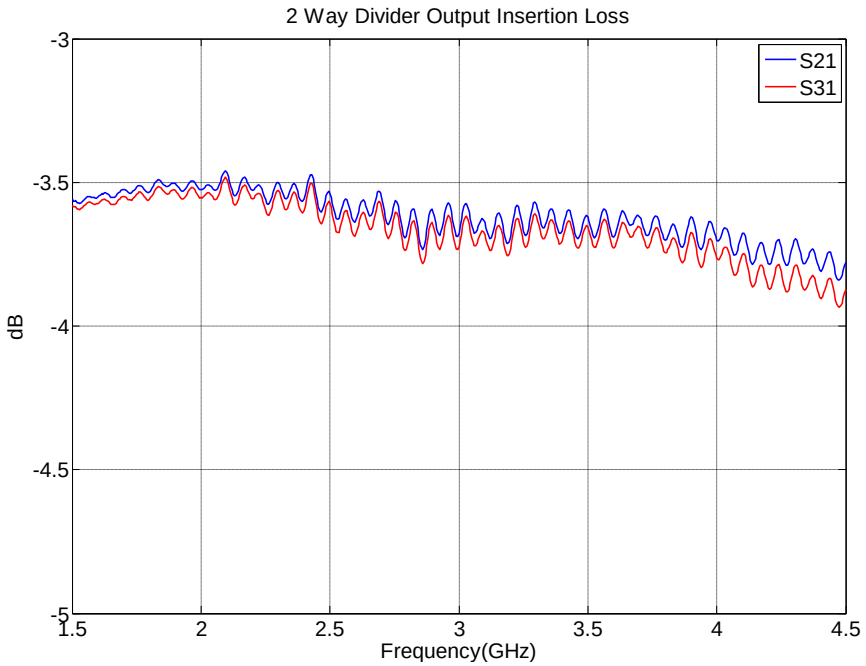

Figure 4.11 Insertion loss characteristics of 2 way divider utilized in 1.5-2 GHz channel

After the placement of diplexer, dividers, and cables, feed network is realized as can be seen in Figure 4.12. SMA connectors are used in all parts of feed network. In order to connect diplexer, splitters and combiners inside this feed network, SUCOFORM® cables [17] with equal length are utilized to maintain phase match at the outputs as much as possible. Circuit schema of this feed network can be seen in Figure 4.13. At the conjunction of different frequency channels, 2 way combiners built with power divider chips are utilized instead of diplexers due to limited number of diplexer.

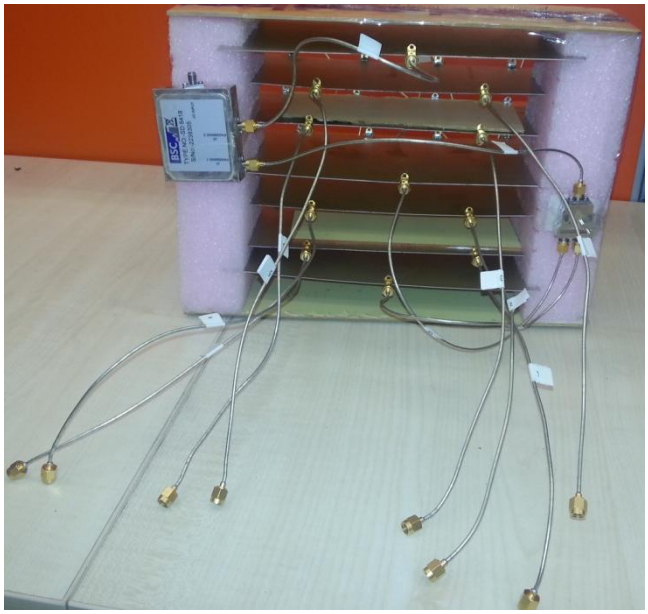

Figure 4.12 Feed network

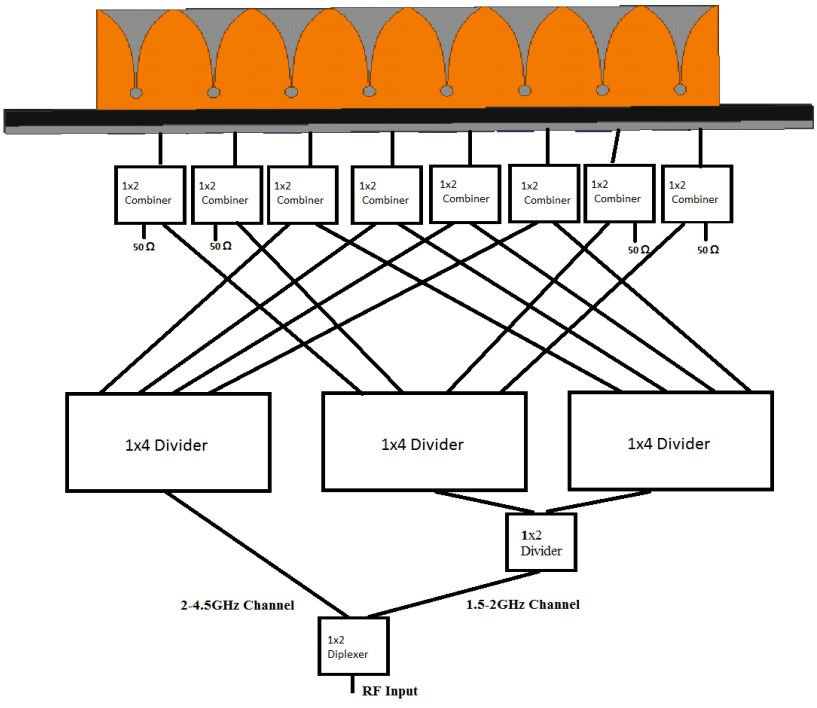

Figure 4.13 Circuit diagram of the feed network

Realized feed network is measured in terms of input return loss and insertion loss of output ports. Output ports are terminated with 50Ω during the measurement. Measurement results can be seen in Figure 4.14 and Figure 4.15.

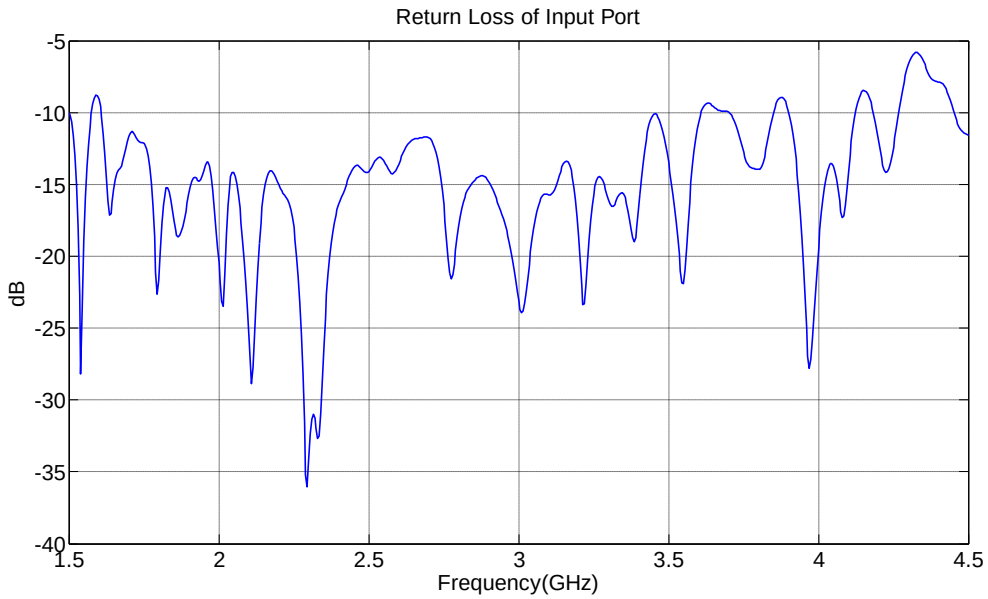

Figure 4.14 Return loss characteristics of feed network

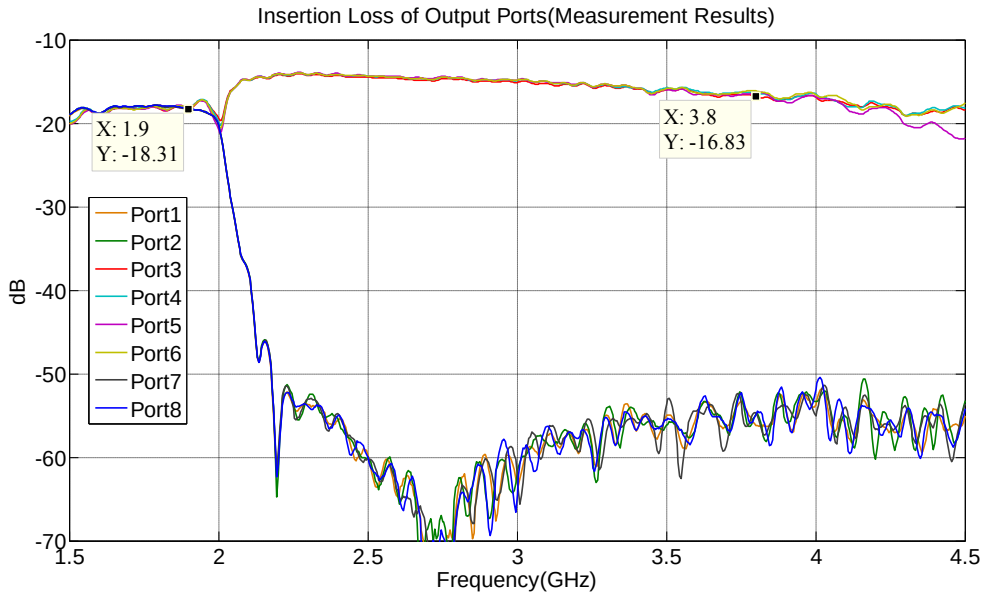

Figure 4.15 Insertion loss characteristics of feed network

As in Figure 4.15, there is a difference in amplitude of output ports. There can be said to be two group of outputs with different power levels in 1.5-4.5 GHz band. Ports 1,2,7,8

and ports 3,4,5,6 are these two mentioned output groups. First group can deliver power to antenna in 1.5-2 GHz band, while the second group delivers in all band. This characteristic is required in order to implement a linear array with changing active region.

This feed network insertion loss is high. For insertion loss calculations of this feed network, the ratio of total power at the output ports to the input port is calculated. This ratio is about -9 dB throughout the band. In order to comprehend the loss dynamics, feed network is investigated in AWR® Design Environment™ [18] simulation program and results of this study are given in the next section of this thesis.

4.2 Loss Dynamics of Feed Network

In order to investigate insertion loss of feed network, measurements performed to characterize the circuit elements of feed network are utilized to create subcircuits in AWR® Design Environment™. Data files showing measurement results are imported to the program and then subcircuits are formed by those imported data. An example of 4 way divider subcircuit can be seen in Figure 4.16.

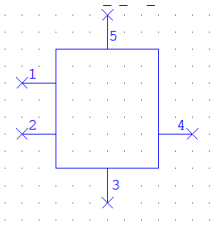

Figure 4.16 4 way divider subcircuit created with measurement data in AWR® Design Environment™

After the creation of all subcircuits required for the simulation designed feed network, simulation model is completed as can be seen in Figure 4.17. In the figure, all sections shown with 2 ports represent cable sections.

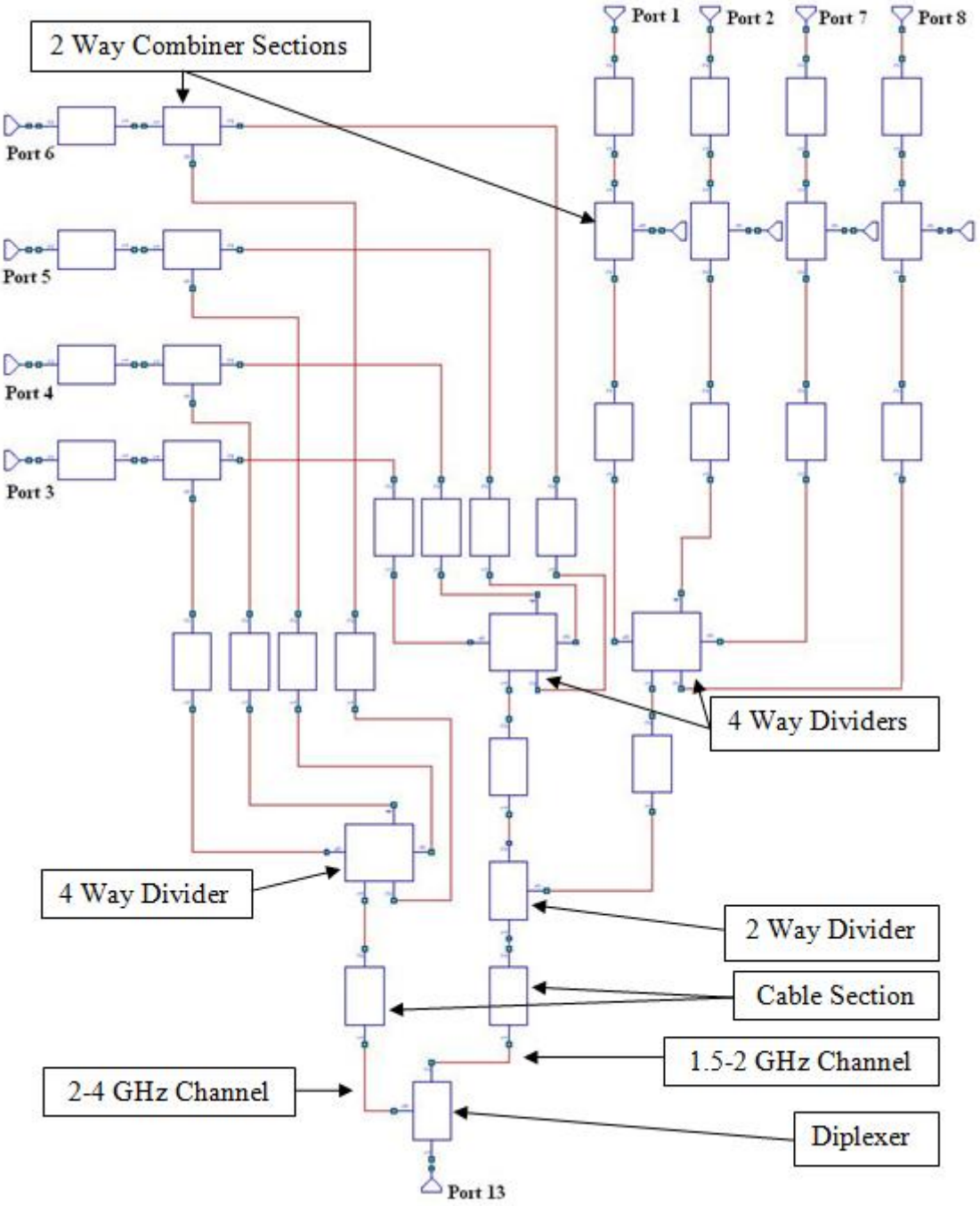

Figure 4.17 Simulation model of feed network

Simulation is performed in AWR® Design Environment™, and the simulation results for input return loss and insertion loss of output ports are given as in Figure 4.18 and Figure 4.19 respectively.

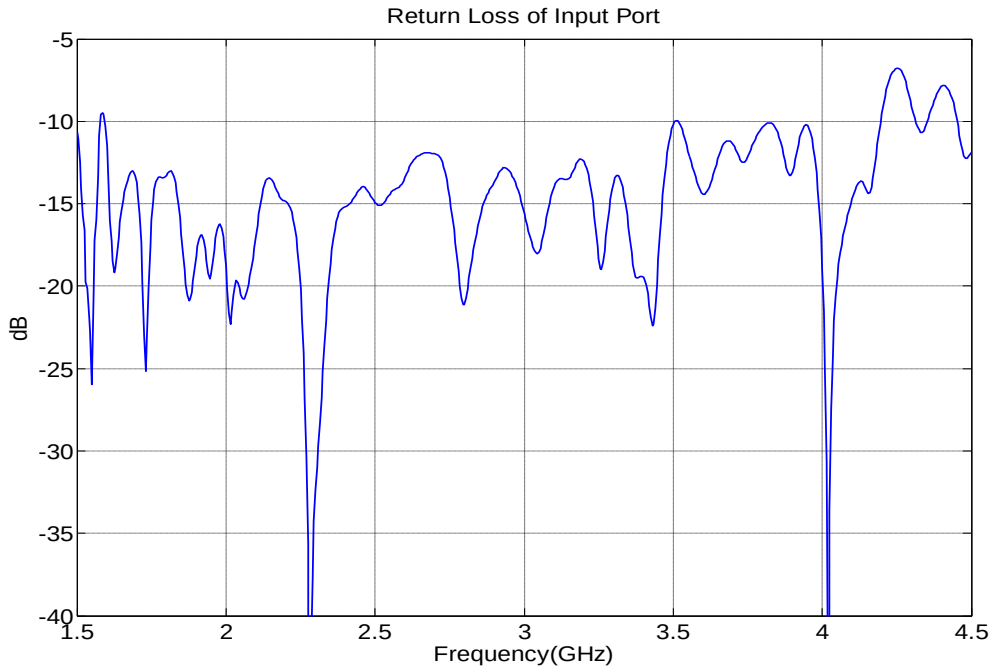

Figure 4.18 Simulation results for return loss of feed network

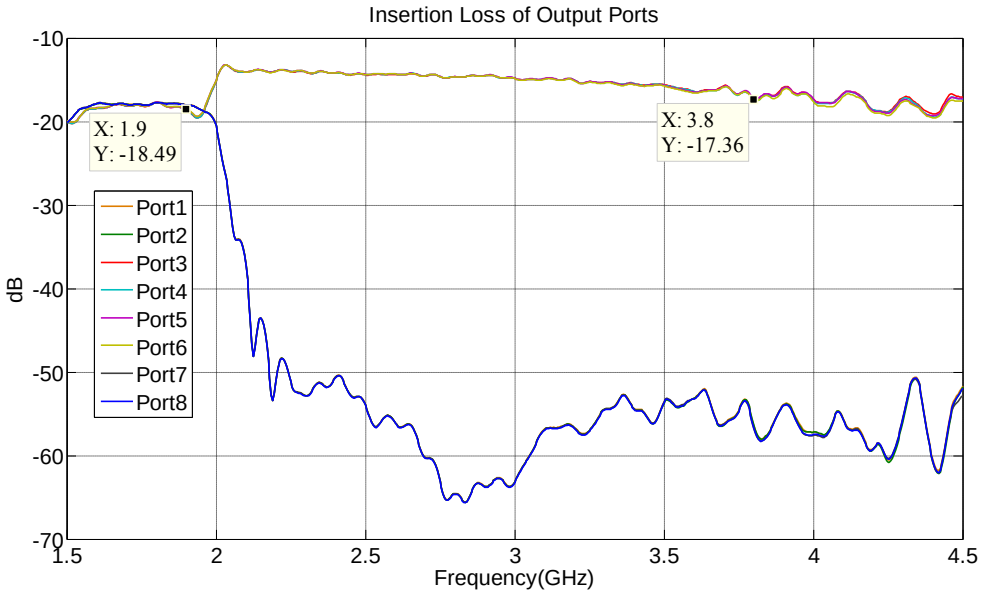

Figure 4.19 Simulation results for insertion loss of output ports of feed network

For input return loss and insertion loss characteristics of output ports in Figure 4.18 and Figure 4.19 are very similar to those in measurements as in Figure 4.15. As a result,

simulation model in AWR® Design Environment™ gives very similar results with the measurement.

In order to compensate for insertion loss of this feed network, some proper choices of elements utilized in feed network are considered. One of these choices is utilization of diplexer rather than 2 way combiner at conjunction of two different frequency channels. Such a choice requires a change in the feed network circuit schema given in Figure 4.20.

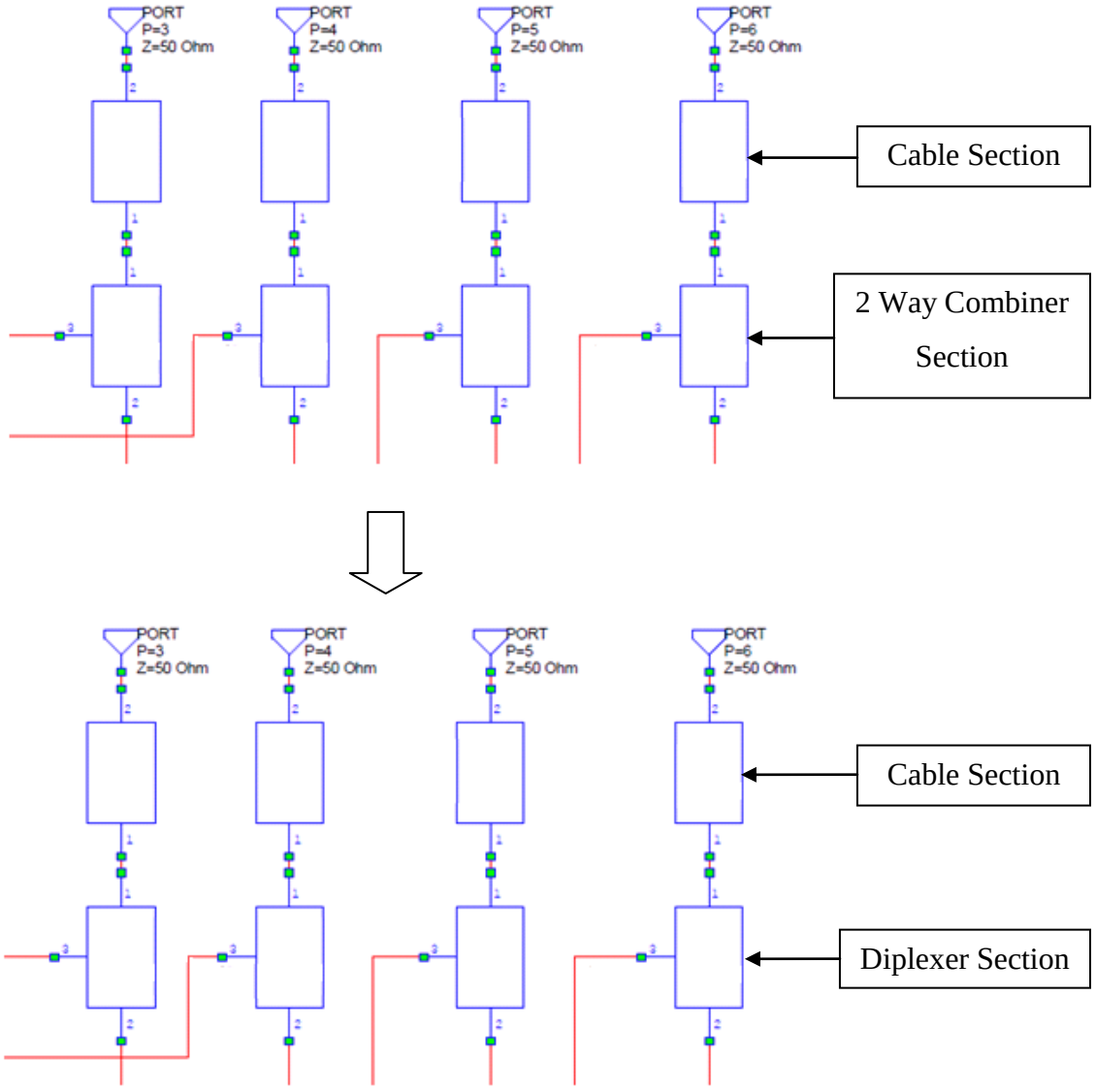

Figure 4.20 Change in simulation model in order to change 2 way combiners with diplexers at conjunction of two different frequency channels

This kind of utilization can compensate for 3 dB or more insertion loss of this feed network. Input return loss and insertion loss of modified feed network can be seen in Figure 4.21 and Figure 4.22 respectively, after the run of simulation model with the mentioned change.

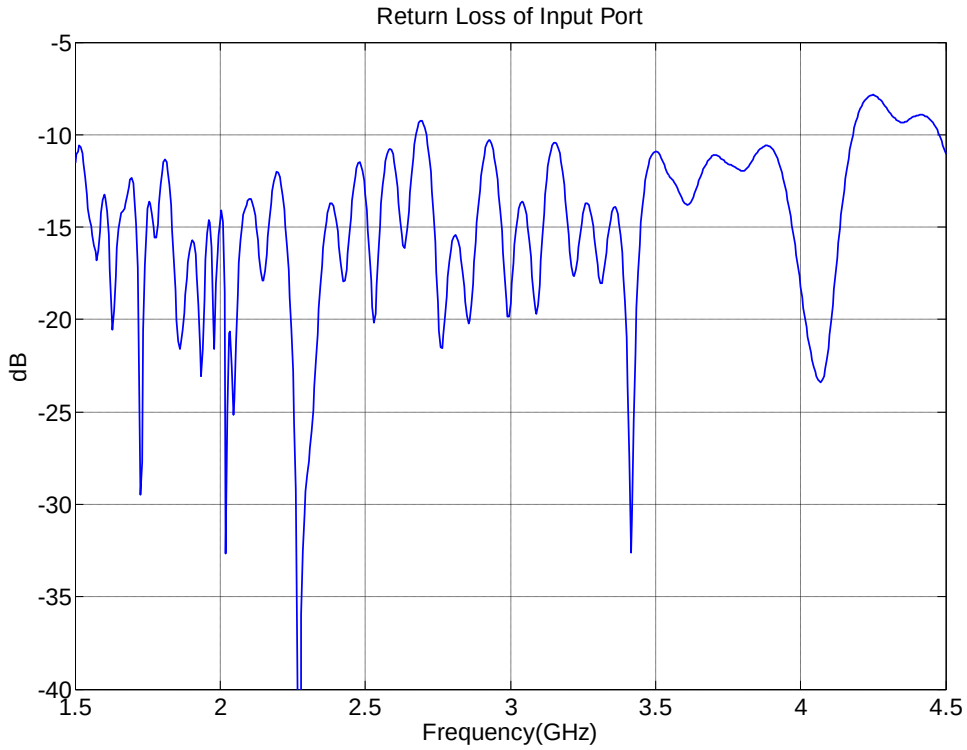

Figure 4.21 Simulation results for return loss of feed network after the change of 2 way combiners with diplexers

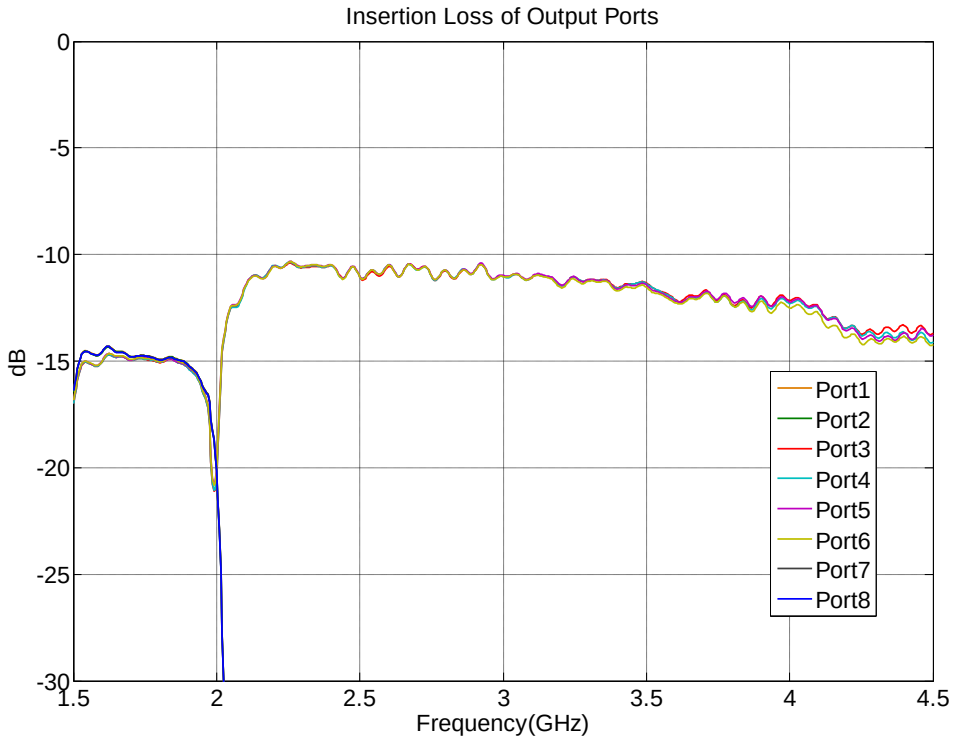

Figure 4.22 Simulation results for insertion loss of output ports in feed network after the change of 2 way combiners with diplexers

With mentioned change of elements in the feed network model, insertion loss of output ports are compensated as expected. This compensation is about 4 dB. The usage of 2 way combiners before the output ports has resulted in such extra loss in feed network. Moreover, input return loss of modified feed network is nearly the same as that of previous feed network. Therefore, utilization of diplexers rather than combiners would be smarter choice for the conjunction of different frequency channels.

After utilizing diplexers at the conjunction of two different frequency channels, another proper choice of elements in the feed network could be utilization of 2 way divider, which exists in 1.5-2 GHz channel, to form 4 way dividers. The reason why this is reasonable is that insertion loss of dividers built with power divider chips is pourer than the mentioned divider especially at high frequencies. Insertion loss performance difference between 2 way divider built with power divider chips and 2 way divider existing in 1.5-2 GHz channel could be seen in Figure 4.7 and Figure 4.11 respectively. The change required to

implement this change in the simulation model of the feed network is given in Figure 4.23 for one of the 4 way dividers in the network. It is noteworthy that 2 stage of 2 way divider with a cable section can form a 4 way divider. This cable section is the same as ones used in the simulation model shown in Figure 4.17.

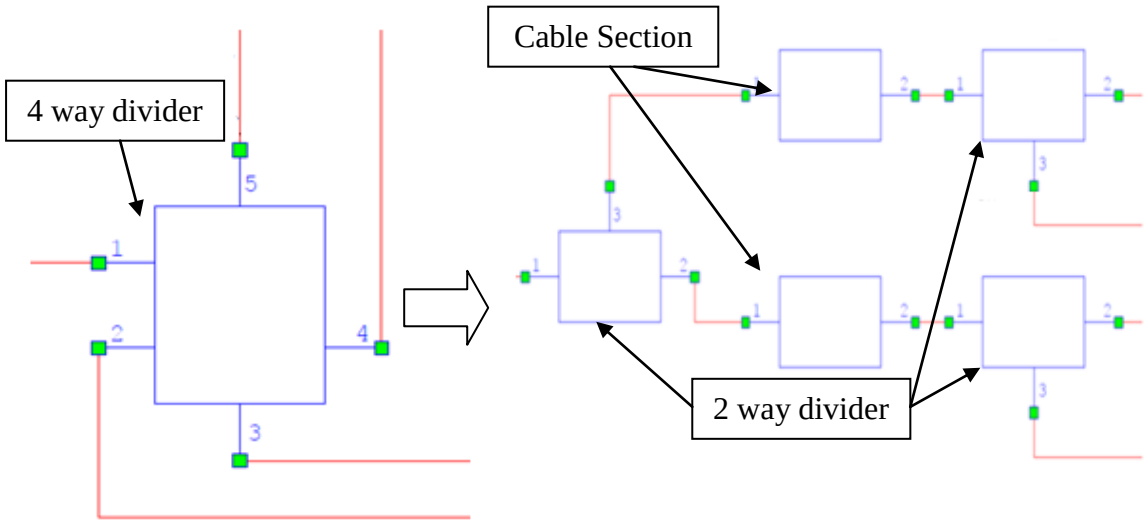

Figure 4.23 Change in simulation model in order to form 4 way dividers with 2 way dividers utilized in 1.5-2 GHz channel

Note that change shown in Figure 4.23 is performed after utilizing diplexer at the conjunction of different frequency channels. Input return loss of modified feed network can be seen in Figure 4.24.

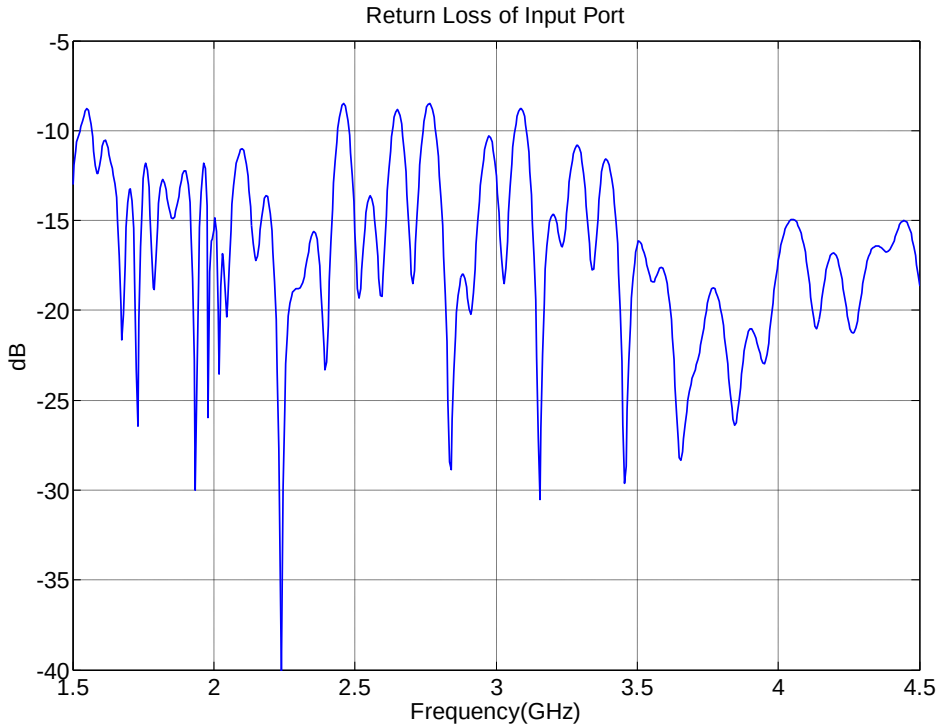

Figure 4.24 Simulation results for return loss of feed network after forming 4 way dividers with 2 way dividers utilized in 1.5-2 GHz channel

As can be seen in Figure 4.24, mentioned change is again reasonable in terms of input return loss. Insertion loss of output ports is given in Figure 4.25.

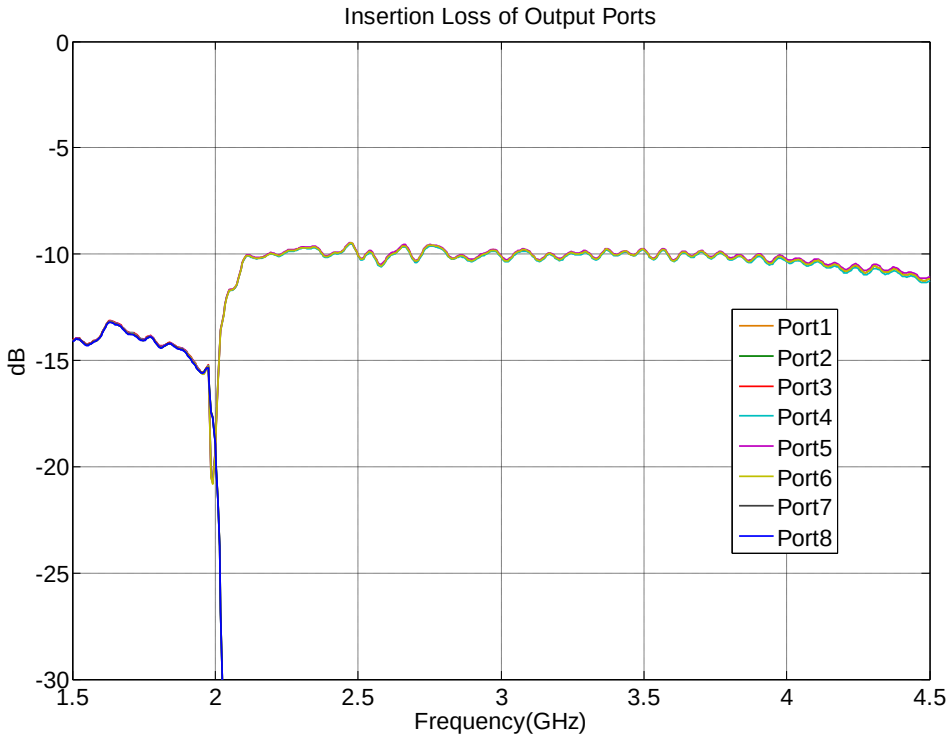

Figure 4.25 Simulation results for insertion loss of output ports in feed network after forming 4 way dividers with 2 way dividers utilized in 1.5-2 GHz channel

With mentioned change of elements in the feed network model, insertion loss of output ports are compensated around 1 dB for 1.5-2 GHz channel, and 2 dB for 2- 4.5 GHz channel. Better compensation at high frequencies with this change is expected since the difference between insertion loss of power divider units and that of 2 way divider existing in the last simulation model increases with increasing frequency in the band. Results show that utilization of 2 way dividers with better insertion loss characteristics instead of power dividing units built with power divider chips outcomes in less insertion loss at the output of the feed network.

4.3 Linear Array Design

A linear array consisting of 8 Vivaldi elements in 1.5-4.5 GHz band is designed in this part of the thesis. Vivaldi antenna was first designed by Gibson [19] with symmetric endfire beam in both E and H planes with moderate gain, and low sidelobes. This antenna basically involves metalized dielectric substrate with an exponentially tapered slot in this

metallization. Thus, it is a tapered slot antenna. Tapered slot antennas are classified as travelling wave antennas. Travelling wave propagation along the antenna structure with a phase velocity under light velocity (v_{ph}<c) can account for high directivity for this antenna.

There is slotline section on Vivaldi antennas. The basic slotline configuration can be seen in Figure 4.26. Height (h), width (b), and permittivity (ϵ_r) of substrate and slot width between metal plates above substrate (w) are important parameters affecting the impedance of slotline section given in Figure 4.26.

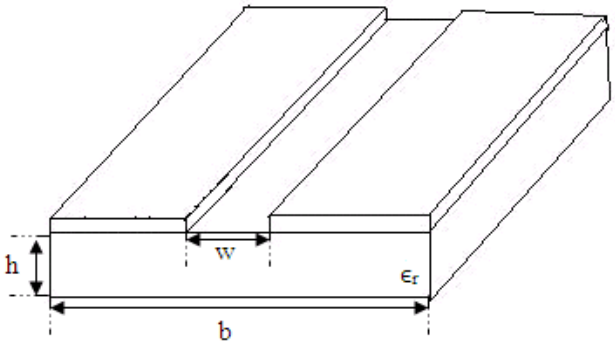

Figure 4.26 Geometric structure of slotline

In order to feed Vivaldi from line, a transition between slotline and the line, from which antenna is fed, is necessary. K. C. Gupta studied many slotline transitions [20]. In this thesis, microstripline is chosen to feed the array. The basic slotline to microstripline transition can be seen in Figure 4.27.

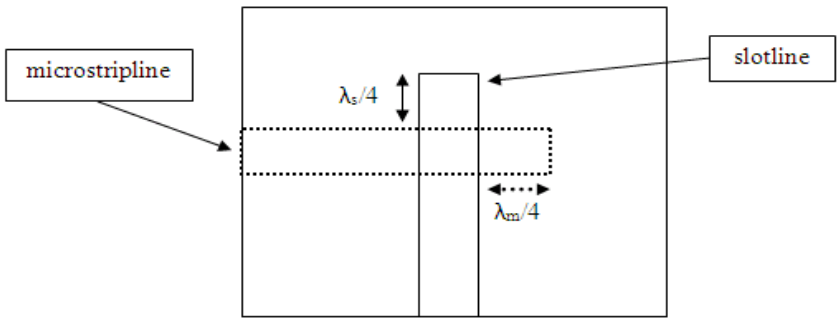

Figure 4.27 Slotline to microstripline transition and equivalent circuit model

Slotline section of Vivaldi starts opening with an exponential rate until the end of substrate after microstrip transition as in Figure 4.28.

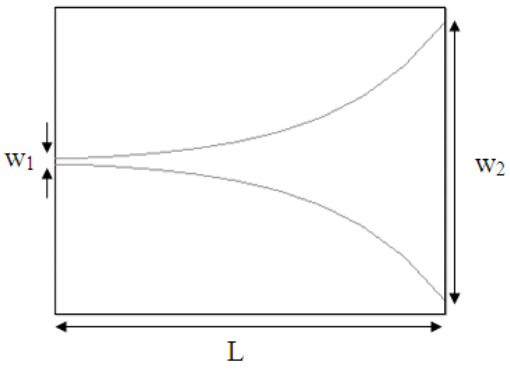

Figure 4.28 Exponential tapered slotline

There are three parameters determining the shape of taper. w_1 is the parameter defined by the microstripline to slotline transmission. w_2 is determined by the frequency band of the antenna. It is determined by λ/2 of the free space wavelength at the minimum operating frequency. This is because of the nonresonant traveling wave mechanism. When the slot width is smaller than λ/2, the velocity of travelling wave is smaller than that of free space and the energy is closely bounded to the surface of the antenna. As the slot width gets λ/2 or larger, phase velocity of the travelling wave reaches to that of free space and the most of the energy is coupled to the air and then radiated. L determines the gain of the antenna. It can affect VSWR of the antenna. The equation of the taper is as the following:

$$y = Ae^{px} + B$$

$$A = \frac{w_2/2 - w_1/2}{e^{pL} - 1} \tag{4.1}$$

$$B = \frac{w_1/2 * e^{pL} - w_2/2}{e^{pL} - 1}$$

where p is the opening rate of the taper.

Single Vivaldi antenna should have nearly λ/2 taper width and λ taper length in order to perform moderately at the frequency of operation. However, an element in antenna array cannot have this size due to element spacing in the array. On the other hand, Vivaldi elements perform better when their taper width is below λ/2 and taper length below λ. This is due mutual coupling between antenna elements. As a result, performance of isolated Vivaldi antennas and Vivaldi antennas in an array are different from each other.

In order to design Vivaldi array, investigating infinite array performance can be smarter way of designing the antenna element since the CPU and requirements of such 3D problems can be very high. Moreover, such problems can last very long for parametric analysis which is very beneficial in designing Vivaldi antennas. In this thesis, Ansoft HFSS^{TM} [21] simulation program is utilized to design Vivaldi antenna element in infinite array. Ansoft HFSS^{TM} allows user to employ periodic boundary conditions through which the periodicity of the array can be defined. Boundaries of the element are defined as master and slave. The phase of slave boundary can be defined as a parameter of the master boundary in order to investigate the scan performance. In this problem, same phases are set for master and slave boundaries, so broadside performance of the array is analyzed. Non periodic boundaries are far from the radiating element in order to absorb unwanted reflections. Infinite model of array antenna is given in Figure 4.29.

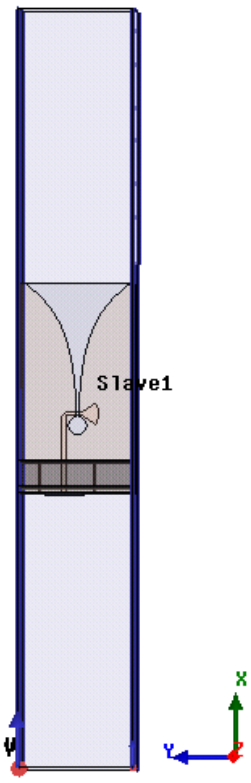

Figure 4.29 Infinite array model of Vivaldi antenna

Infinite array model does not only include the antenna but also the mechanics that can be used in realization of the antenna. Ground plane made of aluminum with 5 mm, and ECCOSORB® LS24 [22] absorber with 0.375 inch thickness that is used in front of this plane to absorb unwanted reflections from ground plane are those mentioned mechanics. Figure 4.30 shows antenna and the mechanics of the array in infinite array model.

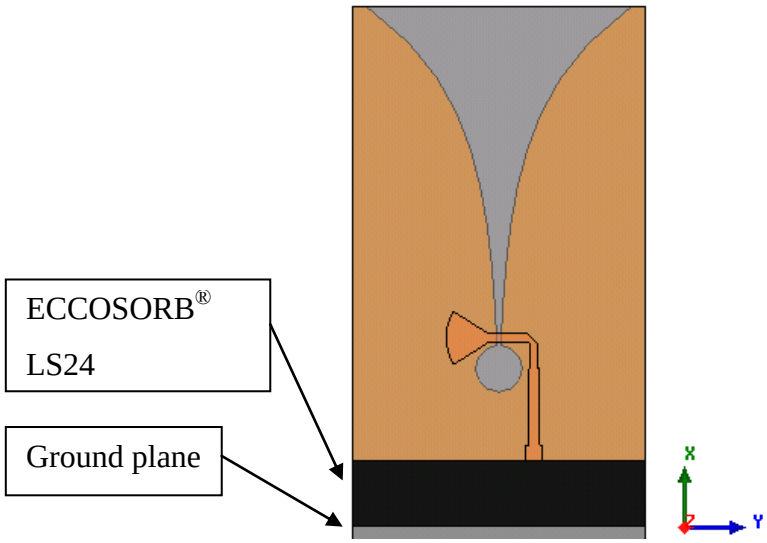

Figure 4.30 Antenna and the mechanics in the infinite array model

For substrate material of this antenna, RT/duroid® 5880 with ϵ_r=2.2 and thickness 31 mil is selected [23]. Microstripline to slotline transmission on the substrate can be seen in Figure 4.31. Microstripline section consists of 4 sections and it ends with an open circuit. Three of them are linear sections with different lengths and widths in order to have a better match to 50Ω feeding line. First section is the radial section ending with open circuit. Second section has a 90° turn with a miter. Slotline has a circular section and it ends with a short circuit. Circular slotline is matched to 50Ω microstripline (4th section), with different shaped sections, i.e. with different impedance sections. Width, length, radius and diameter of all these sections were optimized by genetic algorithm inside Ansoft HFSS™.

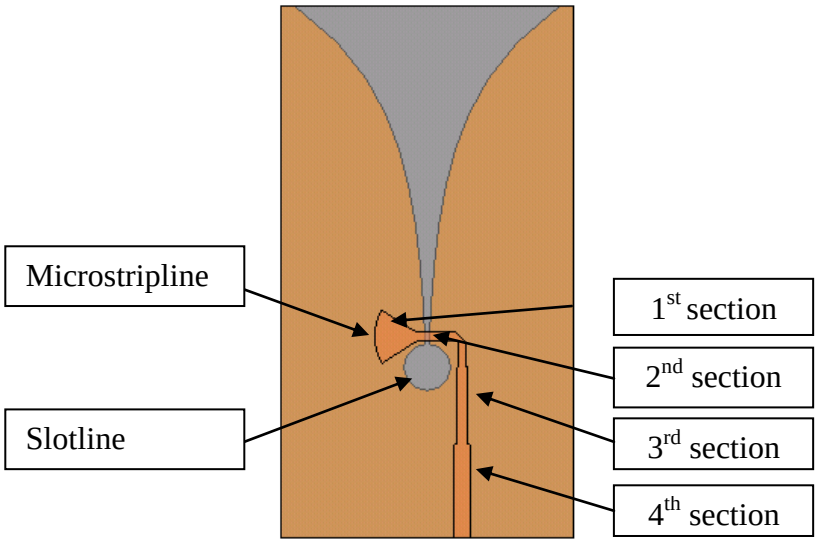

Figure 4.31 Feed design of Vivaldi antenna

Return loss of Vivaldi antenna that is used in finite array can be seen in Figure 4.32.

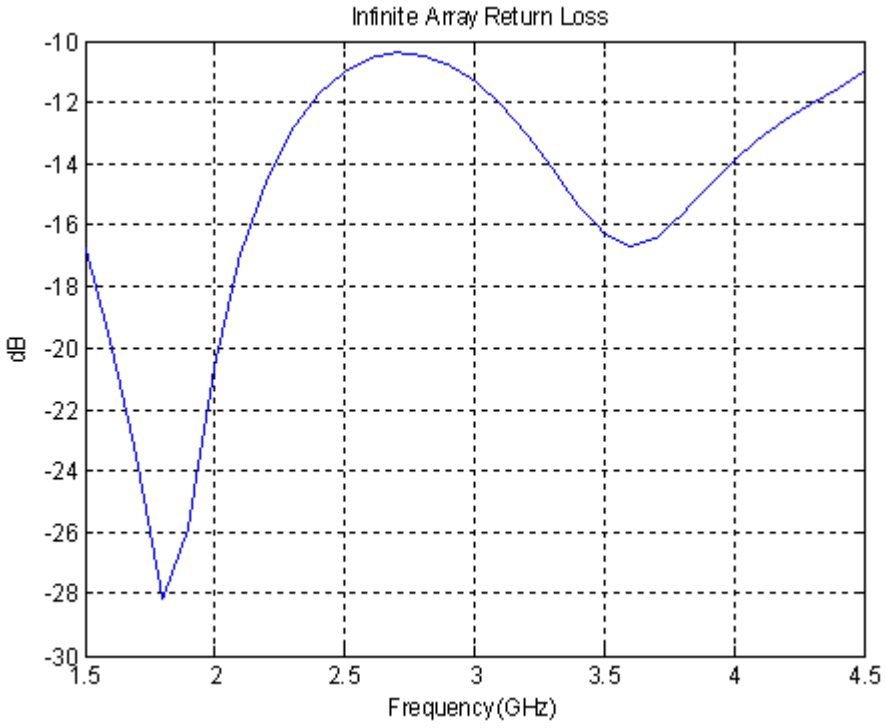

Figure 4.32 Return loss of Vivaldi antenna in infinite array

A linear array of 8 elements with this designed element is modeled to investigate the finite array characteristics. Designed array can be seen in Figure 4.33.

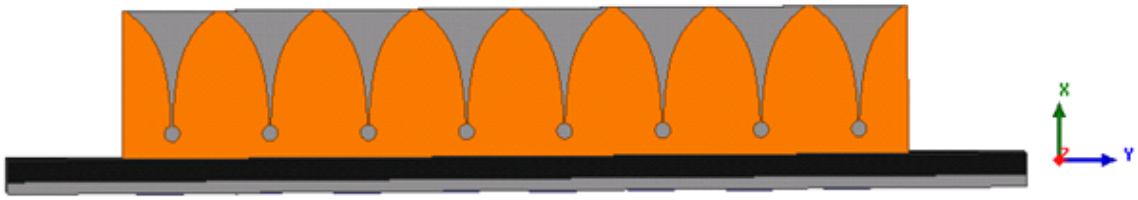

Figure 4.33 Designed linear array with Vivaldi elements

Active S parameters of this finite array are found to be higher than return loss of infinite array in simulation. Although return loss of infinite array is below -10 dB at frequencies below 2 GHz, active S parameters of elements in linear array is worse than this value. Simulation results of S parameters can be seen in Figure 4.34. Array elements perform better for frequencies above 1.8 GHz.

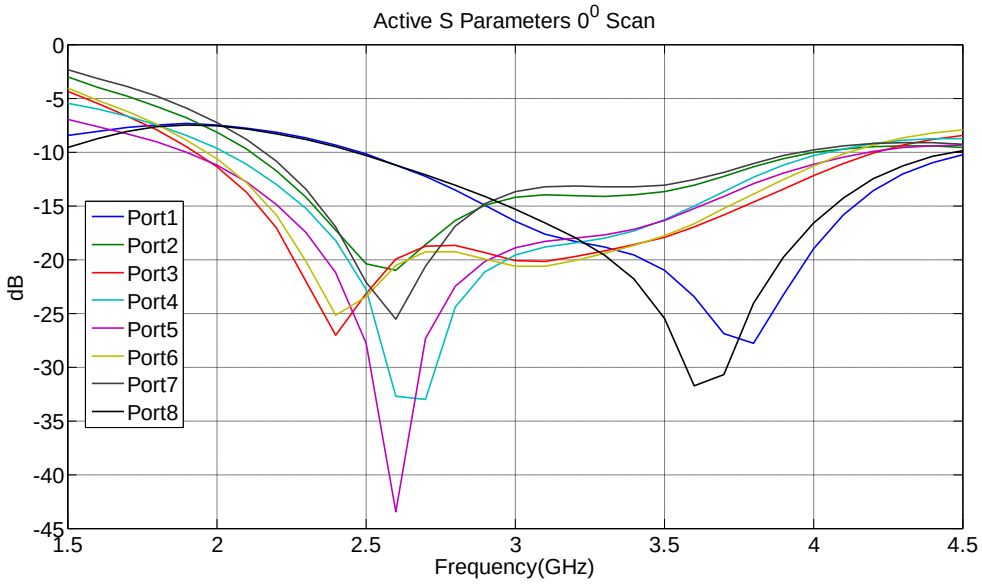

Figure 4.34 Active S parameter of 8 element Vivaldi array

In order to see the performance of this designed array with changing active region, element excitation coefficients are adjusted. The mentioned performance is investigated for frequencies 1.9 and 3.8 GHz frequencies in simulation. For 1.9 GHz frequency all the element coefficients are set to 1, i.e. all elements are active at this frequency. For

3.8 GHz, only 4 elements neighboring the center of the array are active. Array pattern and gain can be seen in Figure 4.35 with these changes.

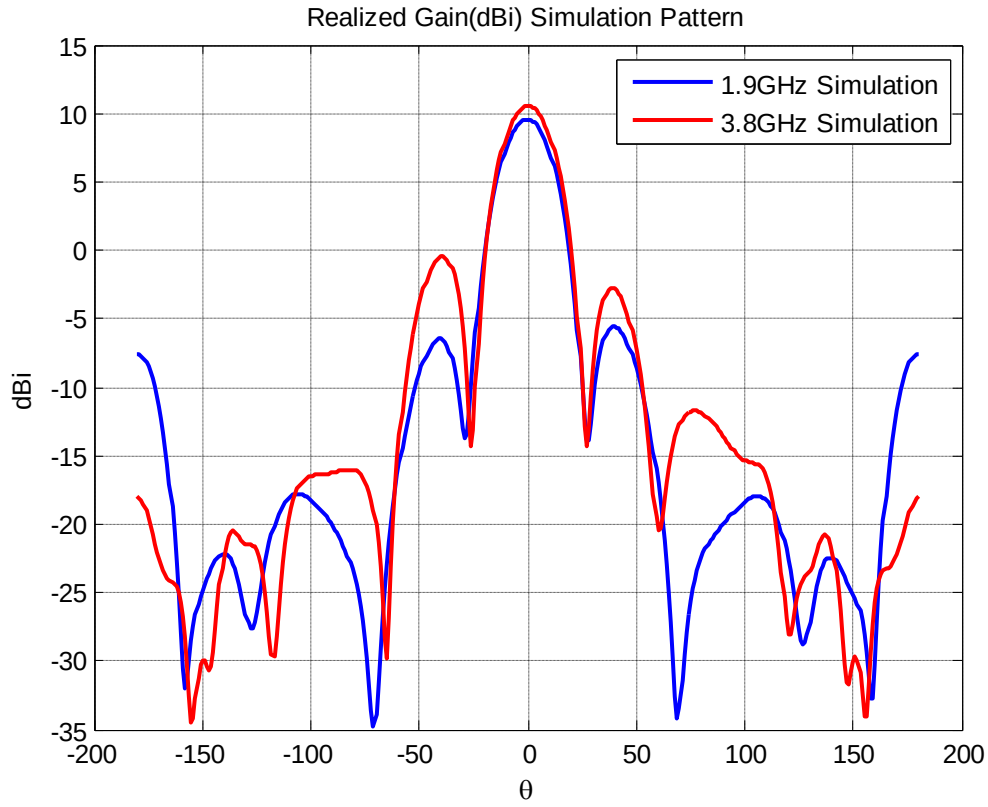

Figure 4.35 Array performance in simulation with implementation of changing active region

Pattern in frequencies 1.9 and 3.8 GHz are very similar in terms of main beam, beamwidth, gain and sidelobe as can be seen in Figure 4.35. As a result, this linear array is manufactured in order to see the required function of the feed network.

After the antenna is manufactured it is important to make some tests in order to check whether the production quality of antenna is good. Measuring S parameters are one of such tests. This antenna's S parameters are measured with a network analyzer [24] and these parameters are compared with simulation. In order to measure S parameter of one element in the array, return loss of this element and mutual coupling of this element with other elements must be measured. These measurements for each element can be regarded

as passive S measurements. During these measurements, other elements are terminated with 50Ω matched load. Figure 4.36 shows the distribution of loads, during passive S parameter measurement for one the ports.

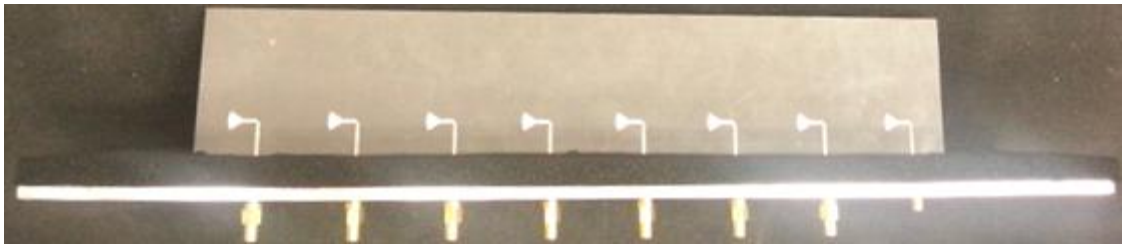

Figure 4.36 Passive S parameter measurement of linear array

After all required passive S measurements are performed, active S parameters of each element are calculated according to (4.2),

$$S_m = \sum_{n=1}^{8} \frac{a_n * S_{mn} * e^{j\phi_n}}{a_m * e^{j\phi_m}} \qquad (4.2)$$

where S_m is active S parameter of m^{th} element. a_m and a_n are the excitation coefficients of m^{th} and n^{th} element and ϕ_m and ϕ_n are the excitation phase of m^{th} and n^{th} element in radians respectively. S_{mn} is mutual coupling between m^{th} and nth element, which is one of the passive S parameters. In calculations, a_m and a_n are set to 1 assuming the uniform excitation of array. Moreover ϕ_m and ϕ_n are 0 due to 0° scan.

Result of this measurement is given in Figure 4.37. Measurements and simulation results are very close, so linear array can operate as expected after production.

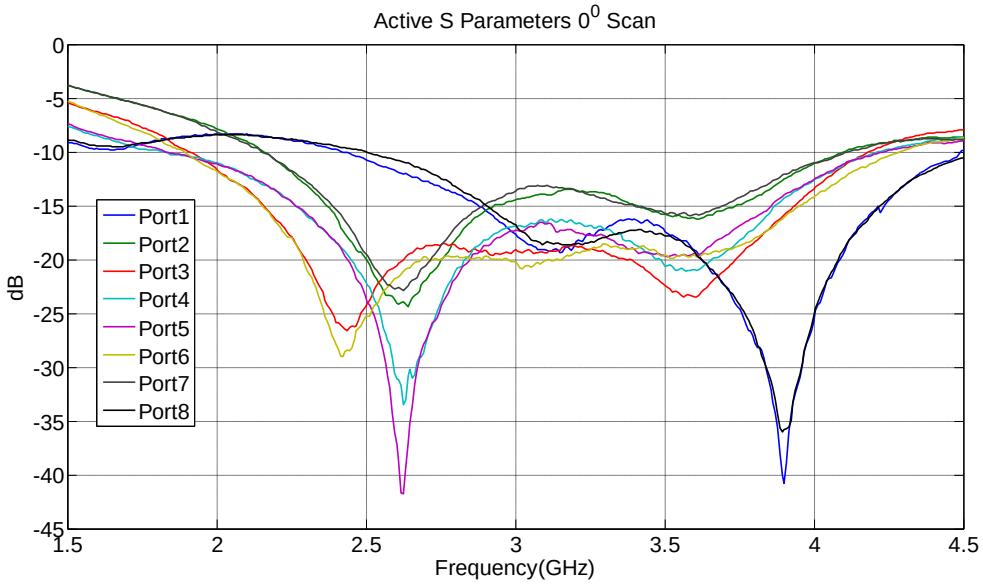

Figure 4.37 Measured active S parameters of Vivaldi array

4.4 Measurement Results

Designed feed network and linear array are integrated before the measurement as in Figure 4.38.

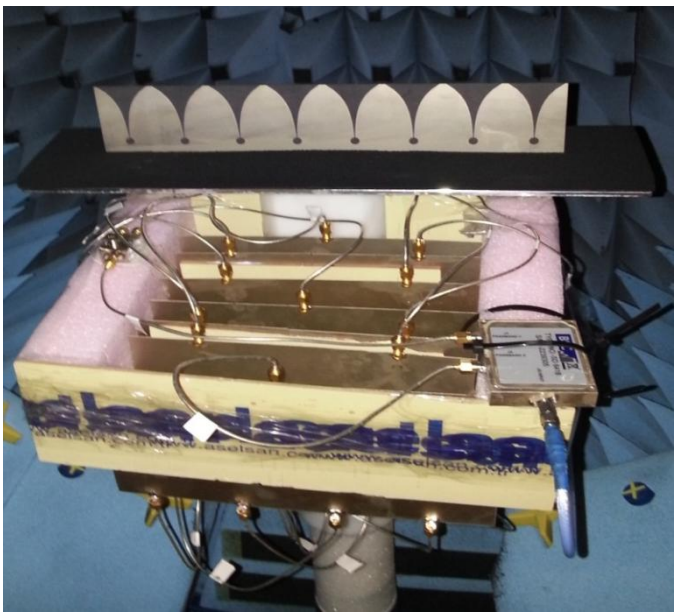

Figure 4.38 Integration of feed network and Vivaldi array in antenna measurement system

Measurement is performed in 1.5-4.5 GHz band for 0° scan in azimuth plane in SATIMO spherical near field antenna measurement system [25]. Then, measurements are compared with simulation in terms of pattern shape and gain of the antenna. Normalized patterns in simulation and measurement can be seen in Figure 4.39. Note that simulation patterns are gathered from simulation in which antenna elements are excited with coefficients that are taken from measurement data of the feed network.

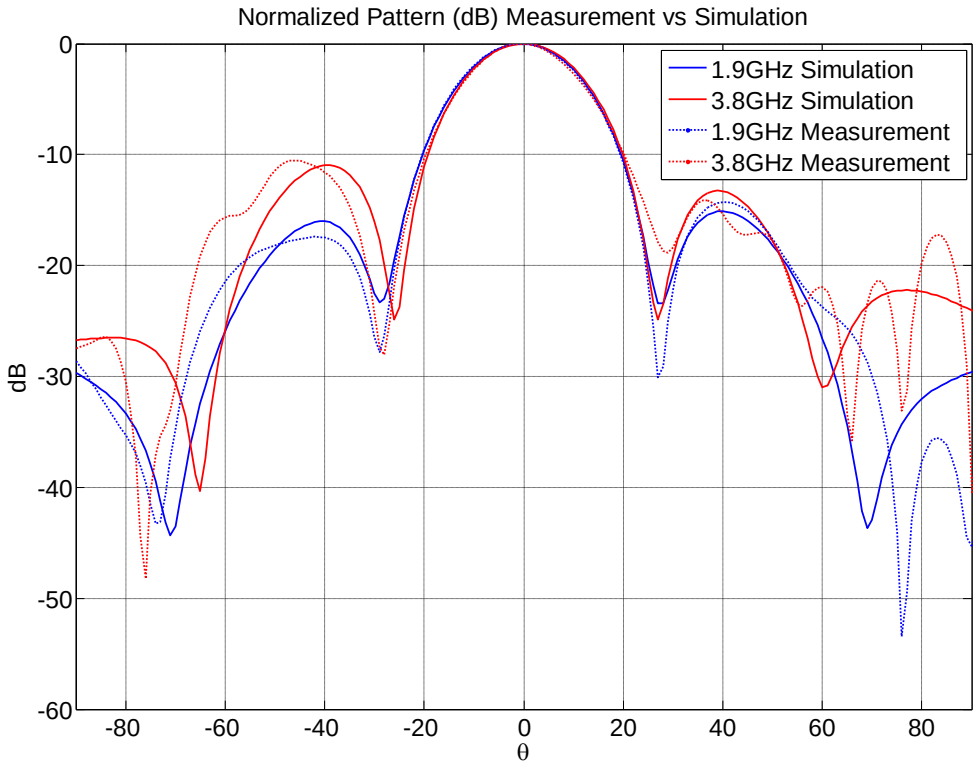

Figure 4.39 Normalized patterns in simulation and measurement

Normalized patterns in simulation and measurement are very similar as seen in Figure 4.39. In order to find the gain of linear array at those frequencies, some calculations about the insertion loss of feed network has to be performed at 1.9 and 3.8 GHz because the measurement system is not calibrated with the feed network. In loss calculations, it is assumed that all power supplied by the feed network is delivered to the antenna array with no return loss. This assumption is valid due to good active S performance of the antenna array at those frequencies. Feed network loss, L_{fn} (dB), is defined in (4.3), where

$S_{m,i}$ represents insertion loss between m^{th} output port and input port. Feed network loss is calculated by summation of insertion loss of all ports at a single frequency.

$$L_{fn}(dB) = 10\log10\left(\sum_{m=1}^{8}|S_{m,i}|^2\right) \quad (4.3)$$

L_{fn} (dB) at 1.9 and 3.8 GHz is added to the gain measured from the system at these frequencies. After this loss correction, gain values can be seen in Figure 4.40.

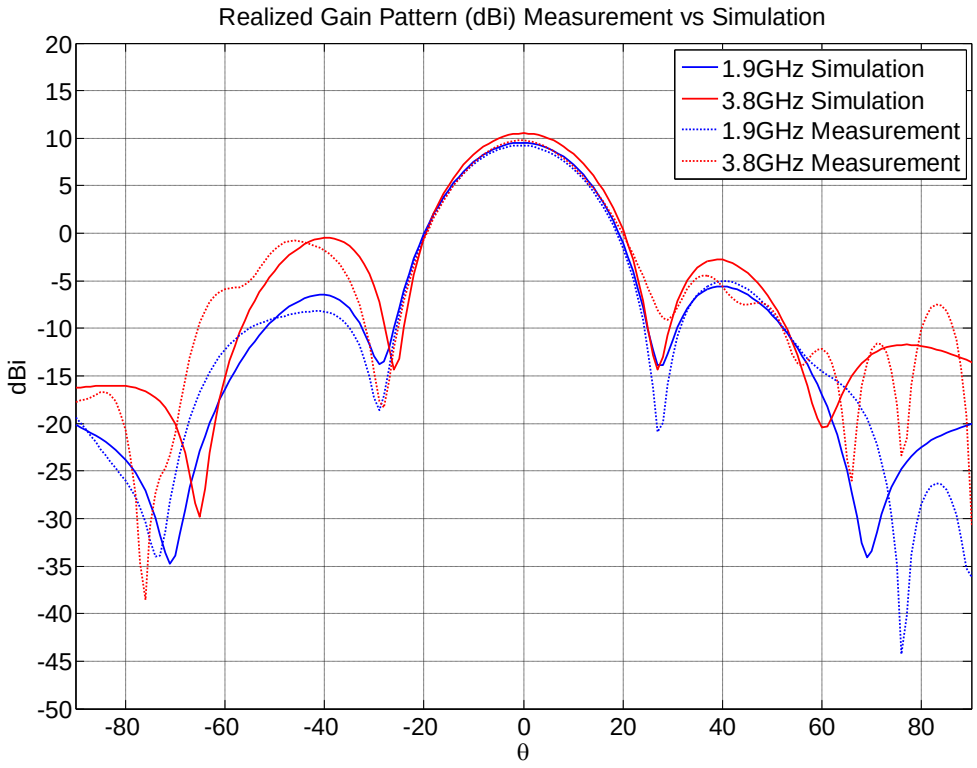

Figure 4.40 Realized gain of linear array in simulation and measurement

In simulation, gain of the linear array is 9.5 and 10.5 dBi at frequencies 1.9 and 3.8 GHz respectively. From measurements, they are calculated as 9.22 and 9.75 dBi. As a result, antenna operation at 1.9 and 3.8 GHz is nearly frequency independent.

CHAPTER 5

CONCLUSIONS

Two methods of wideband array design are studied. The aim of this study is to investigate arrays designed with these methods in terms of wideband behavior. Studies with genetic algorithm and wavelength scaled array concept are performed. Each of these techniques is evaluated by array designs and performance of these designs in wide frequency bands. Moreover, a feed network performing adaptive aperture regions for a linear array with changing frequency is designed. Function of this feed network is also tested with a linear array.

Genetic algorithm is the first method investigated in this thesis. Genetic algorithm is utilized for array antennas with aperiodic spacing to optimize element positions for optimum sidelobe levels and also minimum beamwidth change in operating band. Linear and circular arrays are designed during this study. -23 dB sidelobe levels are achieved for linear array with a minimum of 0.375λ spacing at the design frequency. However, this level is seen to increase up to -10 dB with increasing frequency. Then, this level is optimized to -18 dB within f_0-1.5f_0 with a change in the error criterion of the algorithm. Increasing the minimum element spacing in linear array also increases the sidelobe level at the design frequency. For example, sidelobe level could be optimized to -19 dB rather than -23 dB by increasing the minimum spacing of the array from 0.375λ to 0.5λ. This level is optimized to -17 dB within f_0-1.5f_0 with application of algorithm with the modified error criterion. Algorithm used in designing linear arrays is also applied to circular arrays. Array patterns demonstrating nearly -30 dB Taylor distribution is achieved. Array pattern satisfies -30 dB for sidelobes near mainlobe but can increase up to -25 dB for other sidelobes in the visible space. Besides sidelobe level optimization,

beamwidth optimization is also performed. There is also -13 dB sidelobe level requirement from the patterns so that no grating lobe can exist in them. After the optimization is finished, patterns for linear array satisfy -13 dB sidelobe level requirement. On the other hand, they show that half power beamwidth of the array scales inversely with changing frequency.

Second method which is investigated in this thesis is wavelength scaled array concept. Firstly, in order to examine array factors in the design, GUIs are designed in MATLAB® environment. Some examples of designed wavelength scaled arrays are studied with those GUIs. Frequency independent radiation of those examples is verified with the pattern and beamwidth values gathered from MATLAB®. With wavelength scaled array concept, it was noted that number of elements in array can be smaller than that of an array designed with conventional array design concept, i.e. constant element size and constant inter element spacing. Comparison of this method with conventional concept is performed for different operational bandwidth for linear array. Results show that advantage of wavelength scaled array design concept increases with increasing bandwidth.

In the fourth section of the thesis, realization of a linear array with changing active region with frequency is studied. This concept requires a feed network with switching abilities. Active region of linear array must be adjusted with respect to frequency. For these capabilities of the feed network, a diplexer is utilized, operating in 1-12 GHz band where two channels are separated at 2 GHz. In addition, the feed network also includes 2 way and 4 way power dividers and combiners. For the radiator, a manufactured linear array with 8 Vivaldi elements is used. This array can operate in 1.5-4.5 GHz band. Feed network is measured with network analyzer and its switching characteristic is confirmed with insertion loss measurements. In addition, input insertion loss and output phase difference characteristics of this feed network are also measured for the characterization. Improvement in these characteristics is also investigated in AWR® Design Environment™. In the end of this study, it is concluded that, insertion loss of this network could be less with proper choice of elements in the network. Moreover, these measurements are used in order to set the amplitude coefficients in HFSS™ simulation. Some comparison is performed at the different operating frequencies of the array antenna.

Nearly independent frequency radiation characteristics are observed in simulation results. Pattern measurements of array antenna with this feed network are performed. From the results, it is seen that it is possible to realize an array with changing active region with the designed feed network.

As a result of all studies mentioned, genetic algorithm and wavelength scaled array are suitable methods for wideband array design. These methods demand some future works. It will be inspiring to realize a linear array with aperiodic spacing whose element positions are optimized using genetic algorithm for desired sidelobe level and beamwidth at the design frequency. More linear arrays with different minimum element spacing and bandwidth requirements could be realized in order to see the effects of some parameters in the design mentioned in Chapter 2. Vivaldi antennas could be good candidate for element choice of such arrays. Feed network of such an array should require only dividers and cables due to uniform feeding. Such a realization is also required for wavelength scaled array which is investigated in Chapter 3. However, feed network of such an array could be very complex due to adaptive active region of such arrays as mentioned in Chapter 4. Such a feed network could require design of RF components such as diplexer, multi port dividers and combiners. Therefore, not only array design but also feed network design is crucial for this method. Return loss performance of such an array for both methods could be challenging. For array design, full wave analysis should be investigated with simulation software.

REFERENCES

[1] R. Gunnarsson et al., "Comparison of Wideband Phased Array Concepts for Achieving Frequency Independent Radiation Characteristics", *IEEE Radar Conference, 2008*, pp. 1-6, May 2008.

[2] V. H. Rumsey et al., "Directive Frequency Independent Arrays", *IEEE Transactions on Antennas and Propagation*, Vol. 13, No. 5, pp. 807-809, September 1965.

[3] James K. Breakall, "The Three Dimensional Frequency-Independent Phased Array (3D-FIPA)", *Ninth International Conference on Antennas and Propagation*, Vol. 1, No. 407, pp. 9-11, April 1995.

[4] B. Cantrell et al., "Wideband array antenna concept", *2005 IEEE International Radar Conference*, pp. 680 – 684, May 2005.

[5] Rick W. Kindt et al., "Preliminary Investigations of a Low-Cost Ultrawideband Array Concept", *IEEE Transactions on Antennas and Propagations*, Vol. 57, No. 12, pp. 3791-3799, December 2009.

[6] Rick W. Kindt, "Prototype Design of a Modular Ultrawideband Wavelength-Scaled Array of Flared Notches", *IEEE Transactions on Antennas and Propagation*, Vol. 60, No. 3, pp. 1320-1328, March 2012.

[7] R. G. Hohlfeld and N. Cohen, "Genetic Optimization of Sparse, Frequency Invariant Arrays Using the HCR Principle", *IEEE International Symposium on Phased Array Systems and Technology*, pp. 588-593, October 2003.

[8] R. G. Hohlfeld and N. Cohen, "Self-Similarity and the Geometric Requirements for Frequency Independence in Antennae", Fractals, Vol. 7, pp. 79-84, 1999.

[9] Micah D. Gregory and Douglas H. Werner, "Ultrawideband Aperiodic Antenna Arrays Based on Optimized Raised Power Series Representations", *IEEE Transactions on Antennas and Propagation*, Vol. 58, No. 3, pp. 756-764, March 2010.

[10] Ren et al., "Synthesis of Non-Uniformly Spaced Arrays Using the Fourier Transform and Window Techniques", *IET Microwaves, Antennas & Propagation*, Vol. 3, No. 8, pp. 1245-1253, December 2009.

[11] Milligan, T. A., "Space-Tapered Circular (Ring) Array", *IEEE Antennas and Propagation Magazine*, Vol. 46, No. 3, June 2004.

[12] MATLAB® GUI, <http://www.mathworks.com/discovery/matlab-gui.html>, last accessed on 24/12/2013.

[13] MATLAB®, <http://www.mathworks.com>, last accessed on 24/12/2013.

[14] SD 6418 diplexer information, <http://www.bscfilters.com/>, last accessed on 24/12/2013.

[15] RO4003® information, <http://www.rogerscorp.com/documents/726/acm/RO4000-Laminates---Data-sheet.pdf>, last accessed on 24/12/2013.

[16] Minicircuits power splitter/combiner information, <http://217.34.103.131/pdfs/GP2Y1+.pdf>, last accessed on 24/12/2013.

[17] SUCOFORM® cable information, <http://www.hubersuhner.com/ProdDet/2477980>, last accessed on 24/12/2013.

[18] AWR® Design Environment™, <http://www.awrcorp.com/sites/default/files/BR-MWO-2013.01.09.pdf>, last accessed on 24/12/2013.

[19] Gibson, P. J., "The Vivaldi Aerial", *9th European Microwave Conference*, 1979.

[20] Gupta, K. C., "Microstriplines and Slotlines", Artech House 1979.

[21] Ansoft HFSS™, <http://www.ansys.com/staticassets/ANSYS/staticassets/resourcelibrary/brochure/ansys-hfss-brochure-14.0.pdf>, last accessed on 24/12/2013.

[22] ECCOSORB® LS24 information, <http://www.eccosorb.com/Collateral/Documents/English-US/LS.pdf>, last accessed on 24/12/2013.

[23] RT/duroid® 5880 information, <http://www.rogerscorp.com/documents/606/acm/RT-duroid-5870-5880-Data-Sheet.pdf>, last accessed on 24/12/2013.

[24] Agilent Technologies, <http://www.home.agilent.com/en/pd-1350013-pn-E8363C/pna-microwave-network-analyzer?cc=TR&lc=eng>, last accessed on 24/12/2013.

[25] SATIMO antenna measurement system, <http://www.satimo.com/content/products/starlab>, last accessed on 24/12/2013.

[26] Touchstone file format, < https://awrcorp.com/download/faq/english/docs/Users_Guide/data_files.html>, last accessed on 24/12/2013.

APPENDIX A

SIMULATIONS FOR ANALYSIS AND IMPROVEMENT OF INSERTION LOSS OF FEED NETWORK

For the analysis and improvement of insertion loss of feed network, AWR® Design Environment™ is utilized [18]. In this thesis, analysis of the designed feed network is performed via Microwave Office™ software. Moreover, effect of changing element in some parts of the feed network is also studied for the improvement of insertion loss.

Each component in feed network is measured with network analyzer [24] in obtain S parameters which are utilized in Microwave Office™ to create simulation model of this components. S parameter data are saved in network analyzer menu as touchstone file format [26]. Then, those saved files are imported in Microwave Office™ to create subcircuits. An example of imported data for 3 port diplexer can be seen in Figure A.1.

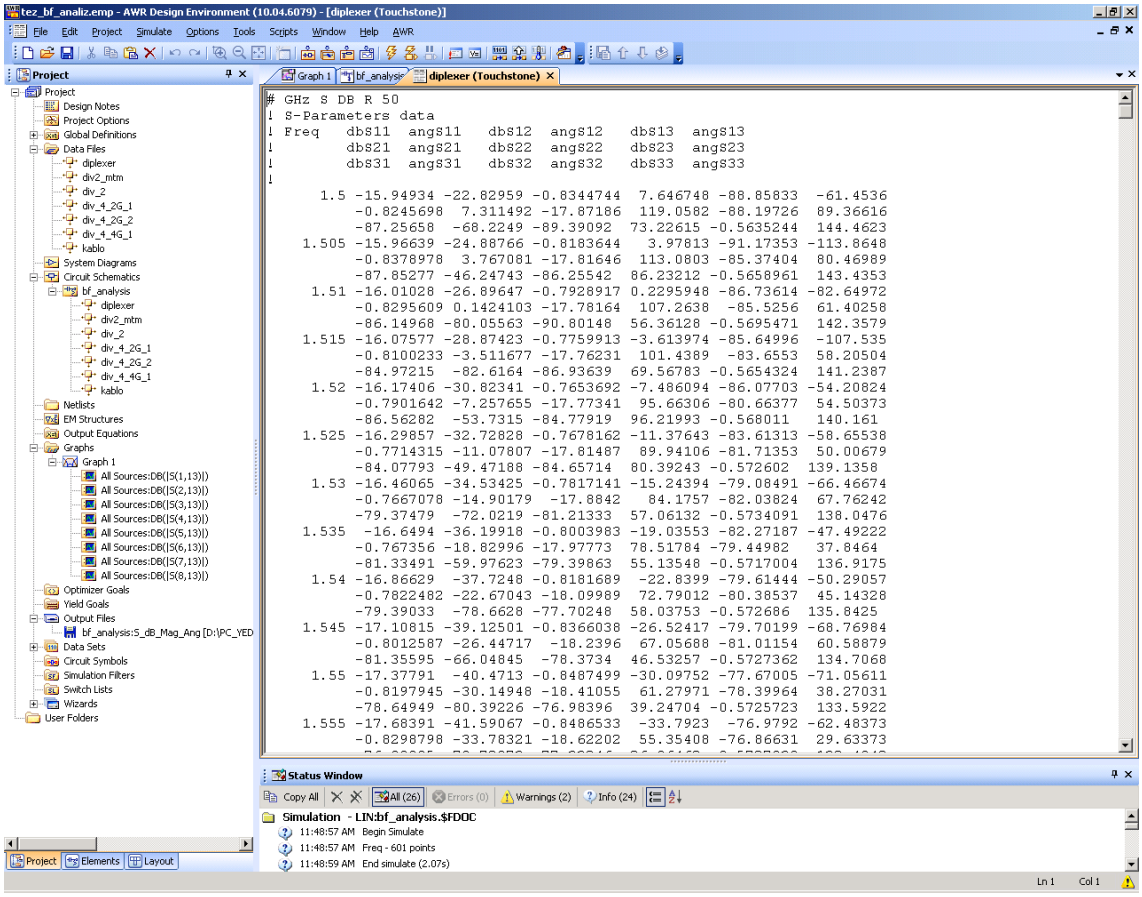

Figure A.1 Imported data for 3 port diplexer

After the import of S parameter data, subcircuit of the measured component can be created using Add Subcircuit Element box as in Figure A.2. Details of this box can be seen in Figure A.3.

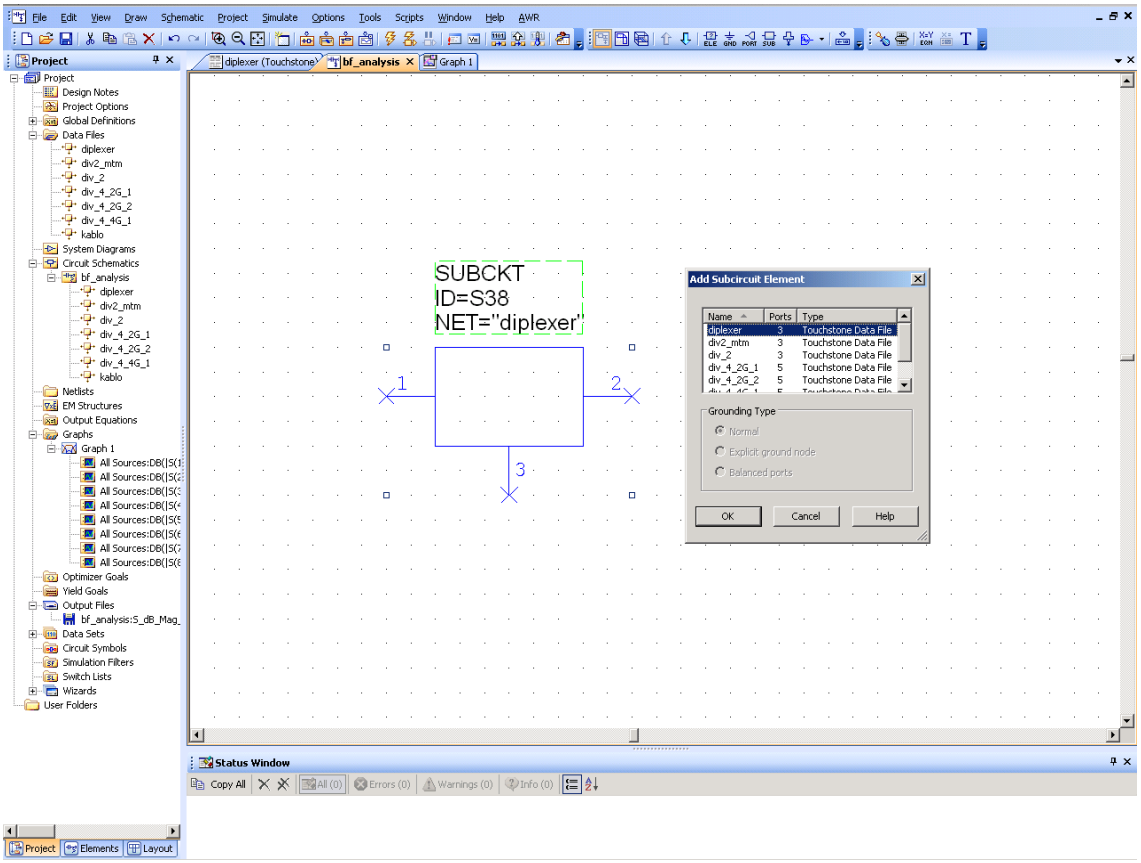

Figure A.2 Creating subcircuit from the imported data

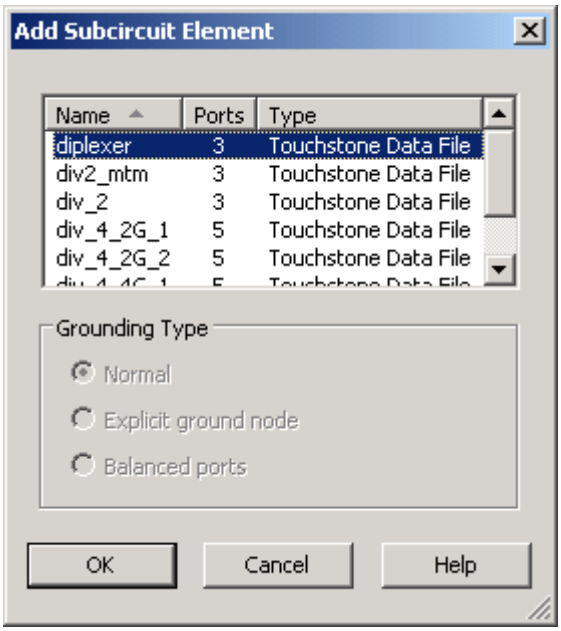

Figure A.3 Add subcircuit element box

As can be seen, there are components with different names and ports in Add Subcircuit Element box. Number of ports for a component which is created from imported data is dependent on the format of touchstone data file.

Each component in feed network in Chapter 4 is created in the same way as the diplexer shown in Figure A.3. Finally, schematic of the feed network in Microwave Office™ is created as seen in Figure A.4.

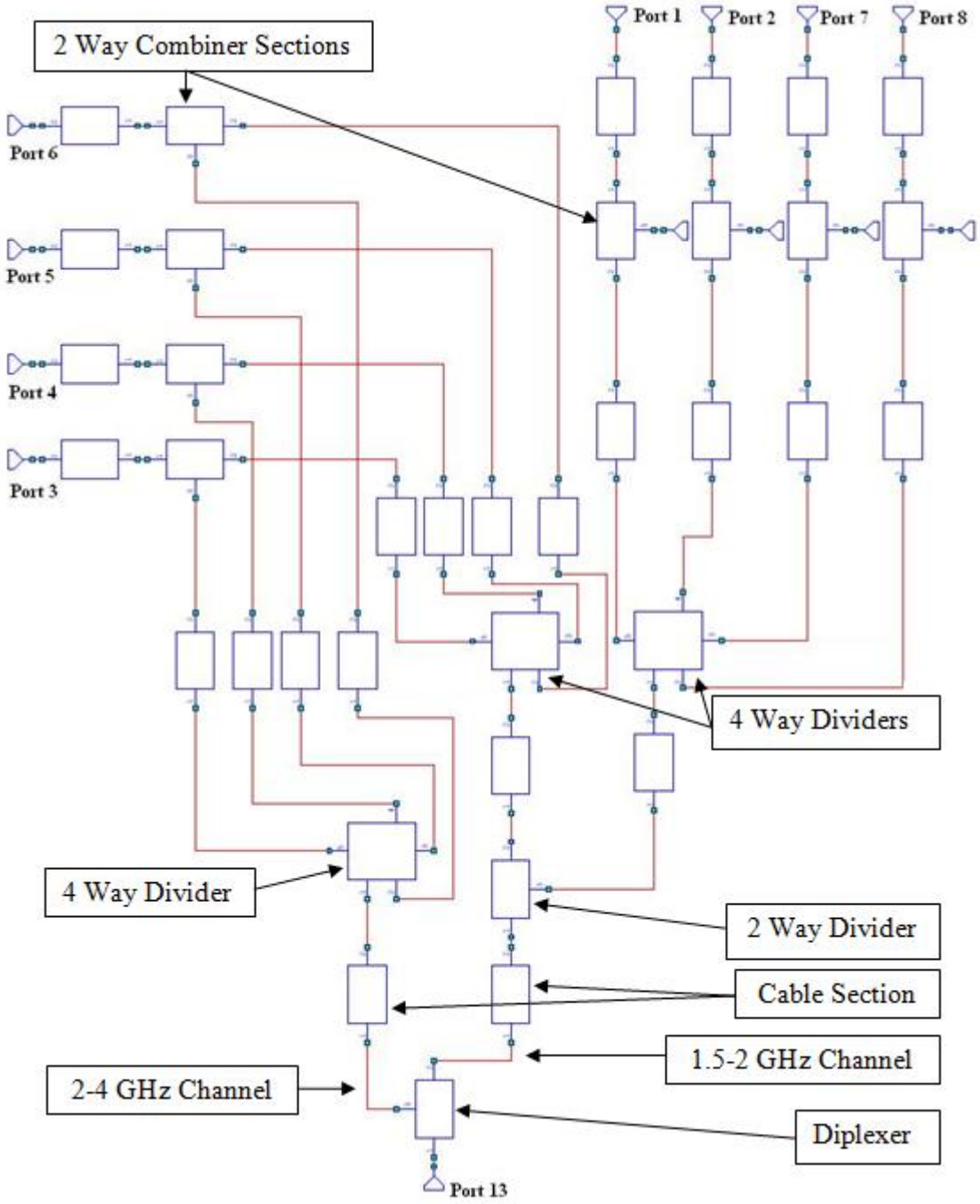

Figure A.4 Circuit schema of feed network

Simulation of the model shown in Figure A.4 is performed for the case in which only one diplexer exists in the circuit. Results of this simulation can be seen in Figure 4.19. Those results and the results obtained from measurements are very similar. Simulations continue

with increasing the number of diplexers utilized in simulation model. Results of the simulation are as expected and can be seen in Figure 4.22.

APPENDIX B

MEASUREMENT OF LINEAR ARRAY

Linear array measurements performed in this thesis can be categorized into two types of antenna measurement concepts. Firstly, S parameter measurement of the antenna is conducted to characterize active return loss of the antenna. Secondly, near field measurement is performed to observe far field radiation of the antenna.

B.1. Active S Measurement of Linear Array

Active S parameters of linear array can be derivated from passive S parameters of the antenna at any desired scan angle. Passive S parameters of linear array can be shown in matrix form as in (B.1).

$$S = \begin{bmatrix} S_{11} & S_{12} & S_{13} & S_{14} & \cdots & S_{17} & S_{18} \\ S_{21} & S_{22} & S_{23} & S_{24} & & S_{27} & S_{28} \\ & & & \vdots & & & \\ S_{71} & S_{72} & S_{73} & S_{74} & & S_{77} & S_{78} \\ S_{81} & S_{82} & S_{83} & S_{84} & \cdots & S_{87} & S_{88} \end{bmatrix} \quad \text{(B.1)}$$

Definition of the entries of this matrix for ports m and n is given in Figure B.1.

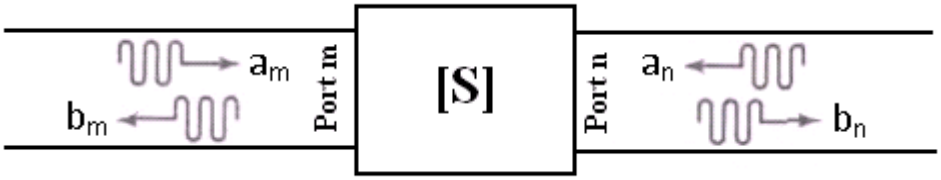

Figure B.1 S parameter definition for ports m and n

As can be seen Figure B.1, wave a is defined as incident wave on ports on m and n, whereas b waves are the reflected or transmitted waves due to incident waves. A 2x2 passive S parameter matrix could be defined using the definition of these waves. S matrix and definition of matrix entries can be seen in (B.2). Definitions require wave a of one port to be zero, which means the mentioned port is terminated with matched load.

$$S = \begin{bmatrix} S_{mm} & S_{mn} \\ S_{nm} & S_{nn} \end{bmatrix}$$

$$S_{mm} = \frac{b_m}{a_m}, a_n = 0$$

$$S_{mn} = \frac{b_m}{a_n}, a_m = 0 \qquad \text{(B.2)}$$

$$S_{nm} = \frac{b_n}{a_m}, a_n = 0$$

$$S_{nn} = \frac{b_n}{a_n}, a_m = 0$$

All entries of passive S parameters of linear array are gathered with measurements performed with network analyzer [24] according to definitions given in (B.2). Then, there is a need for post calculations to apply the effect of excitation coefficients of the array elements in order to calculate active S parameters of this linear array. Active S parameters of each antenna port are calculated via equation (4.2). Calculations performed in MATLAB® environment. Similarity between simulation results and measurements for active S parameters of each port is observed as suggested in Chapter 4.

B.2. Pattern Measurement of Linear Array

Pattern measurement of the linear array given in Chapter 4, is performed with near field measurement in spherical geometry with SATIMO near field measurement system. Overview of this system is given in Figure B.2.

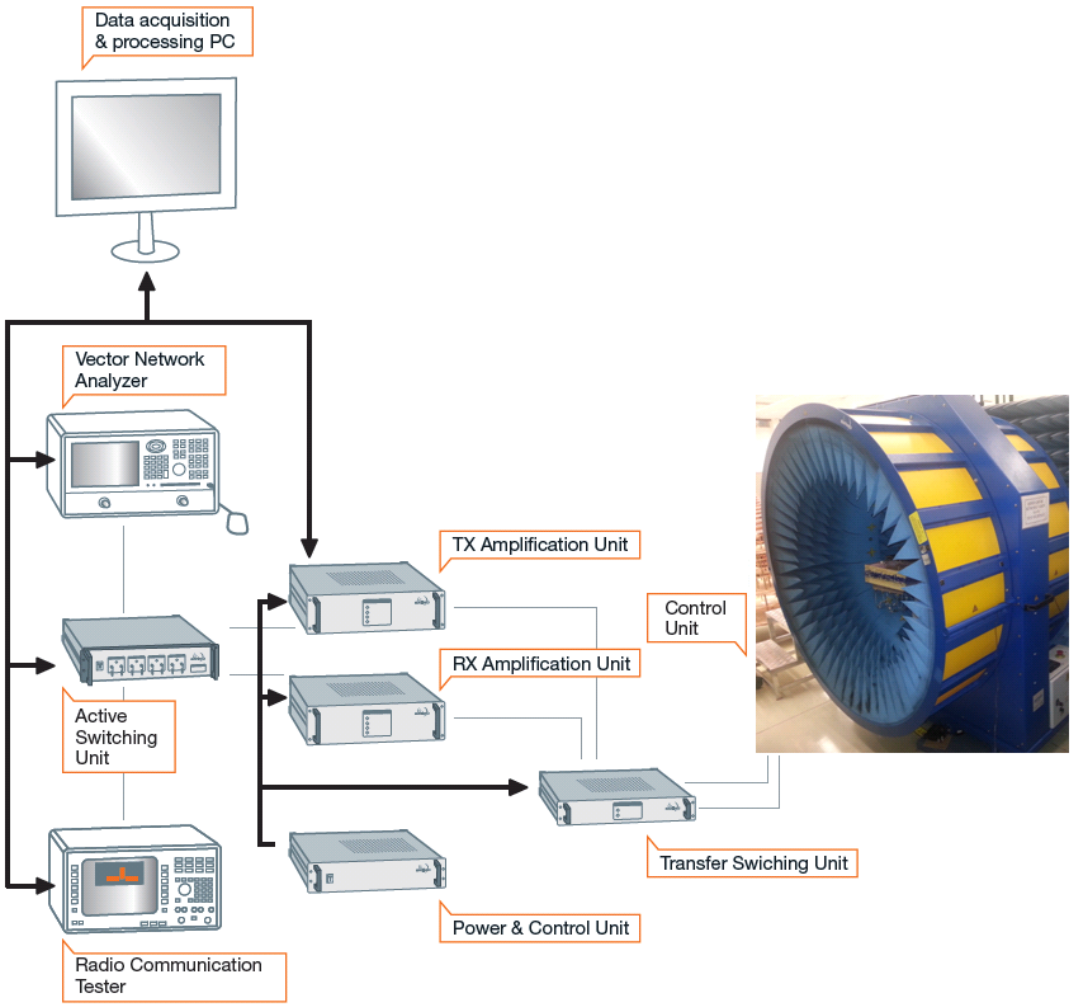

Figure B.2 System overview of antenna measurement system (From [25])

In order to get far field pattern data, some samples in near field of AUT (Antenna Under Test) is taken in control unit. Sampling of the antenna in its near field is performed in data acquisition screen of system software. Sampling of AUT is mainly dependent on antenna size and its maximum operational frequency.

There are dipole probes in order to get samples from AUT. Distribution of these probes and rotations of mechanical parts in control unit can be seen in Figure B.3. These probes could be either receiving antenna or transmitting antenna depending on the size of AUT.

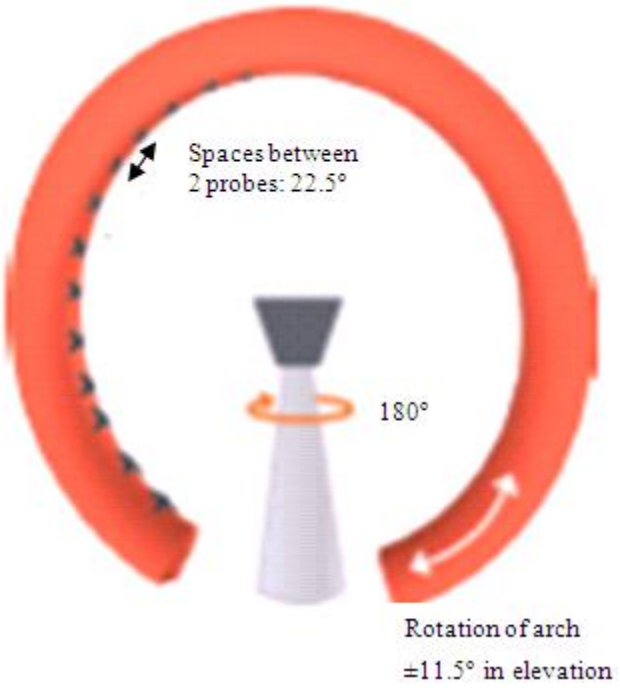

Figure B.3 Probe distribution and rotation in control unit (From [25])

There is need for calibration in this system so as to measure gain of AUT accurately. For gain calibration of this system, there are some antennas with very wideband frequency operation. Gain of such antennas are known and supplied by the manufacturer of the system. Calibration can be performed by measuring such antennas and utilizing the data in such measurement in calibration procedure. Then, it could be possible to measure gain of AUT within ±0.3 dB accuracy.

After calibration procedure, AUT is measured and its pattern data is gathered for major scan axis. Gain data at this stage is not accurate for measured linear array due to loss of feed network which is not taken into account in gain calibration. Then, feed network loss, i.e. sum of insertion loss of output channels in feed network is subtracted from gathered gain data from the measurement as a post processing. As a result of these procedures, gain and the pattern of linear array are found to be very similar to those found in simulation of the antenna. Mentioned results can be seen in Figure 4.40.